HOKKAIDO UNIVERSITY

Title	NMR studies of the structure and dynamics of silicate melts and glasses
Author(s)	Maekawa, Hideki; 前川, 英己
Degree Grantor	北海道大学
Degree Name	博士(理学)
Dissertation Number	乙第4313号
Issue Date	1993-06-30
DOI	https://doi.org/10.11501/3073049
Doc URL	https://hdl.handle.net/2115/49911
Type	doctoral thesis
File Information	000000267480.pdf

Hokkaido University Collection of Scholarly and Academic Papers : HUSCAP

NMR STUDIES OF THE STRUCTURE AND DYNAMICS OF SILICATE MELTS

Hideki Maekawa

1993

NMR STUDIES OF THE STRUCTURE AND DYNAMICS OF SILICATE MELTS

Hideki Maekawa
Department of Chemistry,
Faculty of Science,
Hokkaido University

1993

Sapporo, Japan

CONTENTS

Chap.1. GENERAL INTRODUCTION 1
1-1. Backgrounds and definition of silicate melt and glass structure 1
1-2. Thermodynamics of mixing 5
1-3. Previous structural studies of silicate glasses and melts 7
1-3-1. Raman spectroscopic studies 7
1-3-2. X-ray diffraction method 14
1-3-2-1. Binary silicate systems 14
1-3-2-2. Aluminosilicate systems 16
1-3-3. Neutron diffraction method 20
1-3-4. X-ray emission spectroscopic method 22
1-3-5. Visible spectroscopy and optical basicity 22
1-3-6. X-ray photoelectron spectroscopy 23
1-3-7. X-ray absorption spectroscopy 25
1-3-8. Molecular dynamics calculations 25
1-4. NMR spectroscopy 27
1-4-1. Basic concepts 27
1-4-2. Chemical shifts 28
1-4-3. Application of NMR to silicate glasses and melts 29
1-5 Subjects of the present thesis 33
References 35

Chap.2. STRUCTURAL STUDIES OF BINARY ALKALI SILICATE GLASSES BY MEANS OF ^{29}Si NMR 42
Abstract of Chapter 2 42
2-1. Introduction 42
2-2. Experimental section 44
2-3. Results 44
2-3-1. The effect of Fe_2O_3 on the spectra 44
2-3-2. Peak separation 44
2-3-3. Q_n distribution 48
2-4. Discussion 51
2-4-1. Line width 51
2-4-2. Reliability of the NMR area analysis 51
2-4-3. Changes of the chemical shifts 54
2-4-4. Relation between the optical basicity and chemical shifts 54
2-4-5. Thermodynamic modelling 56
2-5 Summary of Chapter 2 60
References 61

Chap.3. STRUCTURAL STUDIES OF TERNARY SILICATE GLASS SYSTEM Na_2O-Al_2O_3-SiO_2 BY MEANS OF ^{29}Si NMR 63
Abstract of Chapter 3 63
3-1. Introduction 63
3-2. Experimental section 65
3-3. Results 68
3-4. Discussion 70
3-4-1. Compositional dependence of the number of non-bridging oxygen atoms connected to Si atom 70
3-4-2. Chemical shifts 72
3-4-3. Location of AlO_4 tetrahedra 75
3-4-4. Qn distribution 78
3-5 Summary of Chapter 3 79
References 80

Chap.4. A HIGH TEMPERATURE ^{29}Si NMR STUDY OF SODIUM SILICATE MELT 81
Abstract of Chapter 4 81
4-1. Introduction 82
4-2. Description of the apparatus 82
4-3. Experimental section 83
4-4. Results 85
4-4-1. Temperature dependence of the line shapes 85
4-4-2. Effect of temperature on ^{29}Si chemical shifts 88
4-5. Discussion 90
4-5-1. Relationships between chemical shift and melt structure 90
4-5-2. Estimation of the rates of exchange reaction between Q_n species 92
4-6 Summary of Chapter 4 95
References 96

Chap.5. A HIGH TEMPERATURE ^{23}Na NMR STUDY OF COORDINATION NUMBERS OF SODIUM ION IN SILICATE MELTS 97
Abstract of Chapter 5 97
5-1. Introduction 97
5-2. Experimental section 98
5-3. Results 99
5-3-1. ^{23}Na chemical shifts for silicate, borate and other inorganic crystals 99
5-3-2. ^{23}Na chemical shifts of simple ionic liquids 102
5-3-3. ^{23}Na chemical shifts for silicate and aluminosilicate liquids 103
5-4. Discussion 105
5-5. Summary of Chapter 5 106
References 107

Chap.6. DYNAMICS OF INORGANIC NETWORK-GLASS-FORMING SYSTEM: ^{11}B NMR STUDY OF B_2O_3 MELT AND GLASS 108
Abstract of Chapter 6 108
6-1. Introduction 108
6-2. Experimental section 110
6-3. Results 112
6-4. Discussion 117
6-5. Summary of Chapter 6 120
References 121

ACKNOWLEDGEMENTS 123

CHAPTER 1

GENERAL INTRODUCTION

1-1 Backgrounds and definition of silicate melt and glass structure

Characterization of the structure and an understanding of the relationships between the structure and properties of silicate melts and glasses are important in both the earth science and material science: the chemical and physical behavior of magmas dominates many geological processes, and most technological glasses and glass ceramics start off in the molten state. The structure and properties of silicate glasses and melts had been investigated by glass scientists and steel making metallurgists.

Zachariasen(1932), who was a pioneer of structure analysis of glass, presented the structural model of glass as a continuous random network which is absent of periodicity and symmetry. For example, the structure of binary Na_2O-SiO_2 glass can be represented as shown in figure1. The basic units constructing the glass structure are SiO_4 tetrahedra. Because of the strong Si-O sp^3 hybrid orbital between silicon and oxygen atoms, the SiO_4 tetrahedra remains unchanged as basic units for a variation of composition and temperature.

CaO-Na_2O-Al_2O_3-SiO_2 is one of the most important system for glass industries. Metal oxides constructing such multi-component silicate systems have been reduced into three categories e.g., network formers, network modifiers and intermediates. The network former, such as SiO_2, form units of low coordination numbers to construct framework of the network structure by sharing corner oxygen atoms each other, whereas the network modifiers, such as Na_2O, modify the network to loosen the structure, which cause, for example, a descent of the melting points. Intermediates, such as Al_2O_3, can take place either of network former and modifier depending on the variation of composition, temperature and

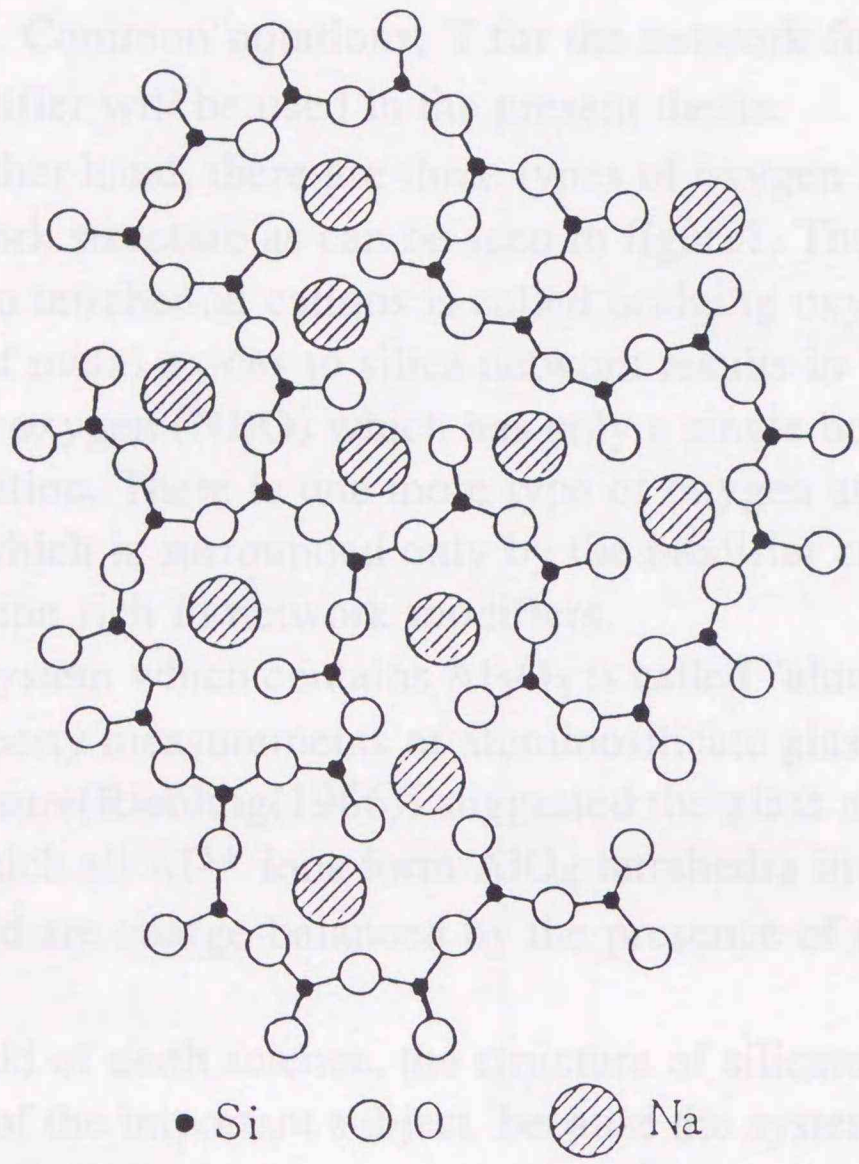

Figure 1. Cartoon suggesting possible structure of sodium silicate glasses(Na_2O-SiO_2).

pressure.

These categories can be classified by the ion-oxygen attraction(I), defined by

$$I=2ze^2/r^2, \qquad (1)$$

where z is the valency, e is the electronic charge, r is the bond length. I, expressed by the electron units, of network formers exceeds 1.6, whereas that of network modifiers is smaller than 0.7. Intermediates have I value of $0.7<I<1.6$. Common notations, T for the network former, M for the network modifier will be used in the present thesis.

On the other hand, there are three types of oxygen atoms in the silicate network structure as can be seen in figure1. The oxygen atom shared by two tetrahedral cations is called bridging oxygen (BO), whereas an addition of metal oxides to silica network results in the formation of non-bridging oxygen (NBO) which has only a single bond to the tetrahedral cation. There is one more type of oxygen atom called "free oxide ion", which is surrounded only by the modifier cations that exist in the composition rich in network modifiers.

Silicate system which contains Al_2O_3 is called "aluminosilicate". Physical property measurements of aluminosilicate glasses and melts at ambient pressure(Riebling(1966)) suggested the glass and melt structure models in which all Al^{3+} ions form AlO_4 tetrahedra in the place of SiO_4 tetrahedra and are charge-balanced by the presence of the network modifiers.

In the field of earth science, the structure of silicate melts have become one of the important subject because the systematic understanding of the rock forming igneous process and magmatic process e.g. the formation and separation of the magma needs more and more information about the silicate melt structure. Natural mafic to intermediate magmas is in the range of M/T=0.5~1.

On the other hand, CaO-Al_2O_3-SiO_2, is the most important system for steel making process especially of the composition rich in CaO.

The composition of silicate melts related with investigation are shown in figure2, together with the crystal structure of corresponding composition.

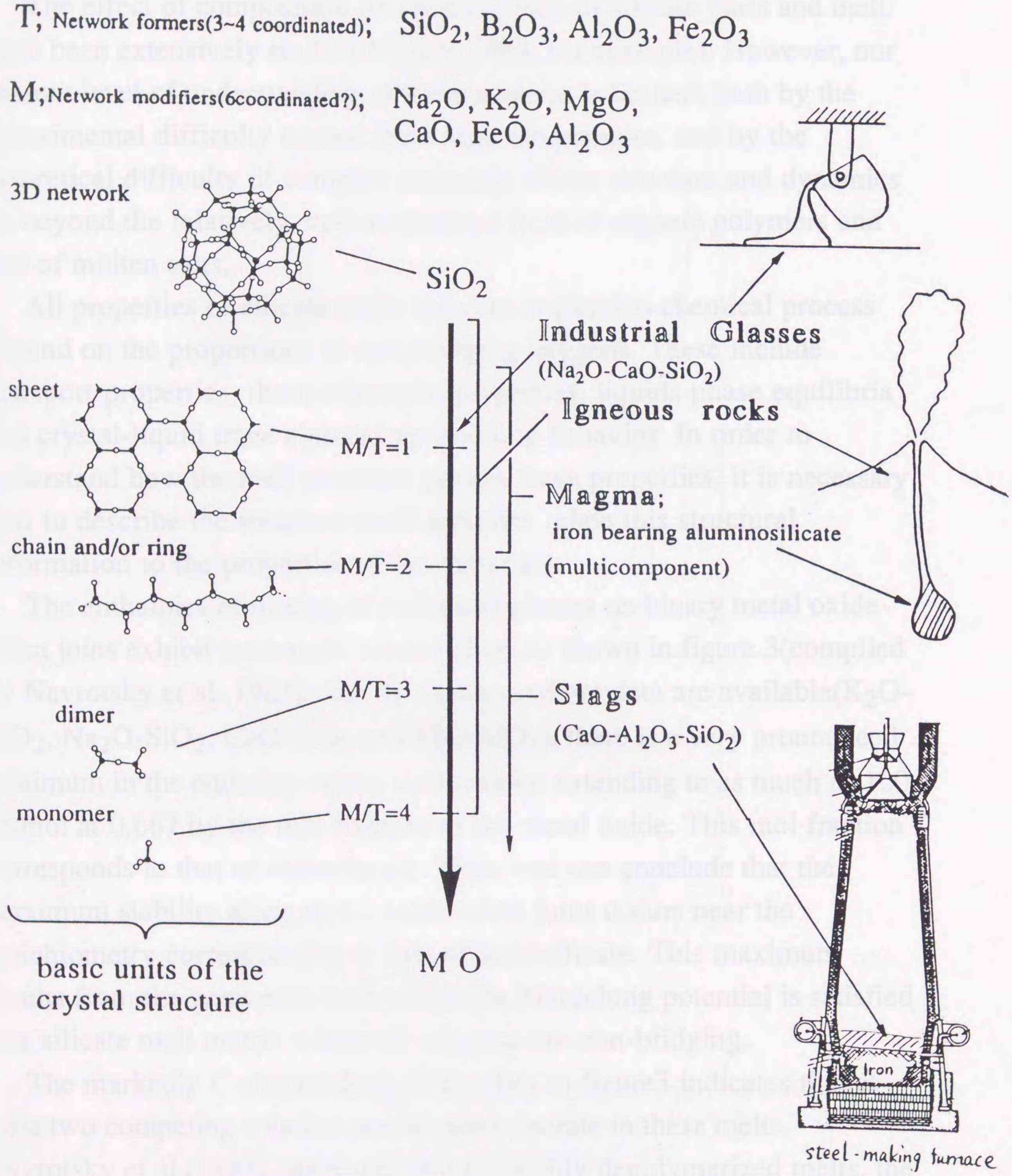

Figure 2. Variation of the structure of silicates as a function of composition.

1-2 Thermodynamics of mixing

The effect of composition on the properties of silicate glass and melt have been extensively studied(Mysen, 1988, for example). However, our present level of understanding of these systems is limited, both by the experimental difficulty caused from high temperature, and by the theoretical difficulty of complex materials whose structure and dynamics lie beyond the relatively well-understood field of organic polymers and that of molten salts.

All properties of silicate melts relevant to physico-chemical process depend on the proportions of non-bridging oxygens. These include transport properties, thermodynamic properties, liquids phase equilibria and crystal-liquid trace element partitioning behavior. In order to understand how the melt structure govern these properties, it is necessary first to describe the structure itself and then relate this structural information to the properties of the materials.

The enthalpies of mixing of melts and glasses on binary metal oxide-silica joins exhibit systematic relationships as shown in figure 3(compiled by Navrotsky et al. 1985). For the systems where data are available(K_2O-SiO_2, Na_2O-SiO_2, CaO-SiO_2 and PbO-SiO_2), there is a very pronounced minimum in the enthalpy versus composition extending to as much as 100 kJ/mol at 0.667 by the mol fraction of the metal oxide. This mol fraction corresponds to that of orthosilicate. Thus, one can conclude that the maximum stability along metal oxide-silica joins occurs near the stoichiometry corresponding to that of orthosilicate. This maximum results from the great ease with which the Mardelung potential is satisfied in a silicate melt matrix where all oxygens are non-bridging.

The markedly C-shaped form of the data in figure3 indicates that at least two competing solution mechanisms operate in these melts. Navrotsky et al.(1985) suggested that for highly depolymerized melts, the equilibria involving silicate anionic units and free oxide ion might dominate and a reaction such as;

$$Si_2O_7^{6-} + O^{2-} \leftrightarrow 2SiO_4^{4-} \qquad (2)$$

was suggested. At higher silica contents the equilibria involving various

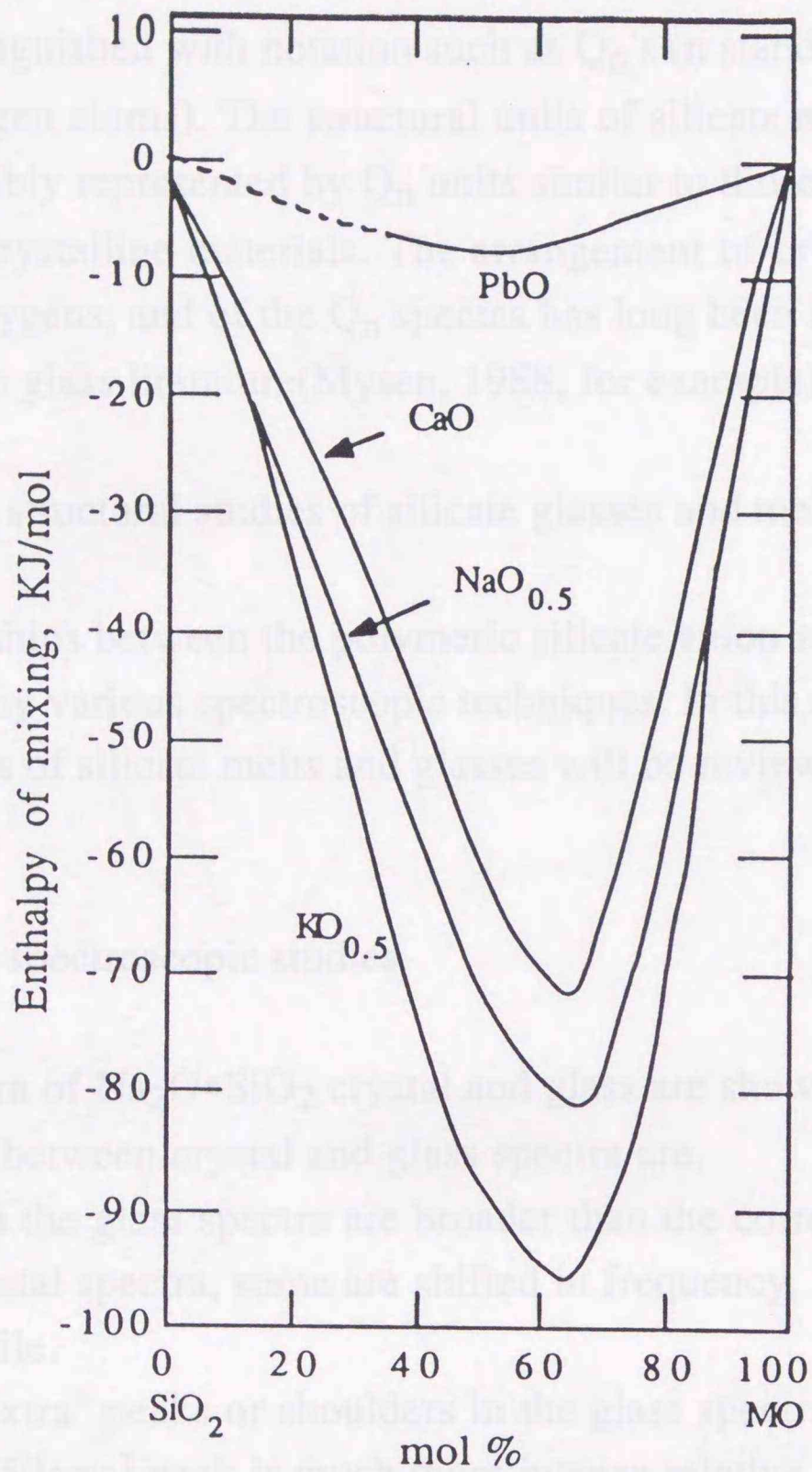

Figure 3. Enthalpy of mixing of glasses on metal oxide-silica joins as indicated on figure(data from Rein and Chipman, 1965; Ostvold and Kleppa, 1969; Eliezer et al., 1978, 1979; and Byker et al. 1981; compiled by Navrotsky et al., 1985).

silicate polymers describe the structure.

The SiO_4 units constructed from different numbers of BO atoms are commonly distinguished with notation such as Q_n's (n stands for numbers of bridging oxygen atoms). The structural units of silicate melts and glasses are possibly represented by Q_n units similar to those corresponding crystalline materials. The arrangement of bridging and non-bridging oxygens, and of the Q_n species has long been a subject of discussion in the glass literature(Mysen, 1988, for example).

1-3 Previous structural studies of silicate glasses and melts

The relationships between the polymeric silicate anion structure have been examined by various spectroscopic techniques. In this section, structural studies of silicate melts and glasses will be reviewed, itemizing each technique.

1-3-1 Raman spectroscopic studies

Raman spectra of $Na_2O \bullet SiO_2$ crystal and glass are shown in figure4. The differences between crystal and glass spectra are,

(1) The peaks in the glass spectra are broader than the corresponding peaks of the crystal spectra, some are shifted in frequency, and some are of peculiar profile.

(2) There are "extra" peaks or shoulders in the glass spectra. In particular, the $850cm^{-1}$ peak is much more intense relative to the strong high-frequency peak than any of the secondary high-frequency peaks of the crystal spectrum.

(3) For frequencies less than $500cm^{-1}$ there is little or no structure in the glass spectra, while crystal spectra are quite complex in this region.

(4) The peak intensities of the crystal spectra are about an order of magnitude larger than those of the glass spectra.

From the fingerprinting technique, that is, comparison of the spectrum of a crystalline material, or perhaps several different materials with known structure, with those of spectra of the glasses or melts of interest,

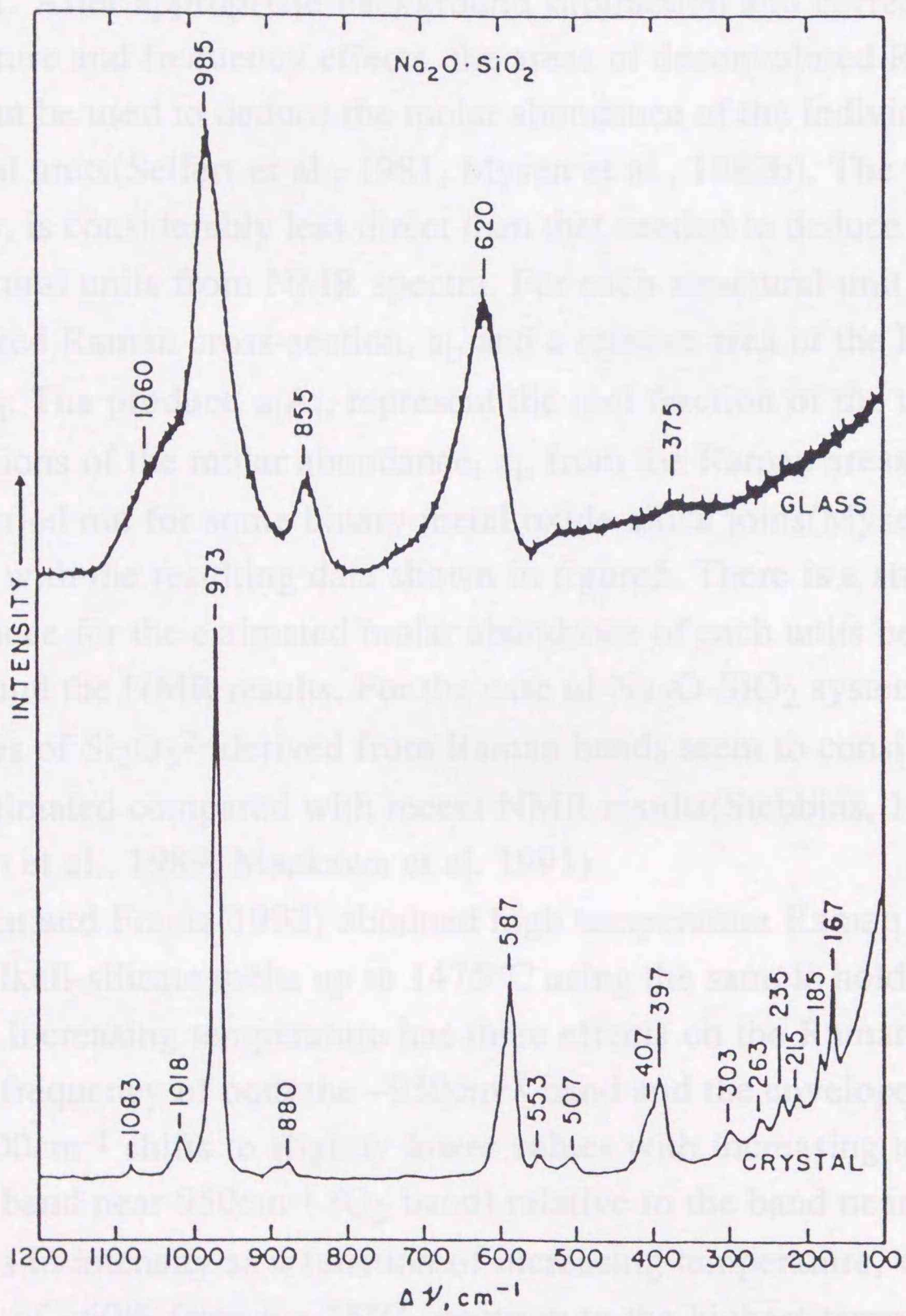

Figure 4. Raman spectra of $Na_2O \bullet SiO_2$ crystal and glass(Brawer and White, 1975).

the Raman bands between 800~1200cm^{-1} have been interpreted to result from stretching vibration of silicon to non-bridging oxygens bonds(Si-O$^-$) in the various structural units. In this interpretation, the bands of each structural units, SiO_4^{4-}(monomer), $Si_2O_7^{6-}$(dimer), $Si_2O_6^{4-}$(chain), $Si_2O_5^{2-}$(sheet), SiO_2(three dimensional network) were assigned as shown in table1. After appropriate background subtraction and correction for temperature and frequency effects, the areas of deconvoluted Raman bands can be used to deduce the molar abundance of the individual structural units(Seifert et al., 1981, Mysen et al., 1982b). The procedure, however, is considerably less direct than that needed to deduce abundance of structural units from NMR spectra. For each structural unit, there is a normalized Raman cross-section, a_i, and a relative area of the Raman band, A_i. The product, a_iA_i, represent the mol fraction of the unit i. Calculations of the molar abundance, x_i, from the Raman areas, A_i, have been carried out for some binary metal oxide-silica joins(Mysen et al., 1982b), with the resulting data shown in figure5. There is a strong discordance for the estimated molar abundance of each units between the Raman and the NMR results. For the case of Na_2O-SiO_2 system, the quantities of $Si_2O_5^{2-}$ derived from Raman bands seem to considerably underestimated compared with recent NMR results(Stebbins, 1987, 1988, Emerson et al., 1989, Maekawa et al. 1991).

Mysen and Frantz(1992) obtained high temperature Raman spectra for binary alkali-silicate melts up to 1475°C using the sample holder shown in figure6. Increasing temperature has three effects on the Raman spectra:
(1) The frequency of both the ~950cm^{-1} band and the envelope centered near 1100cm^{-1} shifts to slightly lower values with increasing temperature.
(2) The band near 950cm^{-1} (Q_2 band) relative to the band near 1100cm^{-1} increases in intensity as a function of increasing temperature, with an increase of ~60% from the 25°C spectrum to the highest-temperature spectrum. A similar increase in intensity with temperature was also noted by Seifert et al.(1981) in the high temperature spectra of sodium aluminosilicate melt.
(3) The intense envelope centered near 1100cm^{-1} broadens with

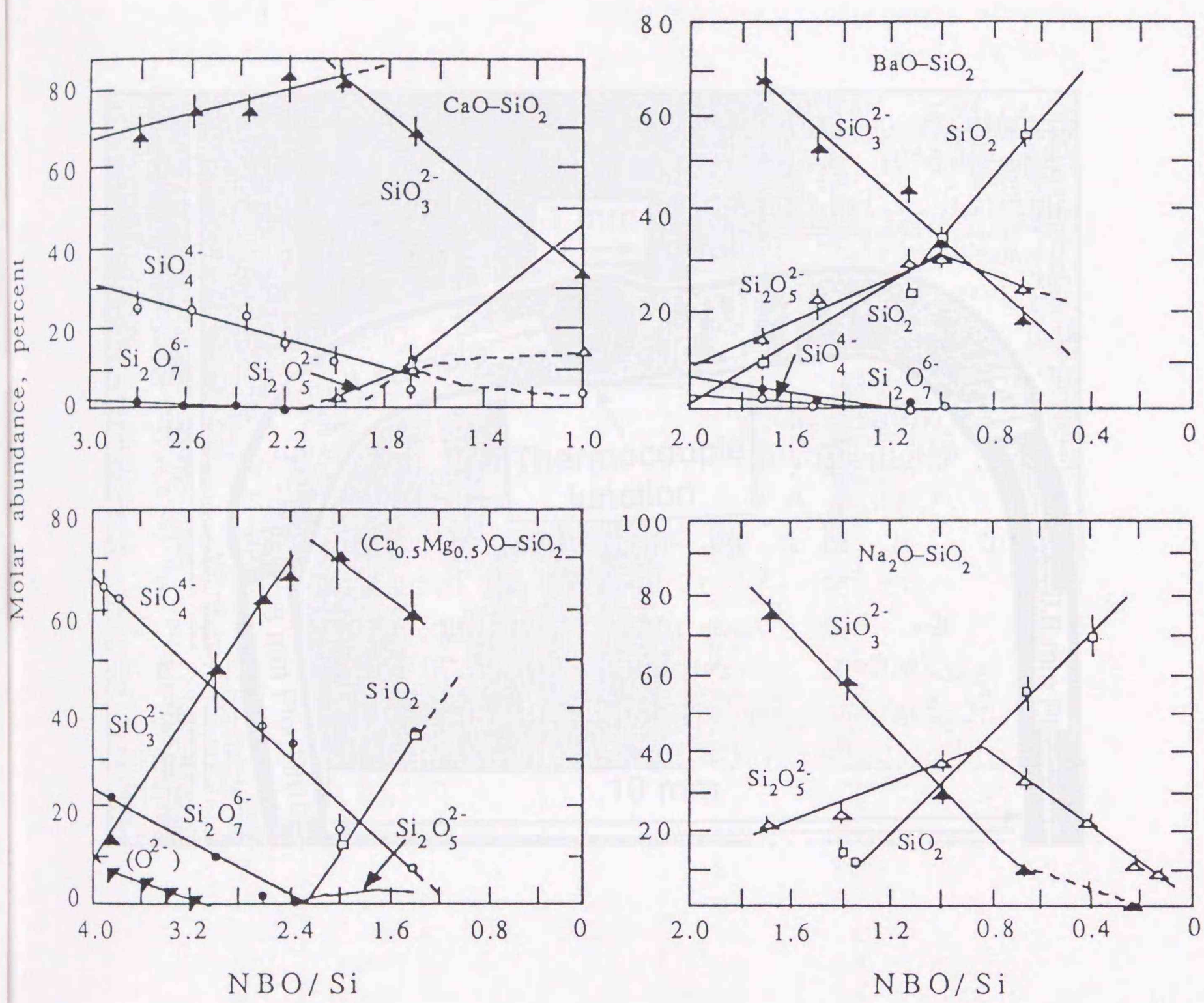

Figure 5. Molar abundance of structural units in quenched melts on metal oxide-silica joins as indicated as a function of bulk melt NBO/Si (Mysen, 1988).

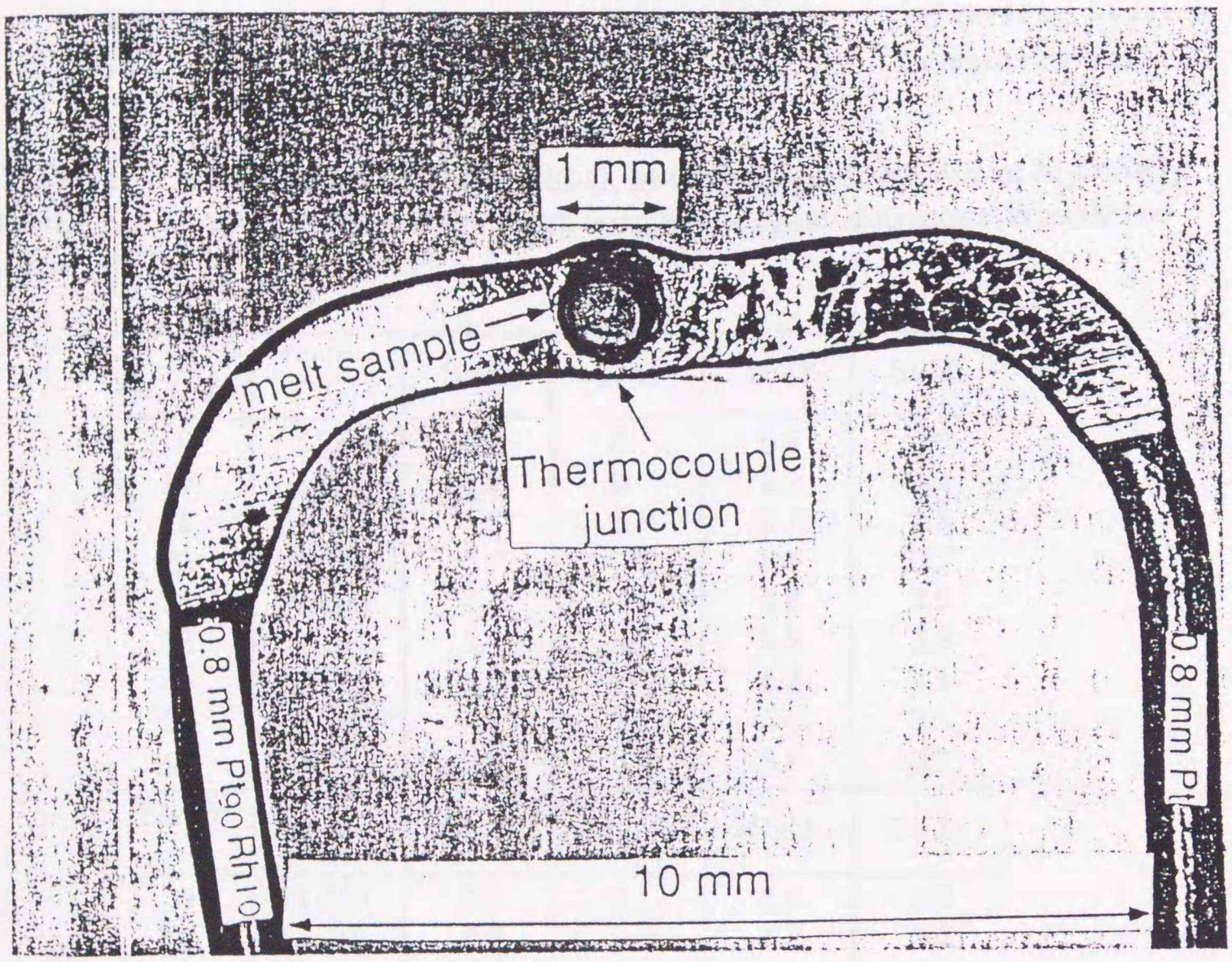

Figure 6. Sample holder made of Pt-$Pt_{90}Rh_{10}$ which serves a dual function as both thermocouple and heater for high temperature Raman spectroscopy(Mysen and Frantz, 1992).

Table 1. Raman frequencies of the stretch vibrations of specific Si-rich anionic structural units in silicate melts(Mysen et al., 1980).

Structural unit	NBO/Si	Frequency(cm^{-1})	mode
SiO_4^{4-}	4	850～880	symmetric stretch
$Si_2O_7^{6-}$	3	900～920	symmetric stretch
$Si_2O_6^{4-}$	2	950～980	symmetric stretch
$Si_2O_5^{2-}$	1	1050～1100	symmetric stretch
SiO_2	0	1060, 1190	symmetric stretch

Table 2. Coordination numbers of Si-O, M-O, O-O and Si-Si pairs of M_2O-SiO_2 (M=Li, Na, K) system obtained from high temperature X-ray diffraction(Waseda and Toguri, 1976).

Li_2O (mole%)	temp. (°C)	Si-O	Li-O	O-O	Si-Si
0	1 750	3.8	0	5.6	3.9
10	1 650	3.8	0 [1]	5.9	4.2
15	1 600	3.5	0 [1]	5.7	3.8
20	1 550	3.7	0 [1]	5.5	3.7
25	1 550	4.1	2.4	5.8	3.9
33	1 150	3.8	4.1	5.5	3.8
40	1 200	4.3	3.7	5.8	4.1
50	1 250	4.1	3.9	5.6	3.5
60	1 200	3.8	3.9	5.6	3.2
Na_2O		Si-O	Na-O	O-O	Si-Si
0	1 750	3.8	0	5.6	3.9
10	1 620	3.7	0 [1]	5.8	3.7
15	1 550	3.8	0 [1]	5.9	3.9
20	1 450	3.9	4.1	5.5	4.2
25	1 200	3.8	5.3	5.6	4.1
33	1 000	4.1	5.9	5.6	3.8
40	1 100	4.1	5.8	5.7	3.9
50	1 200	3.8	5.7	5.8	3.3
60	1 300	3.7	6.1	5.5	3.2
K_2O		Si-O	K-O	O-O	Si-Si
0	1 750	3.8	0	5.6	3.9
10	1 500	3.6	0 [1]	5.5	3.7
15	1 500	3.9	(5.7) [2]	11.3	3.7
20	1 100	4.1	(6.6) [2]	12.2	3.8
25	900	3.8	(7.1) [2]	12.7	3.8
33	1 100	3.9	(7.4) [2]	13.0	3.7
40	1 100	4.2	(7.7) [2]	13.3	3.5
50	1 100	3.9	(8.0) [2]	13.6	3.1

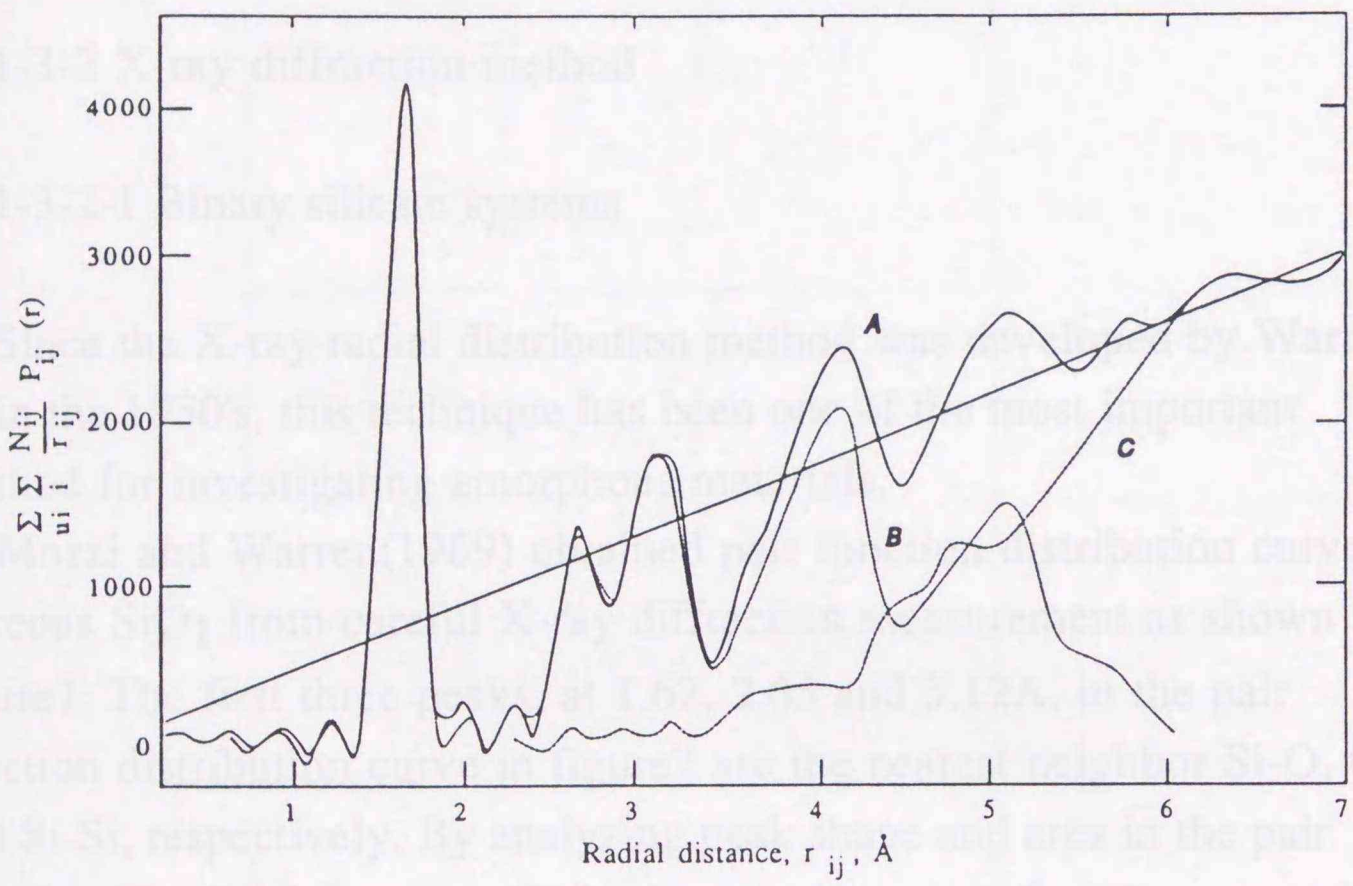

Figure 7. Pair function distribution curve for vitreous SiO_2(Mozzi and Warren, 1969).

temperature (from slightly less than $100cm^{-1}$ in spectra of room temperature glass to >120-$130cm^{-1}$ in the spectra of melts and supercooled liquids).

The temperature dependence is qualitatively consistent with the reaction,

$$Si_2O_5^{2-}(2Q_3) \leftrightarrow SiO_3^{2-}(Q_2) + SiO_2(Q_4) \qquad (2)$$

to shift to the right with increasing temperature, which have been observed from NMR measurements(Stebbins, 1988; Dorfeld, 1988; Maekawa et al. 1991).

1-3-2 X-ray diffraction method

1-3-2-1 Binary silicate systems

Since the X-ray radial distribution method was developed by Warren et al. in the 1930's, this technique has been one of the most important method for investigating amorphous materials.

Mozzi and Warren(1969) obtained pair function distribution curve for vitreous SiO_2 from careful X-ray diffraction measurement as shown in figure7. The first three peaks, at 1.62, 2.65 and 3.12A, in the pair function distribution curve in figure7 are the nearest neighbor Si-O, O-O and Si-Si, respectively. By analyzing peak shape and area in the pair function distribution curve, all the oxygen atoms are found to connect to two silicon atoms, and the Si-O-Si angles distributed widely in the range from 120°~180°.

The radial distribution functions(RDFs) of molten $MgO \bullet SiO_2$, $CaO \bullet SiO_2$, SiO_2 obtained from X-ray diffraction measurements by Waseda and Toguri(1977) are shown in figure8. The coordination number for Si-O and O-O pairs are 4 and 6, respectively, with MgO and CaO concentrations up to 57 mole%. This suggests that molten silicates mainly consist of SiO_4 tetrahedral units at least up to 50mole% MO.

On the other hand, coordination numbers obtained for M_2O-SiO_2 system(M=Li, Na, K) are shown in table2(Waseda and Toguri, 1976). The coordination number of oxygen around silicon atom was 4, independent

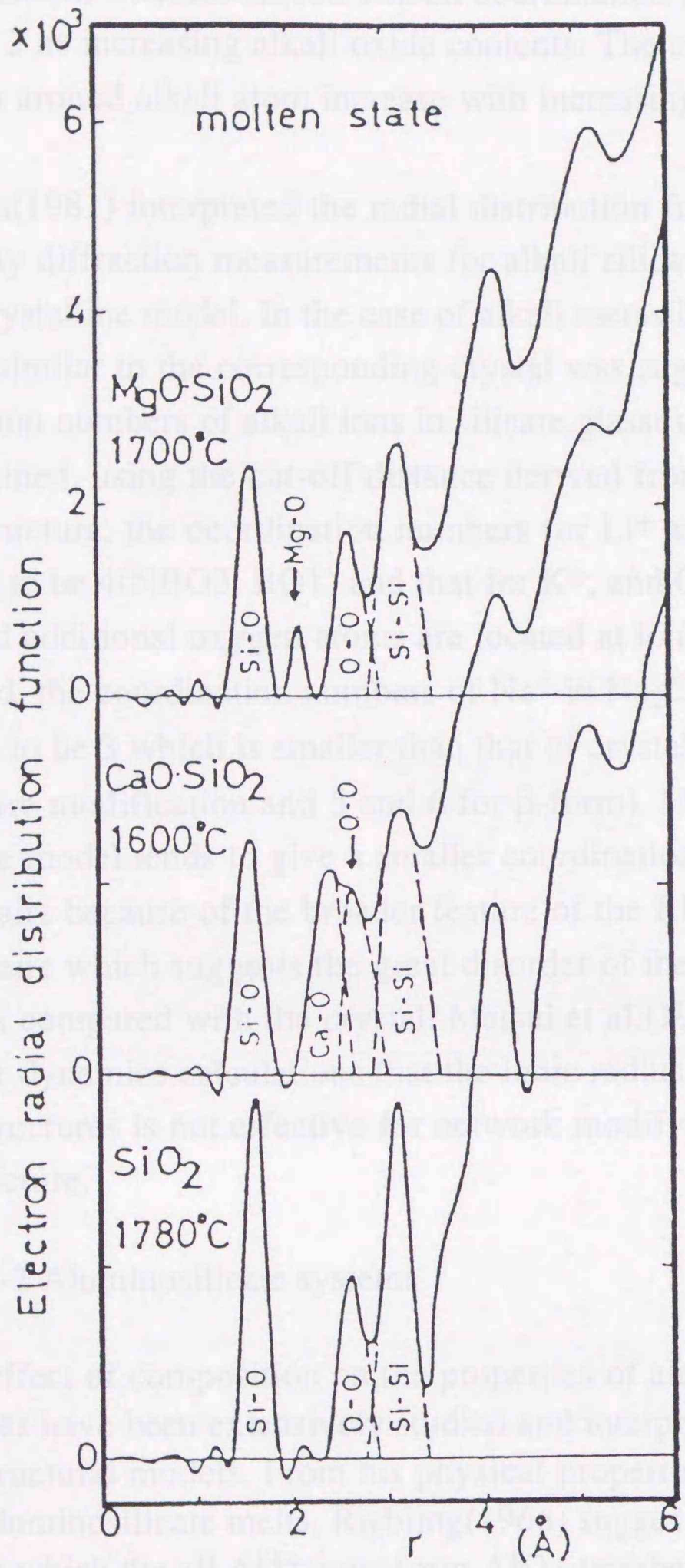

Figure 8. Radial distribution function of molten monosilicates(Waseda and Toguri, 1977).

of composition, whereas silicon-silicon coordination numbers decrease from 4 to 3 as increasing alkali oxide contents. The coordination numbers of oxygen around alkali atom increase with increasing alkali oxide contents.

Imaoka(1981) interpreted the radial distribution functions derived from X-ray diffraction measurements for alkali silicate glass by means of a quasi-crystalline model. In the case of alkali metasilicate glass, the chain structure similar to the corresponding crystal was suggested. Although the coordination numbers of alkali ions in silicate glasses and melts are often ill-determined, using the cut-off distance derived from the corresponding crystal structure, the coordination numbers for Li^+ and Na^+ were estimated to be 4(NBO3, BO1) and that for K^+, and Cs^+ to be 5(NBO4, BO1), and additional oxygen atoms are located at longer distances. On the other hand, the coordination numbers of Na^+ in $Na_2O \bullet 2SiO_2$ glass was estimated to be 3 which is smaller than that of crystal(5 for highest temperature modification and 5 and 6 for β-form). However, the quasi-crystalline model tends to give a smaller coordination numbers for alkali oxygen pairs because of the broader feature of the RDF peak for alkali-oxygen pairs which suggests the great disorder of the coordination polyhedra compared with the crystal. Matsui et al.(1982) suggested from molecular dynamics calculations that the ionic radius concept for the crystal structures is not effective for network modifying cations in the glass structure.

1-3-2-2 Aluminosilicate systems

The effect of composition on the properties of aluminosilicate melts and glasses have been extensively studied and interpreted in terms of simple structural models. From his physical property measurements of sodium aluminosilicate melts, Riebling(1966) suggested the melt structure models in which the all Al^{3+} ions form AlO_4 tetrahedra and are charge-balanced by the presence of the Na^+. Densities, viscosities, refractive indexes and thermal expansivities show drastic changes near the composition of atom ratio [Na]/[Al] = 1. This change was thought to be accompanied by the change of coordination numbers of aluminum from 4

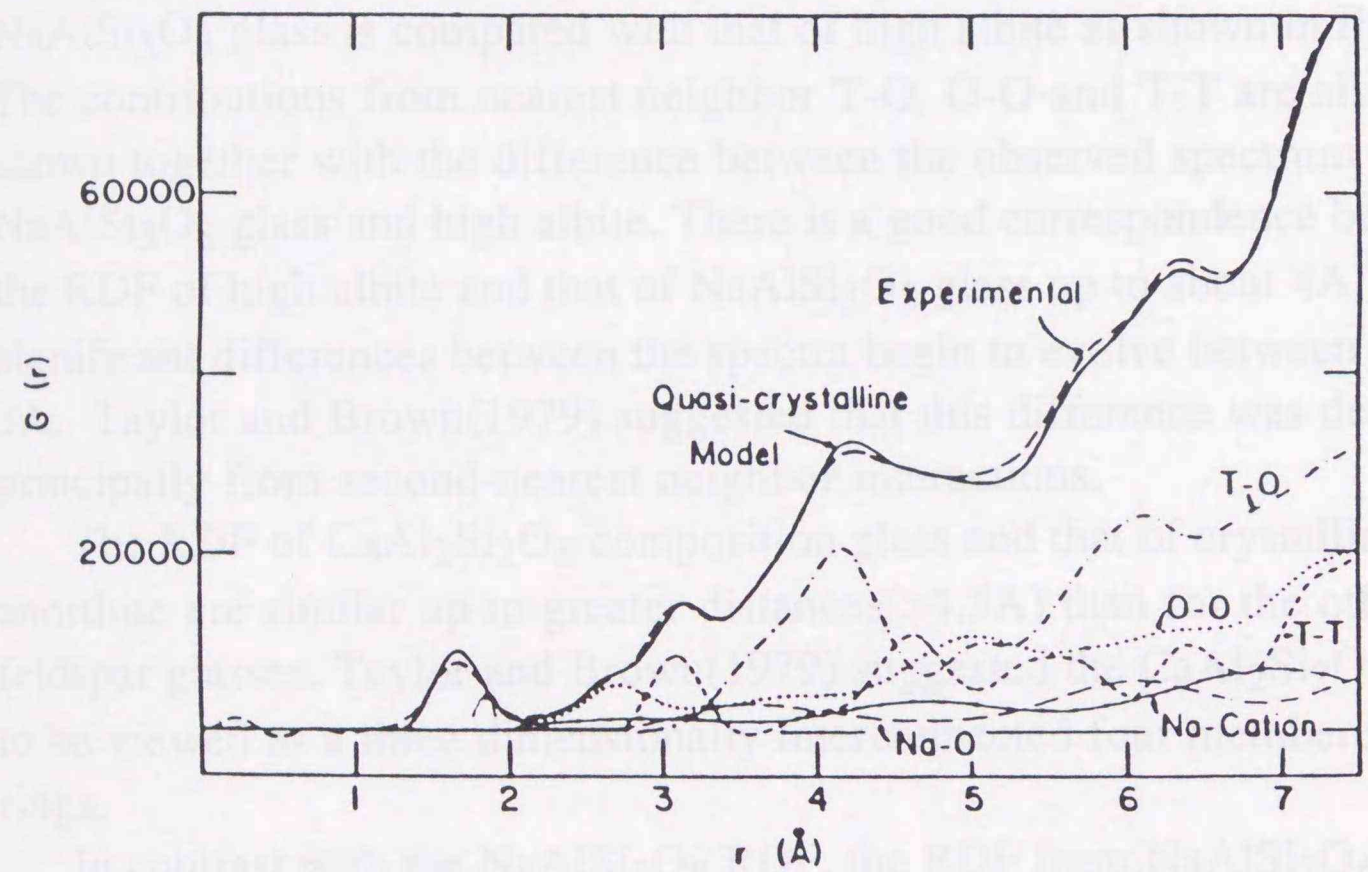

Figure 9. Experimental(-----) and quasi-crystalline model(——) RDFs of the high albite structure. The curves under the solid curve are contributions to the total RDF from five different types of interatomic vectors(Taylor and Brown, 1979a).

to 6 oxygen atoms. Thus, Galant(1959) measured refractive indices of sodium aluminosilicate glasses and proposed a structural model that, in the composition range of [Na]/[Al]>1, all Al^{3+} ions form AlO_4 tetrahedra accompanied by Na^+ ion as the charge compensator and the excess sodium ions modify the silicate network and create NBOs bonded only to one silicon atom. While the observed physical properties suggest the validity of this structural model, spectroscopic observations have not always supported it.

X-ray RDFs of the feldspar glasses($NaAlSi_3O_8$, $KAlSi_3O_8$, $CaAl_2Si_2O_8$) were reported by Taylor and Brown(1979a). The RDF of $NaAlSi_3O_8$ glass is compared with that of high albite as shown in figure9. The contributions from nearest neighbor T-O, O-O and T-T are also shown together with the difference between the observed spectrum from $NaAlSi_3O_8$ glass and high albite. There is a good correspondence between the RDF of high albite and that of $NaAlSi_3O_8$ glass up to about 4A, but significant differences between the spectra begin to evolve between 4 and 5A. Taylor and Brown(1979) suggested that this difference was derived principally from second-nearest neighbor interactions.

The RDF of $CaAl_2Si_2O_8$ composition glass and that of crystalline anorthite are similar up to greater distances(>4.5A) than for the other two feldspar glasses. Taylor and Brown(1979) suggested the $CaAl_2Si_2O_8$ glass to be viewed as a three dimensionally interconnected four membered rings.

In contrast with the $NaAlSi_3O_8$ RDF, the RDF from $NaAlSi_2O_6$ glass shows significant differences with the RDF of crystalline Jadeite(Taylor and Brown, 1979b). In particular, it was concluded that the radial distribution function indicated Al-O distances about 0.2A shorter in the glass than that in crystalline Jadeite, thus being consistent with four coordinated aluminum in the glass as compared with the well-known six-fold coordination of Al^{3+} in crystalline Jadeite. In $NaAlSiO_4$ glass, on the other hand, there is good agreement between the RDF of the glass and that of crystalline nepheline to about 4.5A. From these observations, Taylor and Brown(1979b) concluded that these three compositions on the join $NaAlO_2$-SiO_2 had RDFs best represented by a "stuffed tridymite structure"(tridymite is one of the SiO_2 polymorph.

On the other hand, the structural similarities between the glass and melt of feldspar composition have been suggested by Okuno and

Table 3. Atomic distance(l), its fluctuation(Δl) and coordination number(N) for Si-O and O-O pairs in SiO_2 and $M_2O \bullet 2SiO_2$(M=Li, Na and $Li_{0.63}Na_{0.37}$) glass. <O-Si-O is the mean bond angle at Si atoms(Misawa et al., 1980).

Sample	Si–O				O–O			∠O–Si–O (deg.)
	l (nm)	Δl (nm)	N_{Si-O}	N_{O-Si}	l (nm)	Δl (nm)	N_{O-O}	
SiO_2	0.1613	0.0050	4.0	2.0	0.2628	0.0092	5.7	109.1
$Na_2O \cdot 2\,SiO_2$	0.1631	0.0063	3.9	1.5_6	0.266	0.011	4.9	109.3
$Li_2O \cdot 2\,SiO_2$	0.1624	0.0061	3.9	1.5_6	0.265	0.010	4.4	109.4
$(L\text{-}N)_2O \cdot 2\,SiO_2$ [a]	0.1628	0.0059	4.0	1.6	0.265	0.010	4.8	109.0

[a] $(Li_{0.63}Na_{0.37})_2O \cdot 2\,SiO_2$.

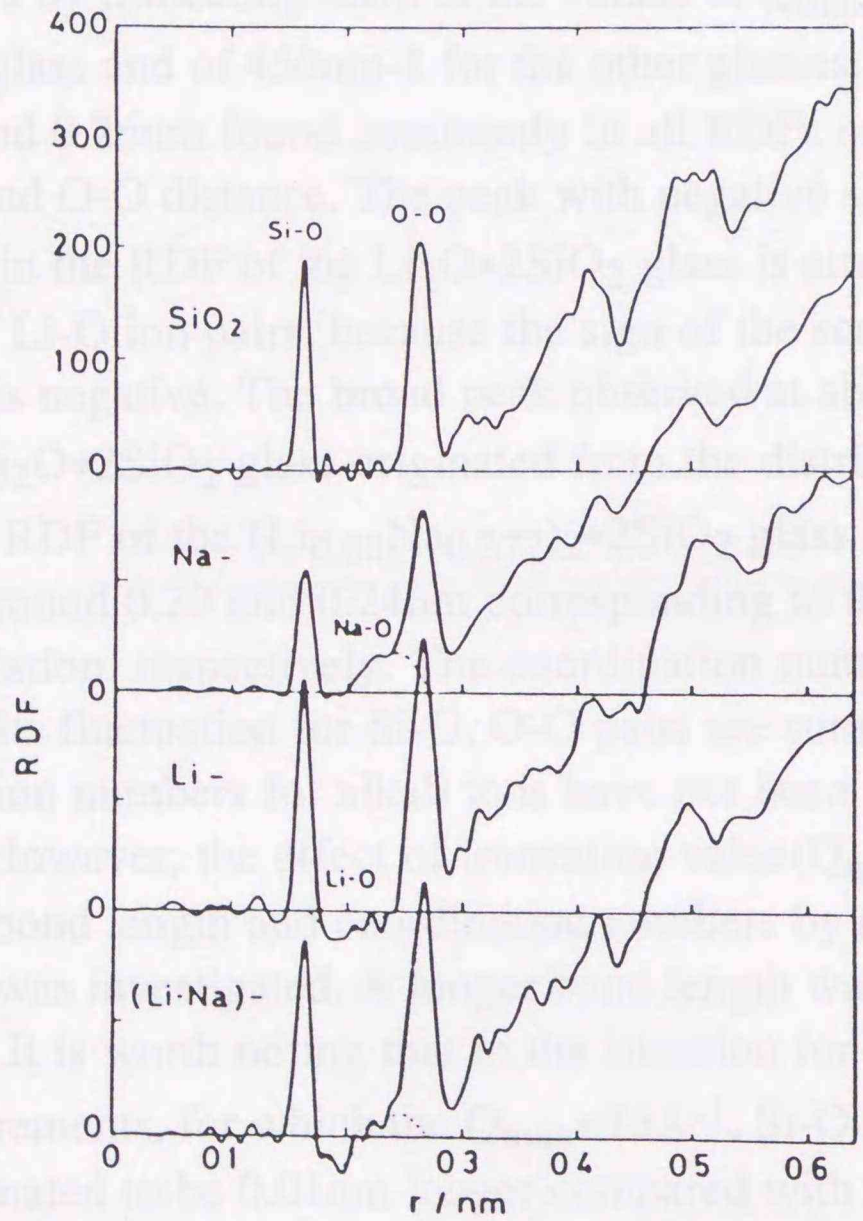

Figure 10. RDFs of SiO_2 and $M_2O \bullet 2SiO_2$(M=Li, Na, $Li_{0.63}Na_{0.37}$) glass. Symbols of Na-, Li-, and (Li-Na)- denote M. Fourier transformation from S(Q) to RDF is truncated at Q_{max}=326nm^{-1} for $Na_2O \bullet 2SiO_2$ glass and 450nm^{-1} for the other glasses(Misawa et al. 1980).

Marumo(1982) for $CaAl_2Si_2O_8$ composition, and Taylor and Brown(1980) for $NaAlSi_3O_8$ composition.

1-3-3 Neutron diffraction method

Misawa et al.(1980) measured structure factors of SiO_2 and $M_2O \bullet 2SiO_2$(M=Na, Li, $Li_{0.63}Na_{0.37}$) glasses using time of flight total neutron scattering with short wave length produced by an electron linear accelerator over a wide range of the scattering vector up to $Q(=4\pi\sin\theta/\lambda)\sim48A^{-1}$. Figure10 is a comparison of the RDF for the four glass samples. The RDFs are obtained by the Fourier transformation of the S(Q) values by truncating them at the values of Q_{max} of $326nm^{-1}$ for $Na_2O \bullet 2SiO_2$ glass and of 450nm-1 for the other glasses. Two sharp peaks around 0.16 and 0.26nm found commonly in all RDFs correspond to the nearest Si-O and O-O distance. The peak with negative sign observed at about 0.20nm in the RDF of the $Li_2O \bullet 2SiO_2$ glass is attributed to the distribution of Li-O ion pairs, because the sign of the scattering amplitude of Li nucleus is negative. The broad peak observed at about 0.24nm in the RDF of the $Na_2O \bullet 2SiO_2$ glass originated from the distribution of Na-O ion pairs. The RDF of the $(Li_{0.63}Na_{0.372})_2 \bullet 2SiO_2$ glass shows the two broad peaks around 0.20 and 0.24nm corresponding to the Li-O and Na-O ion pair correlation, respectively. The coordination numbers, bond distances and its fluctuation for Si-O, O-O pairs are summarized in table3. The coordination numbers for alkali ions have not been presented by their experiments. However, the effect of truncation value(Q_{max}) on the estimation of bond length and coordination numbers by means of RDF peak analysis was investigated. A longer bond length was obtained for $Q_{max}<20A^{-1}$. It is worth noting that in the situation for ordinary X-ray MoKα measurements, for which the $Q_{max}=15A^{-1}$, Si-O bond length would be estimated to be 0.01nm longer compared with the experiments of wider range of the scattering vector.

Gaskell et al.(1991) obtained double-difference scattering function, $S_{CaCa}(Q)$, which originate from Ca-Ca pairs in the $CaO\text{-}SiO_2$ glass, using a subtle trick of isotope ratio for ^{44}Ca. The Fourier transform of $S_{CaCa}(Q)$ is shown in figure11. Surprisingly, there is a strong correlation for Ca-Ca pairs. The first peak at 0.23nm is a ghost which arises from

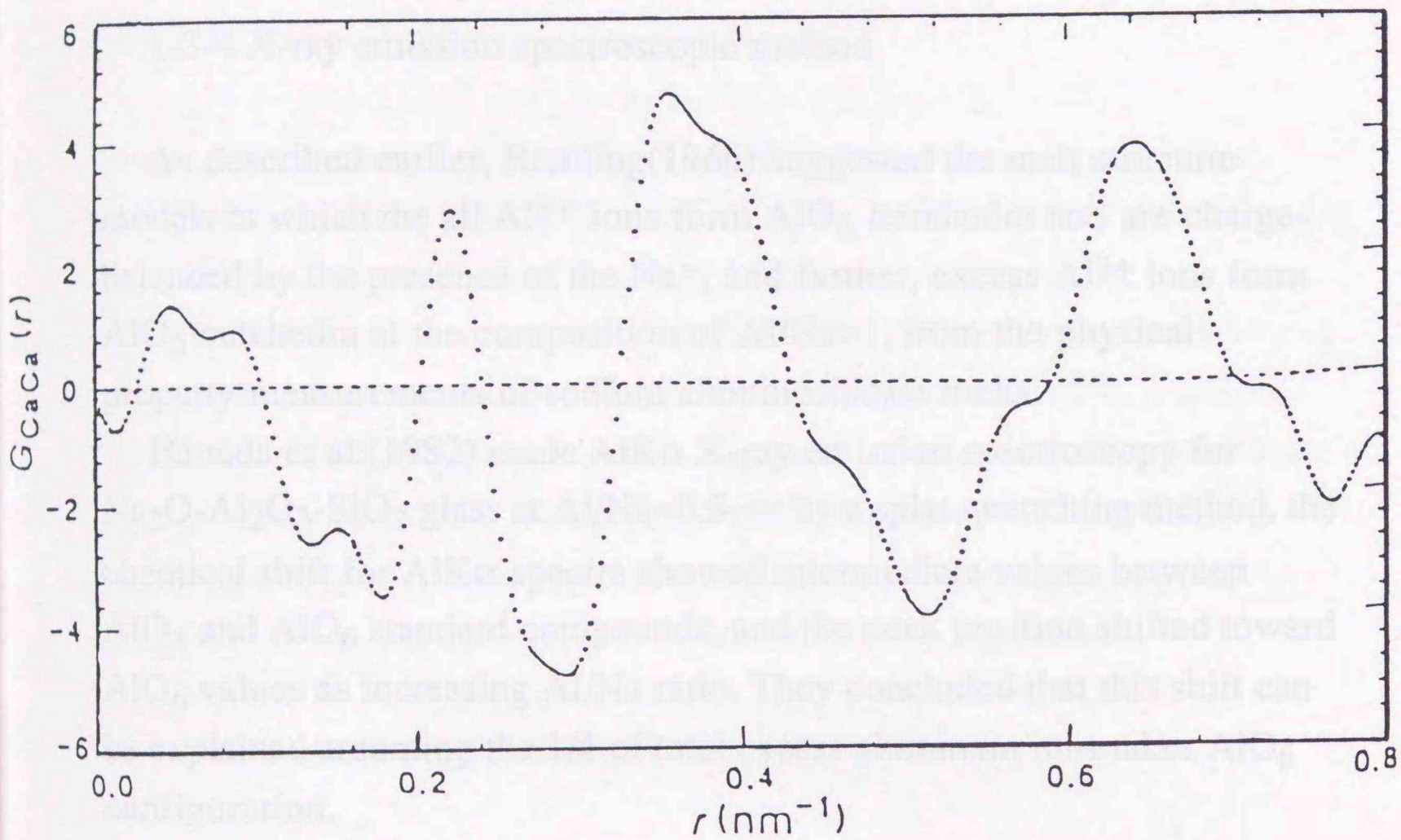

Figure 11. Fourier transform of the double-difference data $G_{CaCa}(r)$ obtained from smoothed $Q(S_{CaCa}(Q)-1)$ data of calcium-calcium pairs for the calcium silicate glass truncated at $Q_{max}=110nm^{-1}$(Gaskell et al., 1991).

inadequate subtraction of the first-difference signals. The strong peak at 0.38nm probably corresponds to the nearest Ca-Ca distance and is close to values found in c-$CaSiO_3$. The strong peak at 0.64nm probably corresponds to the second Ca-Ca neighbors. They concluded that these facts can be well explained by the cubic-close packing of the Ca ions in the silicate glass, which is seen in the crystal structure for c-$CaSiO_3$.

1-3-4 X-ray emission spectroscopic method

As described earlier, Riebling(1966) suggested the melt structure models in which the all Al^{3+} ions form AlO_4 tetrahedra and are charge-balanced by the presence of the Na^+, and further, excess Al^{3+} ions form AlO_6 octahedra at the composition of Al/Na>1, from the physical property measurements of sodium aluminosilicate melts.

Hanada et al.(1982) made AlKα X-ray emission spectroscopy for Na_2O-Al_2O_3-SiO_2 glass at Al/Na=0.5~∞ by a splat quenching method. the chemical shift for AlKα spectra showed intermediate values between AlO_4 and AlO_6 standard compounds, and the peak position shifted toward AlO_6 values as increasing Al/Na ratio. They concluded that this shift can be explained assuming the 1/4 of total excess aluminum ions takes AlO_6 configuration.

The X-ray emission spectroscopy gave in sight on the averaged local coordination state for the atoms in interest. However, nowadays, the coordination numbers of aluminum ion in glass can be more or less easily determined from ^{27}Al NMR spectroscopy.

1-3-5 Visible spectroscopy and optical basicity

Duffy and Ingram(1971) defined the optical basicity for the scale of basicity of the oxide glasses. It is obtained from the peak position of the ultra violet absorption by the Tl^+, Pb^{2+} and Bi^{3+} ions doped into the oxide glass. For the case of Pb^{2+}, the optical basicity Λ_{Pb} is defined as,

$$\Lambda_{Pb} = (60700-\nu)/(60700-29700), \qquad (3)$$

where 60700 is a wave number of isolated Pb^{2+}, 29700 is a wave number

for Pb^{2+} surrounded by the fully ionic oxide ions, that is, the wave number of Pb^{2+} in CaO crystal, ν is a wave number of Pb^{2+} in the sample. Λ_{Pb} represents the tendency of the lone pair electron donation by the oxide ion in the sample, which stands for the Lewis basicity. Λ_{Pb} of glass ranges from 0 to 1, whereas silicate glasses show Λ_{Pb} of 0.45~0.60.

Later, Duffy and Ingram(1976) defined a theoretical optical basicity using the basicity adjustment parameter γ as,

$$\Lambda_{th} = 1-\{(z_A r_A/2)(1-1/\gamma_A)+(z_B r_B/2)(1-1/\gamma_B)+.....), \quad (4)$$

where z is a valency of ion, r is a mole fraction of ion, respectively.

Optical basicities present convenient scale for basicities of glass, though their theoretical meaning of Λ_{th} is not clear. For example, the compositional dependence of the optical basicity depends on the variety of the metal cations used as a probe(Easteal and Morcom, 1979). Klein and Onorato(1980) compared values of Λ_{th} and Λ_{Pb} in sodium aluminosilicate glasses. They found that the Λ_{th} is almost independent of composition, while Λ_{Pb} decreases with increasing sodium oxide contents. Λ_{Pb} and Λ_{th} coincide only at the composition at the ratio Na/Al equals to 1.

1-3-6 X-ray photoelectron spectroscopy

X-ray photoelectron spectroscopy(XPS) has proved to be a powerful analyzing technique for distinguishing between bridging and non-bridging oxygen atoms in glasses. Smets and Lomen(1981) obtained O1s XPS spectra for Na_2O-SiO_2 glasses as shown in figure12. The intensity of the high kinetic energy electron increases with increasing sodium content. This transition is attributed to the NBOs in the silicate network. A shift of the photoelectron lines towards lower binding energies or higher kinetic energies corresponds to an increase of the electron density on the relevant atom. Hence the formal charge difference between the NBO atoms and BO atoms is reflected in an energy shift of the O1s transition in silicate glasses. In the spectra a third peak is attributed to the sodium KL_2L_{23} Auger transition. The amounts of NBOs estimated from the peak intensities increased linearly with increasing sodium oxide contents.

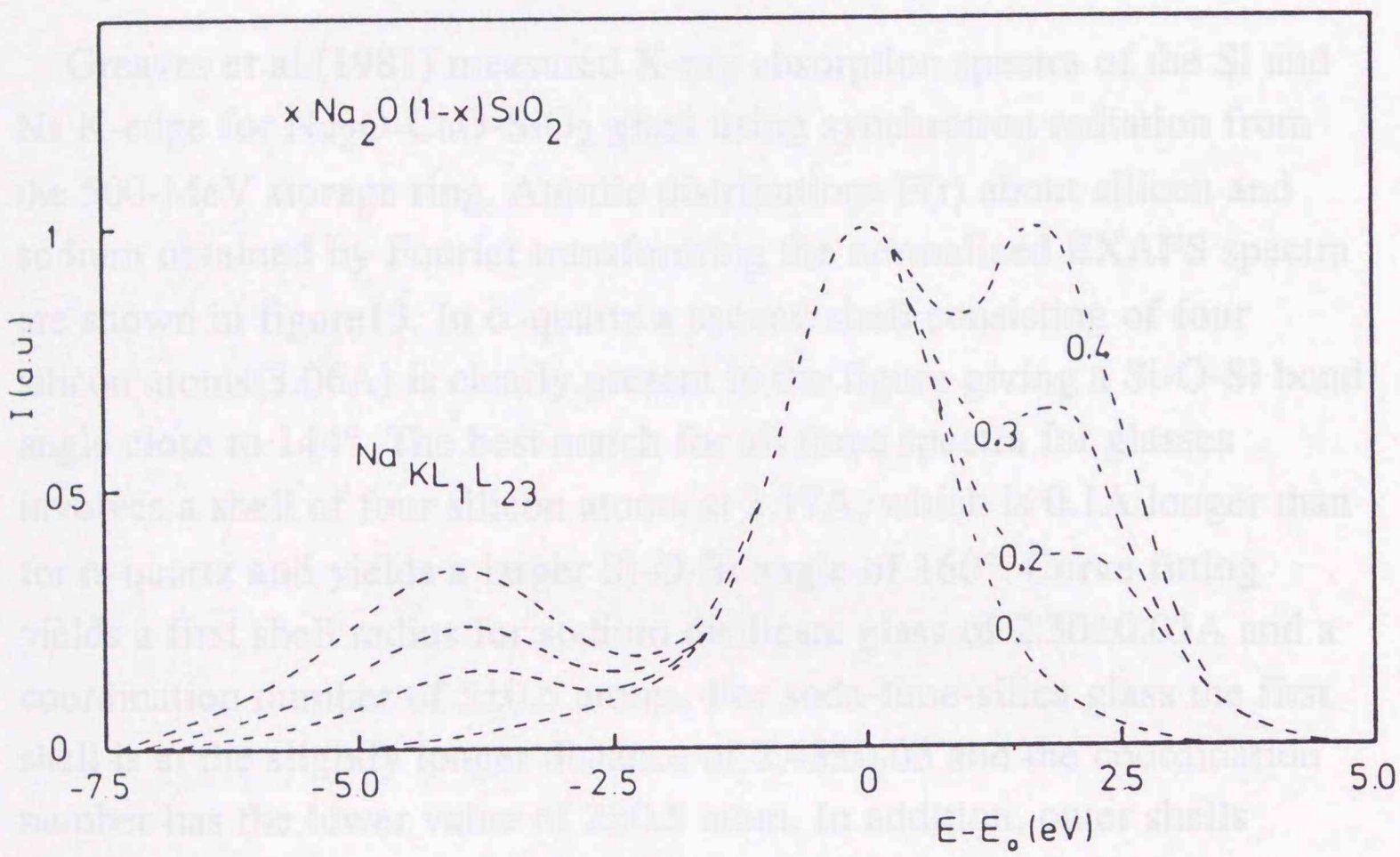

Figure 12. O1s XPS spectra of the sodium silicate glass(kinetic energy scale relative to the energy of the BOs)(Smets and Lommen, 1981).

On the other hand, some XPS measurements have been made on the sodium aluminosilicate glasses with Na/Al>1. Brückner et al.(1980) and Smets and Lommen(1981) concluded from O1s XPS spectra that numbers of NBO(N_{nbo}) goes zero even at the composition [Na]/[Al] > 0.7 and some AlO_6^{3-} might exist at the region of [Na]/[Al] = 1. On the other hand, Tasker et al.(1985) showed that N_{nbo} linearly changed with {[Na] - [Al]}/[Si], and goes zero at [Na]/[Al] = 1.

1-3-7 X-ray absorption spectroscopy

Greaves et al.(1981) measured X-ray absorption spectra of the Si and Na K-edge for Na_2O-CaO-SiO_2 glass using synchrotron radiation from the 500-MeV storage ring. Atomic distributions F(r) about silicon and sodium obtained by Fourier transforming the normalized EXAFS spectra are shown in figure13. In α-quartz a second shell consisting of four silicon atoms(3.06A) is clearly present in the figure giving a Si-O-Si bond angle close to 144°. The best match for all three spectra for glasses involves a shell of four silicon atoms at 3.17A, which is 0.1A longer than for α-quartz and yields a larger Si-O-Si angle of 160°. Curve fitting yields a first shell radius for sodium disilicate glass of 2.30±0.03A and a coordination number of 5±0.5 atoms. For soda-lime-silica glass the first shell is at the slightly longer distance of 2.43±0.03 and the coordination number has the lower value of 2±0.5 atom. In addition, outer shells amounting to an extra four oxygen atoms have been added. This finding is well agrees with the fact that the bond length and coordination numbers of $Na_2O \bullet SiO_2$ and α-$Na_2O \bullet 2SiO_2$ crystal is 2.4 and 5, respectively, whereas the coordination numbers of many multi-component crystals within the spheres of 2.5A is 2~3.

On the other hand, MacKeown(1985) observed Na K-edge EXAFS spectra for sodium aluminosilicate glasses. They concluded that the coordination number of sodium in the whole composition range was obtained to be 5.1~7.6.

1-3-8 Molecular dynamics calculations

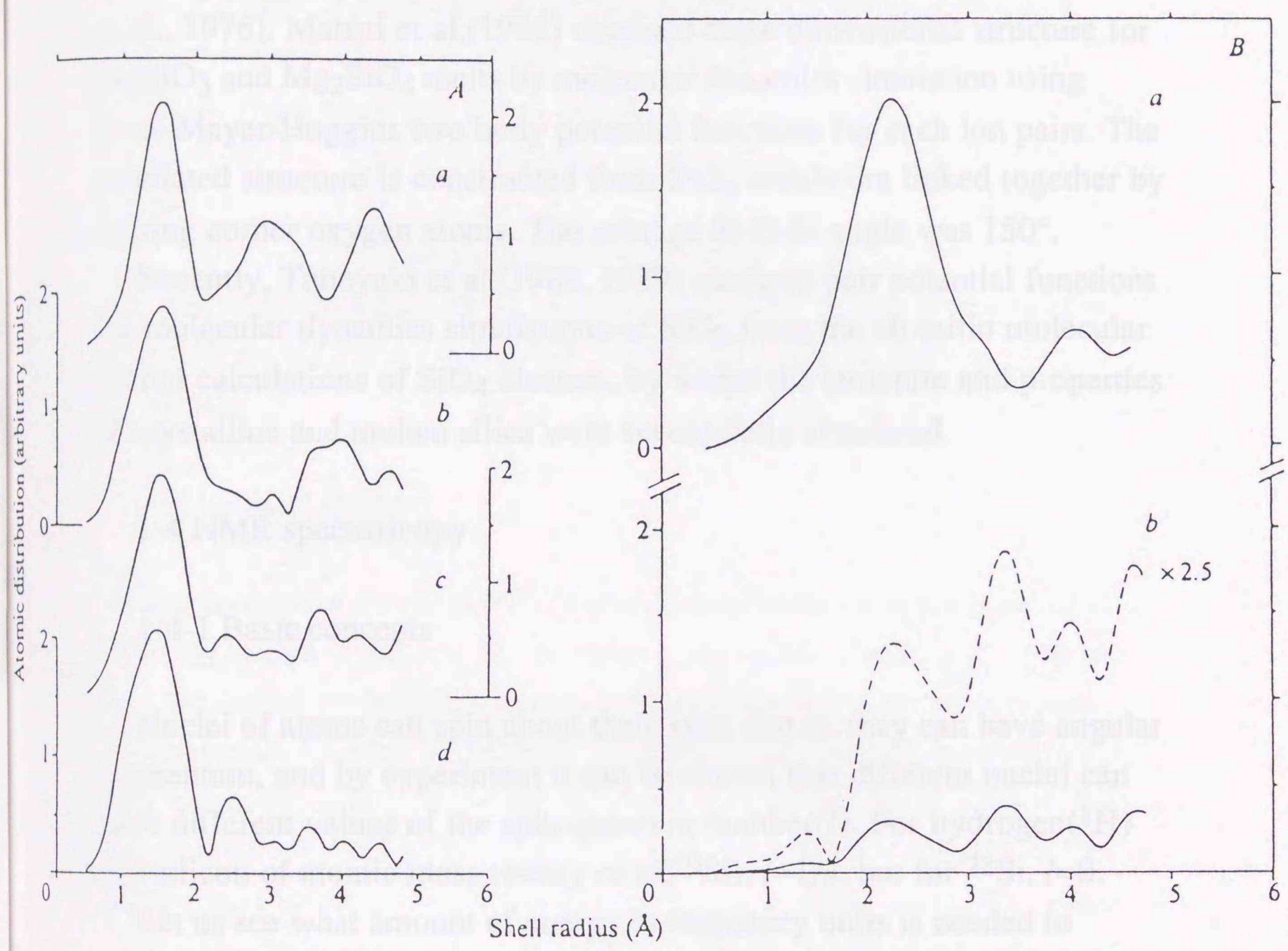

Figure 13. *A*, Atomic distributions F(r) about silicon for; *a*, α-quartz; *b*, silica glass; *c*, sodium disilicate glass; *d*, soda-lime-silica glass. These were obtained by Fourier transforming the normalized EXAFS spectra above the silicon K-edge(6.75A).
B, F(r) about sodium for: *a*, sodium disilicate glass; *b*, soda-lime-silica glass(Greaves et al., 1981).

Molecular dynamics calculations can also be used to describe anion and cation distributions in silicate melts. The application of this method to a molten salts is based on the investigations by Woodcock et al.(Woodcock et al., 1976). Matsui et al.(1982) obtained three dimensional structure for $MgSiO_3$ and Mg_2SiO_4 melts by molecular dynamics simulation using Born-Mayer-Huggins two body potential functions for each ion pairs. The simulated structure is constructed from SiO_4 tetrahedra linked together by sharing corner oxygen atoms. The average Si-O-Si angle was 150°.

Recently, Tuneyuki et al.(1988, 1989) obtained pair potential functions for molecular dynamics simulations of SiO_2 from the ab-initio molecular orbital calculations of SiO_4 clusters, by which the structure and properties of crystalline and molten silica were successfully simulated.

1-4 NMR spectroscopy

1-4-1 Basic concepts

Nuclei of atoms can spin about their axis; that is, they can have angular momentum, and by experiment it can be shown that different nuclei can have different values of the spin quantum number(I). For hydrogen(^1H) and silicon of atomic mass twenty-nine(^{29}Si), I=1/2, but for ^{28}Si, I=0.

Let us see what amount of energy in frequency units is needed to induce a transition between energy levels. The quantized angular momentum p along the direction of the magnetic field z is expressed in units of $h/2\pi$, where h is Planck's constant, as:

$$p=mh/2\pi \text{(if } I=1/2,\ m=1/2 \text{ or } -1/2). \qquad (5)$$

The magnetic moment μ is related to p by a proportionality constant γ, the gyromagnetic ratio. Thus,

$$\mu=\gamma p. \qquad (6)$$

Hence

$$\mu=\gamma mh/2\pi. \qquad (7)$$

Now the energy of interaction, E, between the magnet and nucleus

corresponding to the torque operating to align the spinning nucleus with the magnetic field is given by the product of the strength of the magnetic field H_0 and the magnetic moment μ of the nucleus. Thus,

$$E=-\mu H_0. \qquad (8)$$

Nuclear magnetic resonance is the phenomenon by which transitions between energy states are brought about by applying electromagnetic radiation. Now electromagnetic radiation of radiofrequency ν has energy ΔE given by $h\nu$. Thus at resonance, i.e. when energy is absorbed by the nuclei,

$$\nu = -\gamma H_0(m_2-m_1)/2\pi. \qquad (9)$$

The frequency required for an ordinary ^{29}Si NMR experiment for the transition $m_2=1/2$ to $m_1=-1/2$ at H_0=4.7Tesla magnetic field is 39.76MHz.

1-4-2 Chemical shifts

The determination of chemical shift is the principal application of NMR by which structural information is obtained. The primary reason why the nuclei of the same atomic species in different intramolecular environments resonate at different frequencies is because the electrons around a nucleus alter the magnetic field experienced by it. That is, the actual magnetic field at the nucleus is somewhat different to that of he magnet by a shielding factor(σ) where $H_{(nucleus)} = H_0 - \sigma H_0$. The value of σ cannot be greater than 1; indeed, it is much less than this, since it is a molecular property rather than a quantity contrived in the laboratory. In principle, therefore, H_0 must be known accurately to measure s. The actual value of s depends on the orientation of the molecule relative to the field. For molecules in rapid motion, or by means of magic-angle-sample spinning(MAS), σ is averaged out so that only one isotropic value(σ_{iso}) is observed.

The strength of the magnetic field may fluctuate while making a measurement. Thus establishing a value for s is difficult. In addition, the value of the resonance frequency is magnetic field dependent. It is wise, therefore, to have a measure which is based on difference from a standard

and is independent of magnetic field and can therefore be measured on different machines. This measurement is the chemical shift, and is defined as:

$$d = (\nu_s - \nu_r)/\nu_r \times 10^6, \qquad (10)$$

where ν_s and ν_r are the frequencies of the sample and the reference.

1-4-3 Application of NMR to silicate glasses and melts

A great deal has been learned about silicate glasses and liquids by ^{29}Si NMR studies not described here, as well as by NMR on other nuclei(particularly ^{11}B, ^{19}F and ^{27}Al) over more complex compositions. Much of these works has been reviewed previously(Bray and Holupka, 1985; Dupree et al., 1986; Kirkpatrick, 1988; Eckert, 1990). The information which can be derived from ^{29}Si NMR studies are summarized as follows.

(1). For crystalline silicates, the isotropic chemical shifts vary systematically with silicate structure; thus a silicon nucleus is deshielded (and its chemical shift value becomes less negative) as the numbers of attached bridging oxygen (BO) atoms decrease. The Si atoms surrounded by different numbers of BO atoms are identified as separated peaks in ^{29}Si NMR spectra and commonly distinguished with notation such as Q_n's

(2). Glassy or liquid silicates possess chemical shifts of the similar range as those observed in crystalline silicates having the identical composition. The structural units of glasses or liquids are possibly represented by Q_n units similar to those deduced from the spectra of corresponding crystalline materials.

(3). ^{29}Si chemical shifts are sensitive to the variation of Si-O bond length and Si-O-Si bridging angles as well as to changes of second and third neighbor environments. The relationships between the chemical shift and bridging angle or group electronegativity have been considerably discussed.

^{29}Si NMR spectroscopy has recently been used to accurately count the abundance of Q species in some simple glass compositions. Early data

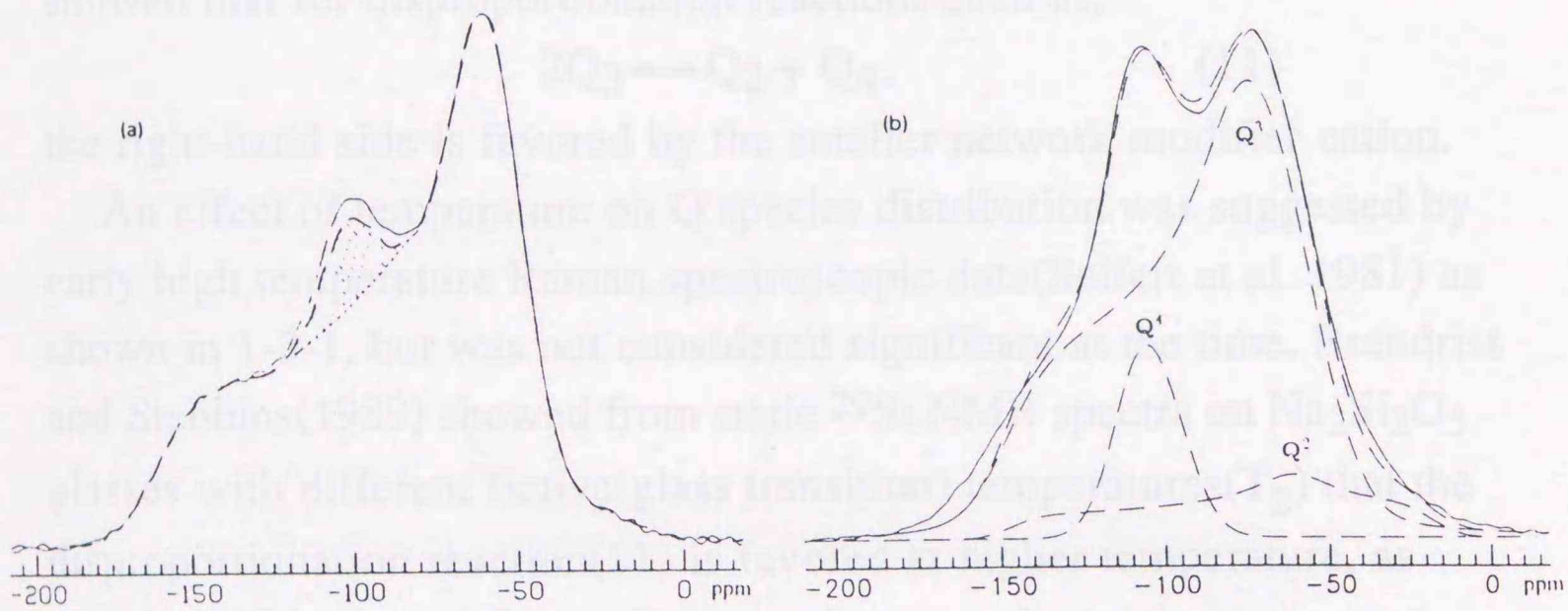

Figure 14. Static ^{29}Si NMR spectra for (a) $Na_2Si_2O_5$ and (b) $Li_2Si_2O_5$ glasses.(Brandriss and Stebbins, 1988; Stebbins and Farnan, 1989). In (a), the cross-hatched area shows the peak resulting from a non-stoichiometric amount of Q_4 sites in an annealed sample with a relatively low fictive temperature. The upper curve in (a) shows the increased abundance of this species in a fast-quenched sample with a higher fictive temperature.

from magic-angle-spinning(MAS) experiments were often ambiguous, with single noisy peaks that were fitted with one to five Gaussian peaks, the number depending on interpretation. The detailed distributions of Q_n species could not be determined, although the distinct difference from statistical distributions are realized.

Recently, as shown in figure14, Brandriss and Stebbins(1988) showed that the static spectra can, for some compositions, be more informative. Here, results for $Li_2Si_2O_5$ and $Na_2Si_2O_5$ glass are compared. The most obvious difference is that the narrow central peak in these spectra, which can be attributed to the relatively symmetrical Q_4 site, is considerably more intense in the Li glass(~11% vs. 6% of the area). They clearly showed that for disproportionation reactions such as,

$$2Q_3 \leftrightarrow Q_2 + Q_4, \qquad (11)$$

the right-hand side is favored by the smaller network modifier cation.

An effect of temperature on Q species distribution was suggested by early high temperature Raman spectroscopic data(Seifert et al. 1981) as shown in 1-3-1, but was not considered significant at the time. Brandriss and Stebbins(1989) showed from static ^{29}Si NMR spectra on $Na_2Si_2O_5$ glasses with different fictive(glass transition) temperatures(T_g) that the disproportionation reaction(11) is favored at higher temperature, as expected if mixing of the species contributes to the total entropy.

However, the systematic dependence of the distributions of Q_n species over wide composition range have not thoroughly been explored.

On the other hand, NMR measurements at high temperature have been made since at least 1964 to study the structure and dynamics of liquid and solid metals, molten salts, ionic conductors, etc.(for a review see Stebbins, 1991). In figure15, data are shown for $K_2Si_4O_9$ liquid(Farnan and Stebbins, 1990). Just above T_g, its static ^{29}Si spectrum is again composed of two major components, an asymmetric uniaxial powder pattern for the Q_3 sites and a narrow Gaussian peak for the Q_4 sites, each of which comprises about half of the total. When the temperature is increased further, these peaks both begin to narrow, as structural motion averages out the orientational effects that give rise to the broad static lines.At high temperature, however, instead of two distinct peaks, as would be expected

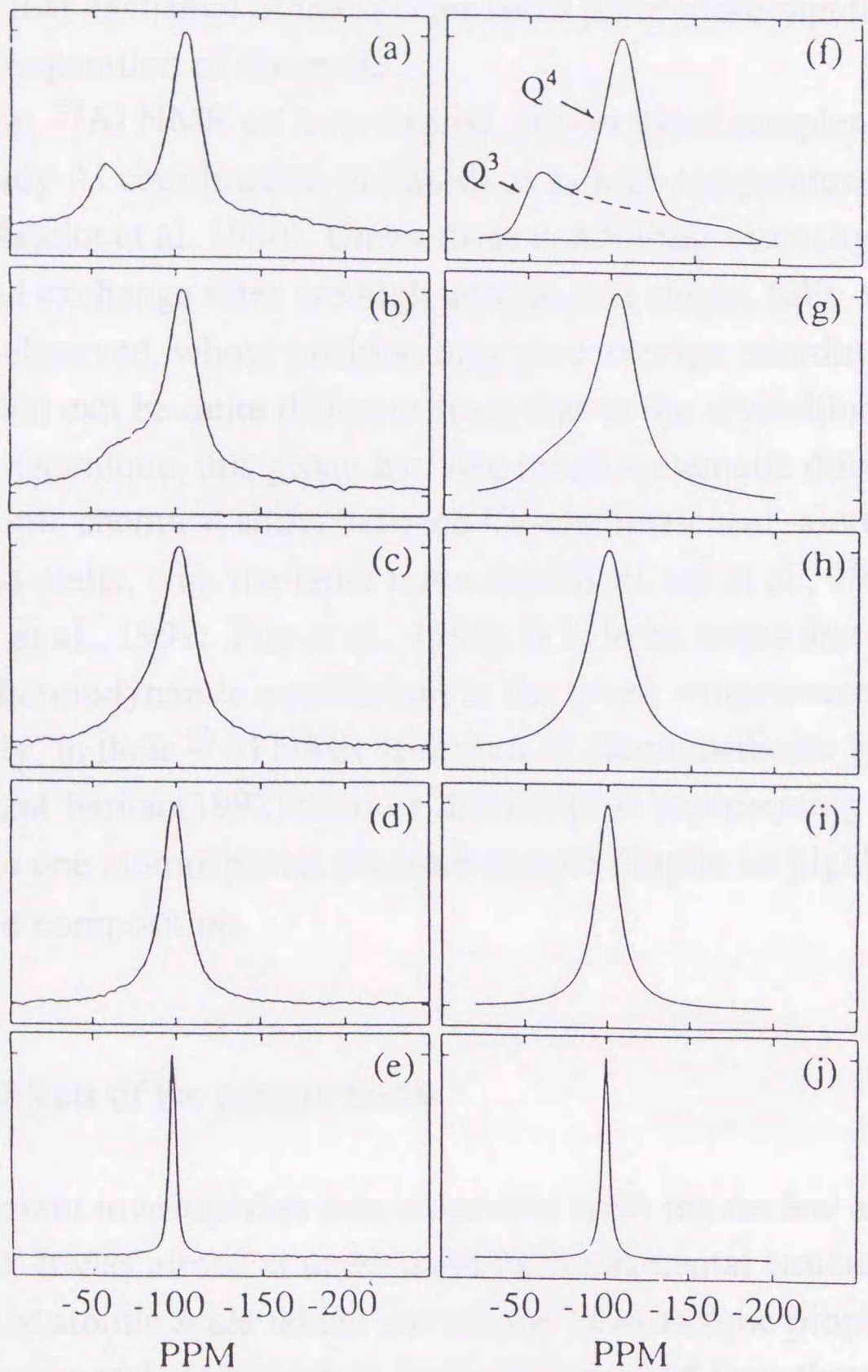

Figure 15. Static ^{29}Si NMR spectra for $K_2Si_4O_9$ glass and liquid (left) and computer simulations of multi-site exchange (right). Temperatures, in °C:(a)697; (b)774; (c)800; (d)847; (e)997. Exchange frequencies in kHz: (f)2; (g)10; (h)25; (i)50; and (j);500. In (f), powder patterns for Q_3 and Q_4 species are indicated(Farnan and Stebbins, 1990).

if the lifetimes of the Q species were long, only a single peak is observed, indicating that exchange of the species takes place more rapidly than the frequency separation of the peaks.

Recently, ^{27}Al NMR on laser-heated, gas-levitated samples has been used to study Al coordination in liquids at as high temperatures as 2100°C(Massiot et al. 1990). Under these conditions, viscosity is low enough and exchange rates are high enough that single, fully averaged peaks are observed, whose position may give average coordination numbers that can be quite different from that in the crystalline phase. Using this technique, this group has also noted systematic differences in ^{27}Al isotropic chemical shifts between Ca-aluminate and -aluminosilicate glasses and melts, with the latter more shielded(Coté et al., 1991; McMillan et al., 1991; .Poe et al., 1991). It is to be noted that the sample is not in thermodynamic equilibrium at the given temperatures.

Recently, in their ^{27}Al NMR spectrum of aluminosilicate glass, Stebbins and Farnan(1992) found a distinct peak representing ~1-3% AlO_6 in an one atomospheric pressure sample despite its highly peralkaline composition.

1-5 Subjects of the present thesis

The present investigation was motivated from the review above mentioned. It was aimed at understanding fundamental structures and processes at atomic scale which govern the macroscopic properties of silicate glasses and melts such as their viscosity and their thermodynamic quantities.

In this thesis, results of investigations on the structure and dynamics of silicates and boron oxide are discussed in relation with the effect of temperature and composition. The Q_n distribution and the local structure around aluminum and sodium in silicate glasses and melts are described. Also, the dynamics of the structural units constructing network is studied by means of NMR line shape and relaxation time measurements

Studies of glass structure have been expected to provide the structure

of the liquid state at temperature of transition from glass to liquid. On the other hand, the direct observations on the liquid state was deadly desired on the melts and the melt-glass transition temperature range. The structural change induced by the liquid to glass transition is a dynamical one, and thus may be closely related to bulk dynamical properties.

In chapter 2, ^{29}Si MAS NMR of binary alkali silicate glasses are described. Special attention was focused on the composition effect of the equilibrium reaction between Q_n species,

$$2Q_n \leftrightarrow Q_{n-1} + Q_{n+1} \quad (n=3,2,1). \quad (12)$$

The compositional dependence of the Q_n distribution has been fully clarified for Li-, Na- and K-silicate glass systems. A proposed thermodynamic model was adopted to interpret the NMR results and to successively explain both of Q_n distributions and thermodynamic activities of Na_2O. Furthermore, the compositional and temperature effects on the binary sodium silicate melt structure is reproduced.

In chapter 3, ^{29}Si MAS NMR investigation of Na_2O-Al_2O_3-SiO_2 join are described. A detailed analysis about the compositional dependence of the Q_n distribution is made. The coordination environments of aluminum ion are interpreted in terms of the acid-base concept.

In chapter 4, a development of high temperature-high resolution probe and its application to sodium silicate melts up to 1200°C are described. Here, they have been applied over a temperature range of 1200°C to silicate, aluminosilicate and borate systems with different nuclei, e.g. ^{11}B, ^{23}Na and ^{29}Si. The ^{29}Si NMR chemical shift and line shape are analysed in terms of the structure and dynamics of this system.

In chapter 5, a high temperature ^{23}Na NMR investigation of the coordination numbers of Na ion in silicate melts is described. ^{23}Na NMR chemical shift of silicates and alunimosilicates in both the crystalline and liquid states are observed. The coordination number of Na ion is estimated to be 6~7 independent of the melt composition.

In chapter 6, high temperature ^{11}B NMR line shape and relaxation time measurements on B_2O_3 are described. The reorientational correlation time for motion of ^{11}B nucleus is interpreted by the α- and β-processes of the glass forming materials.

references for chapter1

Bottinga,Y.(1981)
Thermodynamic modelling of silicate melts in:*Thermodynamics of Minerals Melts* (ed. Newton,R.C. et.al) Springer-Verlag,Berlin Heisenburg pp.207-245

Brandriss,M.E. and Stebbins,J.F.(1988)
Effects of temperature on the structures of silicate liquids: ^{29}Si NMR results
Geochim.Cosmochim.Acta, **52**, 2659-2670

Brawer,S.A. and White,W.B.(1975)
Raman spectroscopic investigation of the structure of silicate glass (I). The binary alkali silicates.
J.Chem.Phys., **63**, 2421-2432

Brawer,S.A. and White,W.B.(1977)
Raman spectroscopic investigation of the structure of silicate glass (II). Soda-alkaline earth-alumina ternary and quaternary glasses
J.Non-crystalline Solids, **23**, 261-278

Bray,P.J. and Holupka,E.J.(1985)
The potential of NMR techniques for studies of the effects of thermal history on glass structure
J.Non-cryst.Solids, **71**, 411-428

Brückner,R, Chun,H.-U., Goretzki,H., and Sammet,M.(1980)
XPS measurements and structural aspects of silicate and phosphate glasses.
J.Non-Crystalline Solids, **42**, 49-60

Coté,B., Massiot,D., Taulelle,F., and Coutures,J.P.(1991)
NMR spectroscopy at very high temperatures
4th Silicate Melt Workshop, Le Howald, March 19-23, 1991(abstract)

Day,D.E. and Rindone,G.E.(1962a)
Properties of Soda Aluminosilicate Glasses:II Refractive Index, Density,Molar Refractivity,and Infrared Absorption Spectra
J.Am.Ceramic.Soc., **45**, 489-496

Day,D.E. and Rindone,G.E.(1962b)
Properties of Soda Aluminosilicate Glasses:II
Internal Friction
J.Am.Ceramic.Soc., **45**, 496-504

De Jong,B.H.W.S. , Schramm,C.M. , Parziale,V.E.(1983)
Polymerization of silicate and aluminate tetrahedra in glasses,melts, and aqueous solutions-IV. Aluminium coordination in glasses and aqueous solutions and comments on the aluminum avoidance principle
Geochim.Cosmochim.Acta, **47**, 1223-1236

Dorfeld, W.G.(1988)
Structural thermodynamics of alkali silicate glasses
Phys.Chem.Glasses, **29**, 179-186

Duffy,J.A. and Ingram,M.D.(1971)
J.Am.Chem.Soc., **93**, 6448

Duffy,J.A. and Ingram,M.D.(1976)
An interpretation of glass chemistry in terms of the optical basicity concept
J.Non-cryst.Solids, **21**, 373-410

Dupree,R., Holland,D., and Williams,D.S.(1986)
The structure of binary alkali silicate glasses
J.Non-cryst.Solids, **81**, 185-200

Easteal,A.J. and Morcom,A.T.(1979)
J.Non-cryst.Solids, **34**, 29

Eckert,H.(1990)
Structural concepts for disordered inorganic solids. Modern NMR approaches and strategies
Ber.Bunsenges.Phys.Chem., **94**, 1062-1085

Eliezer,N., Howwald,R.A., Marinkovic,M., and Elieezer,I.(1978)
Vapor pressure measurements, thermodynamic parameters, and phase diagram in the system potassium oxide-silicon oxide at high temperature
J.Phys.Chem., **82**, 1021-1028

Emerson,J.F., Stallworth,P.E., and Bray,P.J.(1989)
J.Non-cryst.Solids, **113**, 253

Engelhardt,G., Nofz,M., Forkel,K., Wihsmann,F.G., Mägi,M., Samoson,A., and Liippmaa,E.(1985)
Structural studies of calcium aluminosilicate glasses by high resolution solid state ^{29}Si and ^{27}Al magic angle spinning nuclear magnetic resonance
Phys.Chem.Glasses, **26**, 157-165

Farnan,I. and Stebbins,J.F.(1990)
A high temperature ^{29}Si NMR investigation of solid and molten silicates
J.Am.Chem.Soc., **112**, 32-39

Fenn,P.M.(1977)
The nucleation and growth of alkali feldspars from hydrous melts
Canadian Mineral., **15**, 135-161

Fleet,M.E., Herzberg,C.T., Henderson,G.S., Crozier,E.D., Osborne,M.D., and Scarfe,C.M.(1984)
Coordination of Fe,Ga,Ge in high pressure glasses by Mössbauer, Raman and X-ray absorption spectroscopy,and geological implications
Geochim.Cosmochim.Acta, **48**, 1455-1466

Galant,E.I.(1959)
The structure of Glass(Translated from Russian) Consultants Bureau:New York, 1960, Vol.2, 451, Proceedings of the Third All-Union Conference on the Glassy State, Leningrad

Gaskell,P.H., Eckersley,M.C., Barnes,A.C., and Chieux,P.(1991)
Medium-range order in the cation distribution of a calcium silicate glass.
Nature, **350**, 675

Gohshi,Y., Hukuo,Y. and Hori,K.(1972)
Spectrochim. Acta, **B27**, 135

Greaves,G.N., Fontaine,A., Lagarde,P., Raoux.D., and Gurman,S.J.,(1981)
Local structure of silicate glasses.
Nature, **293**, 611-616

Grimmer,A.-R. et. al(1984)
High resolution solid-state ^{29}Si nuclear magnetic resonance spectroscopic studies of binary alkali silicate glasses
Phys.Chem.Glasses, **25**, 105-109

Hamilton,D.L.(1986)
The absence of 6-fold coordinated Al in jadeite melt near the jadeite liquidus.
Geochim.Cosmochim.Acta, **50**, 123-124

Hanada,T., Aikawa,T., and Soga,N.(1982)
Coordination of aluminum in amorphous sodium aluminosilicate films.
J.Non-cryst.Solids, **50**, 397-405

Hanna,R and Su,G-J.(1964)
Infrared Absorption Spectra of Sodium Silicate Glasses from 4 to 30μ
J.Am.Ceramic.Soc., **47**, 597-601
Imaoka,M.(1981)
Bull.Seramics Soc.Japan(in Japanese), **16**, 20-27
Imaoka,M., Hasegawa,H., and Yasui,I.(1983)
X-ray diffraction study of the structure of silicate glasses. Part2. Alkali disilicate glasses
Phys.Chem.Glasses, **24**, 72-78
Kirkpatrick,R.J.(1988)
MAS NMR spectroscopy of minerals and glasses. In: *Spectroscopic Methods in Mineralogy and Geology*. Mineralogical Society of America, (ed.) Hawthorne,F.C., pp341-403
Klein,R.M. and Onorato,P.I.K.(1980)
Phys.Chem.Glasses, **21**, 199
Kushiro,I.(1976)
Changes in viscosity and structure of melt of $NaAlSi_2O_6$ composition at high pressure
J. Geophys. Res., **81**, 6347-6350
Kushiro,I.(1983)
Effect of pressure on the diffusivity of network-forming cations in melts of jadeitic compositions
Geochim.Cosmochim.Acta, **47**, 1415-1422
Lacy,E.D.(1963)
Aluminum in glasses and melts
Phys.Chem.Glasses, **4**, 234-238
Lowenstein,W.(1954)
The distribution of Aluminum in the tetrahedra of silicates and aluminates
Am.Mineral., **39**, 92-96
Maekawa,T., Kikuchi,N., Sumita,S., and Yokokawa,T.(1978)
X-ray fluorescence spectroscopy of binary silicate glasses
Bull.Chem.Soc.Jpn., **51**, 780-782
Maekawa,H., Maekawa,T., Kawamura,K, and Yokokawa.T(1991)
The structural groups of alkali silicate glasses determined from ^{29}Si MAS-NMR.
J.Non-cryst.Solids, **127**, 53-64
Massiot,D., Taullele,F., and Coutures,J.P.(1990)
Structural diagnostic of high temperature liquid phases by ^{27}Al NMR
Colloq.Phys., **51**, C5-425-431
Matson,D.W. and Sharma,K(1985)
Structures of sodium alumino- and gallosilicate glasses and their germanium analogs.
Geochim.Cosmochim.Acta, **49**, 1913-1924
McMillan,P., Piriou,B. and Navrotsky,A.(1982)
A raman spectroscopic study of glasses along the joins silica-calcium aluminate,silica-sodium aluminate,and silica-potassium aluminate
Geochim.Cosmochim.Acta, **46**, 2021-2037

McMillan,P.F., Poe,B.T., Coté,B., Massiot,D., and Coutures,J.P.(1991)
^{27}Al NMR linewidth for SiO_2-Al_2O_3 liquids: structural relaxation and a mechanism for viscous flow in high silica aluminosilicate liquids and glasses
Eos(Trans.Am.Geophys.Union), **72**, 572(abstract)

Matsui,M., Kawamura,K., and Syono,Y.(1982)
Molecular dynamics calculations applied to silicate system: Molten and vitreous $MgSiO_3$ and Mg_2SiO_4 under low and high pressures.
(ed.)S.Akimoto and M.H.Manghnani, Center Academic Pub. Tokyo/Dordrecht, pp511-524

Matsui,M., Kawamura,K.(1983)
Computer simulation of structure of silicate melts and glasses,
in "Material Science of the Earth's Interior"
(ed.)I.Sunagawa, Terra Sci. Pub. Co., 3-23

McKeown,D.A., Waychunas,G.A., and Brown Jr,G.E.(1985)
EXAFS and XANES study of the local coordination environment of sodium in a series of silica-rich glasses and selected minerals within the Na_2O-Al_2O_3-SiO_2 system.
J.Non-cryst.Solids, **74**, 325-348

Misawa,M., Price,D.L., and Suzuki,K.(1980)
The short-range structure of alkali disilicate glasses by pulsed neutron total scattering
J.Non-cryst.Solids, **37**, 85-97

Morikawa,H., Miwa,S., Miyake,M., Marumo,F., and Sata,T.(1982)
Structural analysis of SiO_2-Al_2O_3 glasses.
J.Am.Ceram.Soc., **65**, 78-81
Morikawa,H., Miwa,S., Miyake,M., Marumo,F., and Sata,T.(1982)
Structural analysis of SiO_2-Al_2O_3 glasses.
J.Am.Ceram.Soc., **65**, 78-81
Mozzi,R.L. and Warren,B.E.(1969)
The structure of vitreous silica
J.Appl.Cryst., **2**, 164-172

Mysen,B.O., Virgo,D. and Scarfe,C.M(1980)
Relations between the anionic structure and viscosity of silicate melts - a Raman spectroscopic study
Am.Mineral., **65**, 690-710

Mysen,B.O., Finger,L.W., Seifert,F.A., and Virgo,D.(1982a)
Curve fitting of Raman spectra of silicate glasses
Am. Mineral., **67**, 686-695

Mysen,B.O., Virgo,D., and Seifert,F.A.(1982b)
The structure of silicate melts: Implications for chemical and physical properties of natural magma
Reviews of Geophysics, **20**, 353-383

Mysen,B.O.(1988)
"Structure and properties of silicate melts" in *Developments in Geochemistry 4*, Elsevier, New York

Mysen,B.O. and Franntz,D.(1992)
Raman spectroscopy of silicate melts at magmatic temperatures:Na_2O-SiO_2, K_2O-SiO_2 and Li_2O-SiO_2 binary compositions in the temperature range 25-1475°C
Chem.Geol., **96**, 321-332

Navrotsky,A., Hon,R., Weill,D.F., and Henry,D.J.(1980)
Thermochemistry of glasses and liquids in the systems $CaMgSi_2O_6$-$CaAl_2Si_2O_8$-$NaAlSi_3O_8$, SiO_2-$CaAl_2Si_2O_8$-$NaAlSi_3O_8$ and SiO_2-Al_2O_3-CaO-Na_2O
Geochim.Cosmochim.Acta, **44**, 1409-1423

Navrotsky,A., Geisinger,K.L., McMillan,P., and Gibbs,G.V.(1985)
The tetrahedral framework in glasses and melts-influences from molecular orbital calculations and implications for structure, thermodynamics, and physical properties.
Phys.Chem.Minerals, **11**, 284-298

Ohtani,E., Taulelle,F, and Angell,C.A.(1985)
Al^{3+} coordination changes in liquid aluminosilicates under pressure
Nature, **314**, 78-81

Okuno,M and Marumo,F(1982)
The structure of anorthite and albite melts.
Mineral.J., **11**, 180-196

Poe,B.T., McMillan,P.F., Angell,C.A., Coté,B., Massiot,D., and Coutures,J.P. (1991)
^{27}Al NMR spectroscopy and molecular dynamics simulations of SiO_2-Al_2O_3 and CaO-Al_2O_3 liquids
Eos(Trans.Am.Geophys.Union), **72**, 572

Richet,P.(1984)
Viscosity and configurational entropy of silicate melts
Geochim.Cosmochim.Acta, **48**, 471-483

Richet,P., Bottinga,Y., and Téqui,C.(1984)
Heat capacity of sodium silicate liquids
Commun.Am.Ceram.Soc., C-6-8

Riebling,E.F.(1966)
Structure of sodium aluminosilicate melts containing at least 50 mole% SiO_2 at 1500°C
J.Chem.Phys., **44**, 2857-2865

Rigden,S.M., Ahrens,T.J., and Stolper,E.M.(1984)
Densities of liquid silicates at high pressures
Science, **226**, 1071-1073

Sakka,S and MacKenzie,J.D.(1971)
Relation between apparent glass transition temperature and liquidus temperature for inorganic glasses
J.Non-cryst.Solids, **6**, 145-162

Sakka,S and Matusita,K.(1976)
J.Non-cryst.Solids, **22**, 57

Seifert,F., Mysen,B.O., and Virgo,D(1982)
Three-dimensional network structure of quenched melts(glass) in the system SiO_2-$NaAlO_2$,SiO_2-$CaAl_2O_4$ and SiO_2-$MgAl_2O_4$
Am.Mineral., **67**, 696-717

Shimizu,N. and Kushiro,I.(1984)
Diffusivity of Oxygen in jadeite and diopside melts at high pressures
Geochim.Cosmochim.Acta, **48**, 1295-1303

Smets,B.M.J and Lommen,T.P.A(1981)
The structure of germanosilicate glasses, studied by X-ray photoelectron spectroscopy.
J.Non-crystalline Solids, **46**, 21-32

Smets,B.M.J and Lommen,T.P.A(1982)
The structure of glasses and crustalline compounds in the system $PbO-SiO_2$, studied by X-ray photoelectron spectroscopy.
J.Non-crystalline Solids, **48**, 423

Stebbins,J.F., Murdoch,J.B., Schneider,E, Carmichael,I.S.E., and Pines,A.(1985)
A high-temperature high-resolution NMR study of ^{23}Na ^{27}Al and ^{29}Si in molten silicates.
Nature, **314**, 250-252

Stebbins,J.F.(1987)
Identification of multiple structural species in silicate glasses by ^{29}Si NMR
Nature, **330**, 465-467

Stebbins,J.F.(1988)
Effects of temperature and composition on silicate glass structure and dynamics:Si-29 NMR results
J.Non-cryst.Solids, **106**, 359-369

Stebbins,J.F.(1991)
Nuclear magnetic resonance at high temperature
Chem.Rev., **91**, 1353-1373

Stebbins,J.F. and Farnan,I.(1992)
Effects of high temperature on silicate liquid structure: a multinuclear NMR study
Science, **255**, 586-589

Stein,D.J., Stebbins,J.F., and Carmichael,I.S.E.(1986)
Density of molten sodium aluminosilicates
J.Am.Ceram.Soc., **69**, 396-399

Tasker,G.W, Uhlmann,D.R., Onorato,P.I.K., Alexander,M.N., and Struck,C.W.(1985)
Structure of sodium aluminosilicate glasses : X-ray photoelectron spectroscopy
Journal de Physique, **C8**, 273-280

Taylor,M.(1979)
A quasi-crystalline model for interpretation of radial distribution functions: Theory and experimental confirmation
J.Appl.Cryst., **12**, 442-449

Taylor,M. and Brown,G.E.(1979a)
Structure of mineral giasses-I.
The feldspar glasses $NaAlSi_3O_8$,$KAlSi_3O_8$,$CaAl_2Si_2O_8$.
Geochim.Cosmochim.Acta, **43**, 61-75

Taylor,M. and Brown,G.E.(1979b)
Structure of mineral glasses II. The SiO_2-$NaAlSiO_4$ join.
Geochim.Cosmochim.Acta, **43**, 1467-1473

Taylor,M. and Brown,G.E.(1980)
Structure of mineral glassas III.
$NaAlSi_3O_8$ supercooled liquid at 805°C and the effects of thermal history.
Geochim.Cosmochim.Acta, **44**, 109-117

Tsuneyuki,S., Tsukada,M., Aoki,H., and Matsui,Y.(1988)
First-principles interatomic potential of silica applied to molecular dynamics.
Phys.Rev.Lett., **61**, 869

Tsuneyuki,S., Tsukada,M., Aoki,H., and Matsui,Y(1989)
Nature, **339**, 209-211

Verweij,H(1979a)
Raman study of the structure of alkali germanosilicate glasses(I) sodium and potassium metagermanosilicate glasses
J.Non-cryst.Solids, **33**, 41-53
Verweij,H(1979b)
Raman study of the structure of alkali germanosilicate glasses(II) lithium,sodium and potassium digermanosilicate glasses
J.Non-cryst.Solids, **33**, 55-69
Virgo,D., Mysen,B.O. and Kushiro,I.(1980)
Anionic constitution of 1-atmosphere silicate melts : implications for the structure of igneous melts
Science, **208**, 1371-1373
Waff,H.S(1975)
Pressure-induced coordination changes in magmatic liquids
Geophys.Res.Lett., **2**, 193-196
Warren,B.E. and Pincus,A.G.(1940)
Atomic consideration of immiscibility in glass systems.
J.Am.Ceram.Soc., **23**, 301
Waseda,Y. and Toguri,J.M.(1976)
Tetsutohagane(in japanese), **62**, 1493-1502
Waseda,Y. and Toguri,J.M.(1977)
The structure of molten binary silicate systems $CaO-SiO_2$ and $MgO-SiO_2$.
Metallugical Transactions B, **8B**, 563-568
Waseda,Y. and Toguri,J.M.(1978)
The structure of the molten $FeO-SiO_2$ system
Metallugical Transactions B, **9B**, 595-601
Woodcock, L.V., Angell,C.A., and Cheeseman,P.(1976)
Molecular dynamics studies of the vitreous state: Simple ionic systems and silica
J.Chem.Phys., **65**, 1565-1577
Zachariasen,W.H.(1932)
The atomic arrangement in glass
J.Am.Chem.Soc., **54**, 3841

CHAPTER 2

STRUCTURAL STUDIES OF BINARY ALKALI SILICATE GLASSES BY MEANS OF ^{29}Si NMR

Abstract of Chapter 2

Lithium, sodium, and potassium silicate glasses containing 20-54mol% alkali oxide were investigated by ^{29}Si Magic Angle Spinning Nuclear Magnetic Resonance (MAS-NMR) spectroscopy. In each spectrum, two to three distinct peaks were identified for individual glass. The distributions of SiO_4 structural units Q_n, where n is the number of bridging oxygen atoms attached to Si atom, were determined as a function of composition. The equilibrium constants of the reactions,

$$2Q_n \leftrightarrow Q_{n-1} + Q_{n+1} \quad (n=3,2,1),$$

were determined. The reaction proceeds to the right direction as cationic power of alkali ion (Z/r) increased (Li > Na > K) at the same alkali oxide concentration. The apparent equilibrium constants of the above reactions were compared with those from a proposed thermodynamic model. The ^{29}Si chemical shifts assigned to each structural unit increased linearly as a function of alkali oxide content. Whereas the slope of these lines became gentle as numbers of attached bridging oxygen atoms(BO) decreased corresponding to the difference of bridging angle, bond length and local structure distribution around the structural unit under consideration. The averaged chemical shifts also increased linearly with an increase of alkali oxide contents. The relationship between the averaged chemical shifts and the theoretical optical basicity were established.

2-1. Introduction

The examination of compositional dependence of the structure and other various physical properties of alkali silicate glasses is a fundamental problem in glass chemistry as well as in earth science. The relationships between the polymeric silicate anion structure and composition of the glasses have been examined by various spectroscopic techniques ;e.g., XRD[1-4], IR[5], X-ray emission spectroscopy[6,7], laser Raman spectroscopy[8-13], EXAFS[14,15] and XPS[16]. Since the ^{29}Si MAS-NMR measurement for zeolites was made by Lippma et al. [17], this technique has been applied extensively to many crystalline and glassy silicates [18-27].

The information which can be derived from ^{29}Si NMR studies are summarized as follows.

(1). For crystalline silicates, the isotropic chemical shifts vary systematically with silicate structure; thus a silicon nucleus is deshielded (and its chemical shift value becomes less negative) as the numbers of attached bridging oxygen (BO) atoms decrease. The Si atoms surrounded by different numbers of BO atoms are identified as separated peaks in ^{29}Si NMR spectra and commonly distinguished with notation such as Q_n's (n stands for numbers of bridging oxygen atoms).
(2). Glassy or liquid silicates possess chemical shifts of the similar range as those observed in crystalline silicates having the identical composition. The structural units of glasses or liquids are possibly represented by Q_n units similar to those deduced from the spectra of corresponding crystalline materials.
(3). ^{29}Si chemical shifts are sensitive to the variation of Si-O bond length and Si-O-Si bridging angles as well as to changes of second and third neighbor environments. The relationships between the chemical shift and bridging angle or group electronegativity have considerably been discussed.

In the previous reports concerning the MAS-NMR measurements on binary alkaline silicate glasses[18,19], the detailed distributions of Q_n species could not be determined due to limited S/N ratio, although the distinct difference from statistical distributions are realized i.e; the distribution of Q_n species can be explained on the basis of a model where each alkali ion addition results in one non-bridging oxygen to give one or two species Q_n and Q_{n-1} whose relative amounts can be determined from the concentration of alkali oxide. Recently, careful NMR measurements on sodium silicate glasses of approximately the di-silicate composition carried out by Stebbins[20] made it possible to discuss the equilibrium of reaction (1) quantitatively,

$$2Q_n \leftrightarrow Q_{n-1} + Q_{n+1} \quad (n=3,2,1). \quad (1)$$

However, the systematic dependence of the distributions of Q_n species over wide composition range have not thoroughly been explored.

On the other hand, the effect of variation of the modifying cations on the structure of silicate glasses have been discussed[8,12,21,22]. Enthalpies of solution of glasses of binary metal oxide-silica joins in a solvent increased in the order of cationic power of the metal cation (Z/r, where Z is valency and r is ionic radius). In di-silicate glasses, the observed increments of ^{29}Si MAS-NMR line width with increase of Z/r [22] was interpreted by the reaction,

$$2Q_3 \leftrightarrow Q_2 + Q_4, \quad (2)$$

to proceed to the right direction and to result in the chemical shift dispersion.

In the present paper, we tried to determine the detailed distributions of structural units in variety of alkali silicate glasses. The results will be

compared with the thermodynamic properties and also with the proposed thermodynamic model.

2-2 Experimental Section

Sample glasses were prepared from reagent grade Li_2CO_3, Na_2CO_3, K_2CO_3 and SiO_2. Mixed starting materials were carefully melted in platinum crucible at 1540 K for 3 hours. Then the samples were quenched by water or liquid nitrogen. All samples were optically clear.

Measurements of ^{29}Si MAS-NMR was made by Bruker MSL-200 spectrometer operating at 4.7 Tesla (39.76 MHz for ^{29}Si). A pulse width of 3 μs(45°pulse) and dead time of 20 μs were used. Typical repetition time was 2.5 s. The spectrum was accumulated 1500 times. Samples in an alumina or a zirconia sample holder were spun at the magic angle(54.74°) with respect to the external magnetic field. Spinning rate was 3500-4000Hz which kept the spinning side band intensities less than 1% relative to the intensity of the main peak. External chemical shift standard, Q8M8, was used as a secondary standard whose chemical shifts (M site) was set to 11.51 ppm from TMS. Spin-lattice relaxation time (T_1) for Si nucleus in silicate glasses are generally very long (a few min to hour). The relaxation of ^{29}Si nuclear spins can be acccerated by the spin diffusion from paramagnetic centers [28,29]. Therefore in order to increase relaxation rate 0.1 wt% Fe_2O_3 was addeed to all the samples studied.

2-3. Results

2-3-1 The effect of Fe_2O_3 on the spectra

No appreciable changes were observed on the profiles of spectra at different repetition times (0.1 ~ 20s). However, short repetition time led to poor S/N ratios. No significant effects were observed with different contents of Fe_2O_3 (varying 0.01 ~ 1.0wt%) except that the peak intensities from less polymelyzed sites (for example, Q_2 site in $3Na_2O \bullet 4SiO_2$ glass) decrease as Fe_2O_3 contents increased. The decrement of the peak intensities might be caused by Fe_2O_3 which acts as a network-former in glass network structure just like Al_2O_3.

2-3-2 Peak separation

A series of MAS-NMR spectra of Na_2O-SiO_2 glasses are shown in

figure 1. All spectra were well reproduced by Gaussian functions. The results of peak separation are summarized in Table 1. The normalized standard deviation ($\sigma[y(x)_{obs} - y(x)_{cal}]/N_i$) for peak separation was within 1% for each glass. However, near the stoichiometric composition (for example, $Na_2O \bullet 2SiO_2$ glass), the main peak(assigned to Q_3) and the sub-peaks (Q_2, Q_4) overlapped each other and led to a peak separation somewhat ambiguous. As mentioned by Stebbins[20], the broad line spectra can be used for quantitative estimation of Q_4 site population. Because the spectra consist of combination of line profiles contributed from asymmetrical sites (Q_3 or Q_2 sites; containing contribution from chemical shift anisotropy) and tetrahedral symmetrical site (Q_4 site which has isotropic chemical shift), they can easily be separated into each of the components.

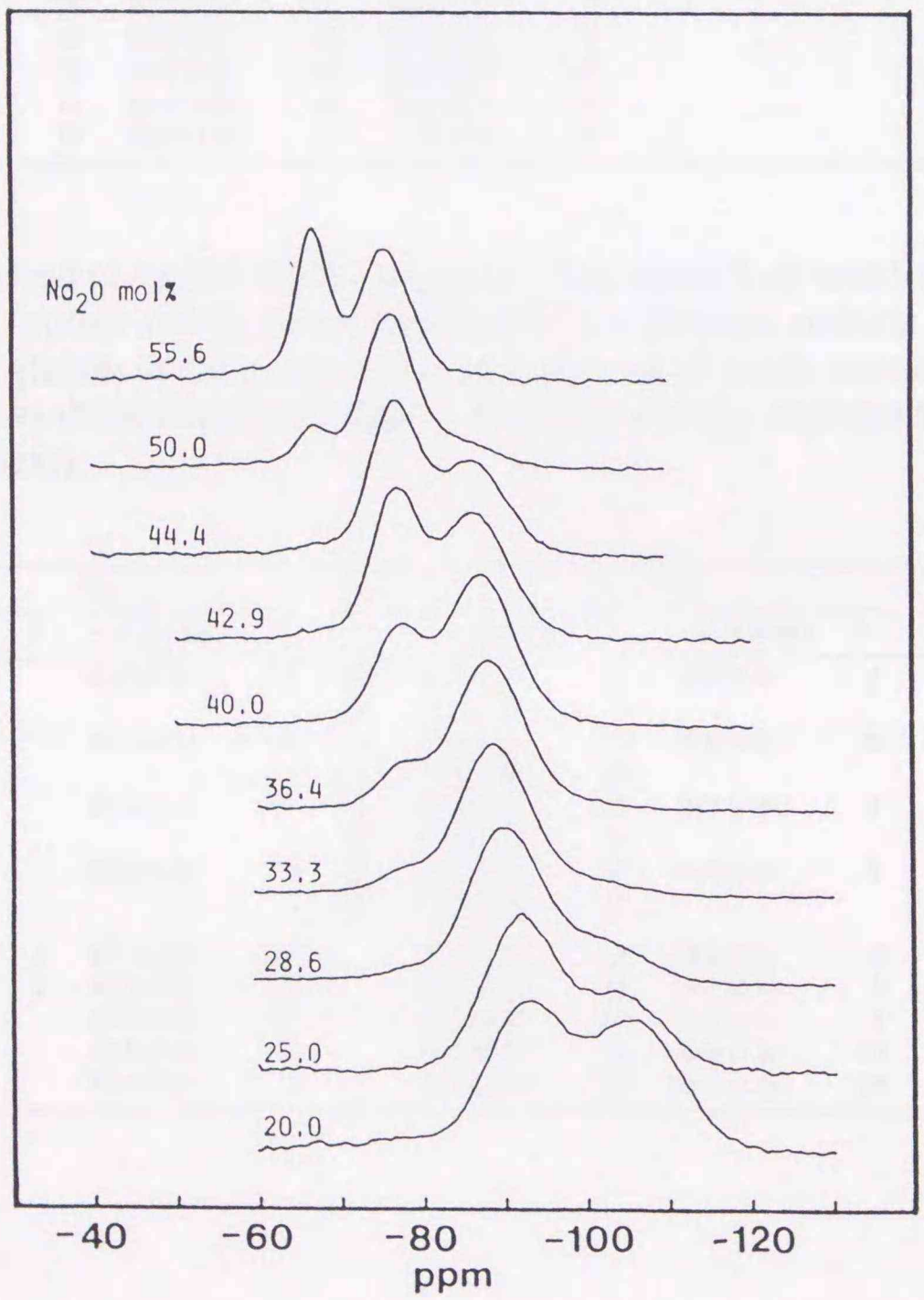

Figure 1. Composition variation of the ^{29}Si MAS NMR spectra of sodium silicate glasses(Na_2O-SiO_2).

Table 1. Observed chemical shifts (σ (ppm)), line width(half width at half maximum; hwhm (ppm)) and Q_n distributions (I(%)) in lithium, sodium and potassium silicate glasses.

mol% M_2O		MAS						Broad line				
		Q_4		Q_3		Q_2		Q_2+Q_3			Q_4	
		− σ (hwhm)	I	− σ (hwhm)	I	− σ (hwhm)	I	$\sigma_{xx}=\sigma_{yy}$	σ_{zz}	I	σ	I
K_2O	20.0	105.1 (5.7)	49	94.3 (4.9)	51			−47	−186	51	−106	49
	27.3	103.3 (5.6)	25	92.5 (5.0)	72	82.9 (3.0)	3	−48	−177	76	−103	24
	28.6	102.5 (5.6)	22	92.0 (5.0)	74	82.5 (4.0)	4	−49	−174	80	−102.5	20
	33.3	103.3 (5.6)	7	90.8 (5.5)	86	79.5 (3.5)	7	−51.5	−170	93	−100.5	7
	36.4	102.0 (6.0)	5	90.0 (5.4)	81	80.5 (4.2)	14	−50	−168	96	−99	4
Na_2O	20.0	105.6 (6.5)	50	92.2 (5.6)	48	78.0 (4.0)	3					
	25.0	104.1 (6.2)	38	91.7 (5.1)	61	78.0 (4.0)	1					
	28.6	100.4 (6.5)	27	89.6 (4.8)	68	78.0 (4.0)	5					
	33.3	99.5 (6.0)	11	88.7 (4.8)	79	77.7 (4.0)	10					
	36.4	99.0 (6.0)	7	88.2 (4.8)	76	77.6 (3.8)	17	−51	−165	95	−108	5
Li_2O	25.0	107.1 (6.9)	38	92.3 (6.3)	53	81.0 (5.1)	9					
	28.6	105.3 (6.7)	32	92.0 (6.1)	59	80.7 (5.0)	10					
	33.3	102.7 (6.9)	22	91.0 (5.8)	63	81.1 (4.8)	15					
	36.4	100.0 (6.8)	17	89.8 (5.6)	62	80.2 (4.5)	21					
	40.0	96.4 (6.8)	15	88.0 (5.5)	57	79.5 (4.0)	26					

Table 2. Observed chemical shifts (σ (ppm)), line width(half width at half maximum; hwhm (ppm)) and Q_n distributions (I(%)) in lithium, sodium and potassium silicate glasses at the composition of higher alkali oxide contents. Symbols are same as those denoted in table 1. Both Q_2 and Q_2' represent two types of Q_2 species(see text).

mol% M_2O		Q_4		Q_3		Q_2			Q_1		Q_0	
		− σ (hwhm)	I	− σ (hwhm)	I		− σ (hwhm)	I	− σ (hwhm)	I	− σ (hwhm)	I
K_2O	40.0			89.9 (5.3)	67	Q_2	82.5 (4.2)	27	70.8 (2.4)	1		
						Q_2'	77.2 (2.3)	5				
	42.9			89.7 (5.3)	51	Q_2	82.4 (4.2)	38	70.8 (2.4)	1		
						Q_2'	77.0 (2.3)	10				
	44.4			89.0 (5.3)	41	Q_2	82.2 (4.2)	43	70.8 (2.4)	2		
						Q_2'	77.0 (2.3)	14				
	50.0			89.0 (5.3)	9	Q_2	81.7 (4.0)	47	70.8 (2.4)	7		
						Q_2'	76.2 (2.3)	37				
Na_2O	40.0	99.0 (6.0)	2	87.1 (5.0)	68		76.9 (3.4)	29	68.0 (3.0)	2		
	42.9	96.0 (5.0)	2	86.3 (5.0)	54		76.6 (3.3)	41	67.4 (2.8)	3		
	44.4			86.0 (5.0)	47		76.5 (3.5)	50	66.8 (2.5	3		
	50.0			84.8 (5.0)	16		76.0 (3.6)	70	66.8 (2.5)	13	59.0 (3.0)	1
	55.6			85.0 (5.0)	3		75.5 (3.7)	54	66.7 (2.4)	39	59.5 (3.0)	4

An example of peak separation of broad line spectrum for $2K_2O \bullet 5SiO_2$ glasses is shown in Figure 2.(a). The spectrum contains contributions from Q_4 and Q_3 sites separated into each peak.The Q_2 site may contribute to the spectrum, however, in the present investigation, the Q_2 peak was included in the Q_3 peak. The estimated Q_4 site population are summarized in table 1.

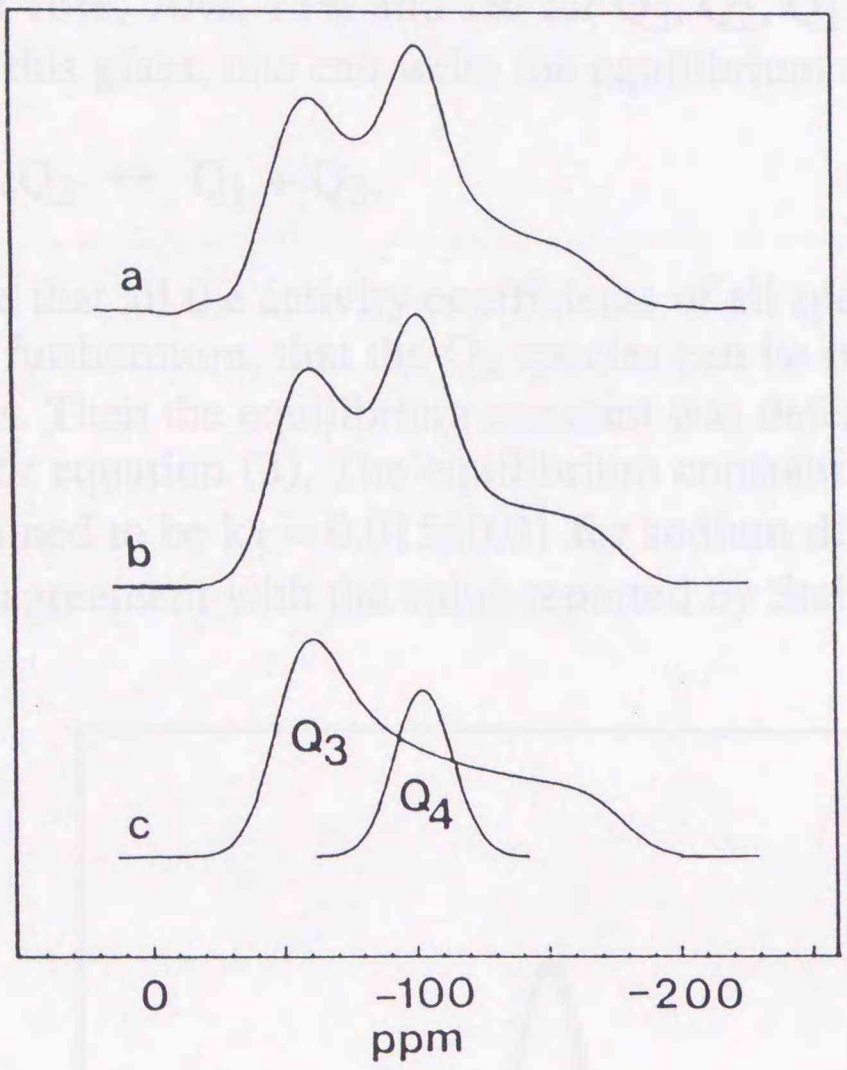

Figure 2. ^{29}Si static NMR spectrum for $2K_2O \bullet 5SiO_2$ glass. (a) experiment; (b) simulation of (a) using two line shape functions shown in (c).

2-3-3 Qn distribution

The distributions of the structural units, Q_n, seem to be governed by the equilibrium constants for equation (1). For example, in sodium metasilicate glass as shown in figure 3, NMR spectra consist of at least three different peaks assigned to Q_1, Q_2, Q_3 (and perhaps Q_0 though the separeted peak is not shown in the figure), and were clearly resolved. Peak areas were 16%, 70%, 13% and 1% for Q_3, Q_2, Q_1 and Q_0 sites respectively. In this glass, one can write the equilibrium reaction,

$$2Q_2 \leftrightarrow Q_1 + Q_3. \qquad (3)$$

Let us assume that all the activity coefficients of all species are equal each other and, furthermore, that the Q_n species can be treated as real chemical species. Then the equilibrium constant was determined as k_2=0.04±0.01 for equation (3). The equilibrium constant for equation (2) was also determined to be k_3 = 0.015±0.01 for sodium disilicate glass. This is in close agreement with the value reported by Stebbins[20] (0.011±0.005).

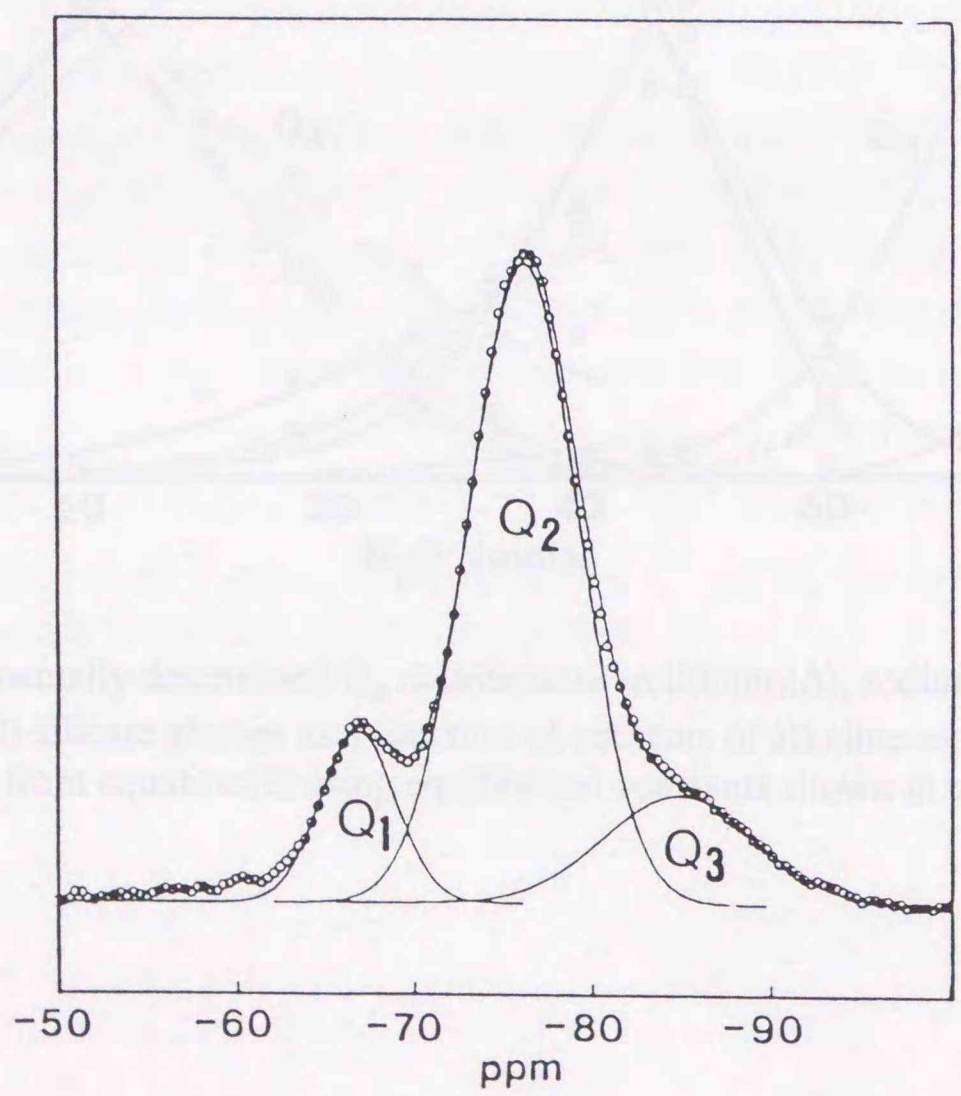

Figure 3. ^{29}Si MAS NMR spectra of sodium meta-silicate glass($Na_2O \bullet SiO_2$).

Qn distributions of potassium, sodium and lithium silicate glasses are shown as functions of alkali contents in fig.4. The distributions of Q_n's are well fitted with reaction(1) using k_n's (k_3 , k_2 and k_1; corresponding to n=3,2,1) which are listed in table 3.

The effect of network-modifying cations to Q_n distributions is clearly seen. Greater Z/r value ($Li^+ > Na^+ > K^+$) makes the equation (1) to proceed to the right direction more intensely. This trend agrees with the results from Raman spectroscopy [8,12] and NMR on the compositions of disilicate and metasilicate glasses[21,22].

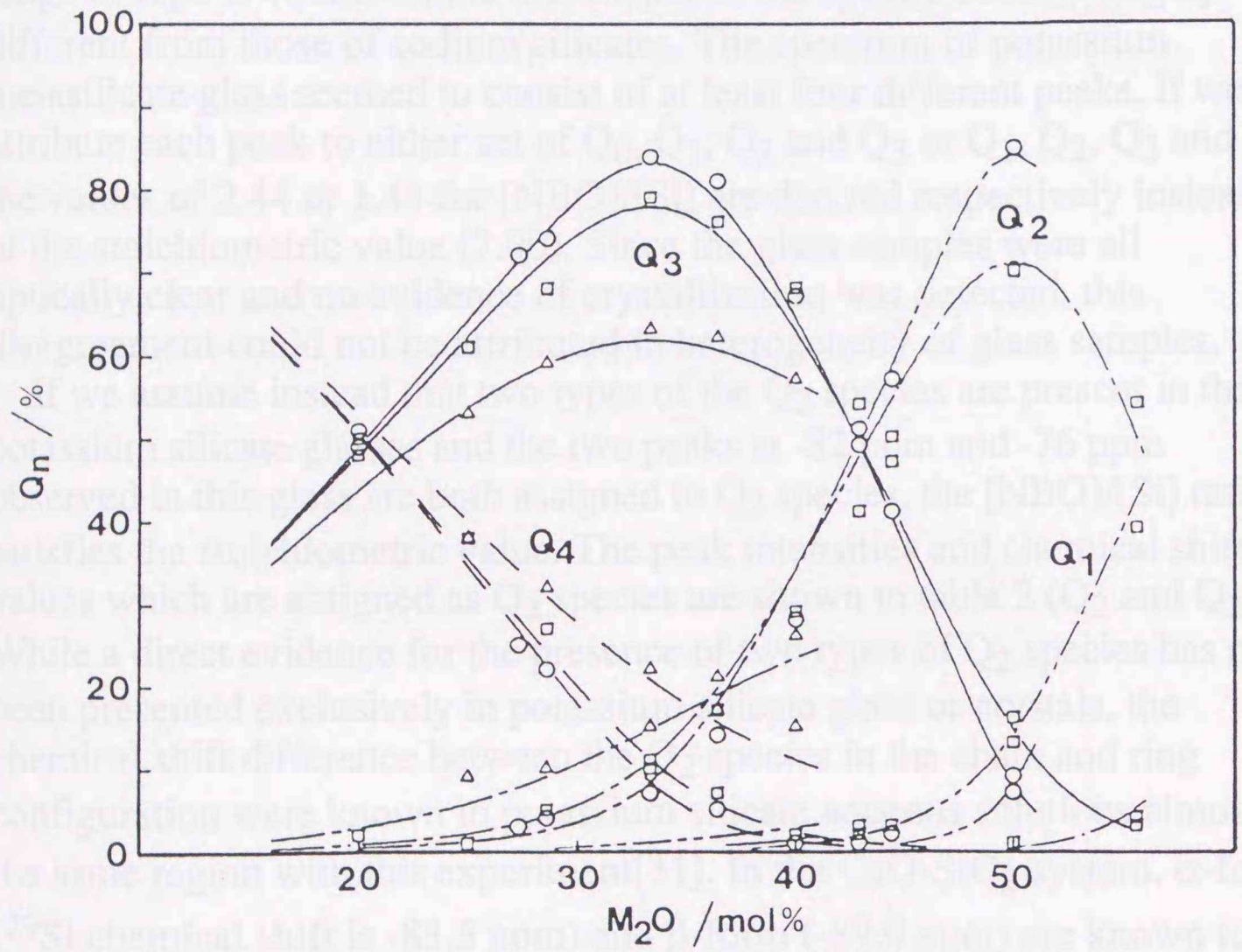

Figure 4. Experimentally determined Q_n distributions in lithium(Δ), sodium (❑) and potassium(○) silicate glasses as a function of contents of alkaline oxide. Fitted lines were calculated from equation(1) using equilibrium constants shown in table 3.

Table 3. Equilibrium constants for equation(1) determined so as to reproduce the Q_n distribution shown in figure4.

	Li_2O-SiO_2	Na_2O-SiO_2	K_2O-SiO_2
k_3	0.08	0.02	0.01
k_2	0.30	0.06	0.01
k_1		0.14	0.02

On the other hand, in potassium silicate glasses beyond the composition range of $K_2O \geq 40$ mol%, the line shapes of the spectra became largely different from those of sodium silicates. The spectrum of potassium metasilicate glass seemed to consist of at least four different peaks. If we attribute each peak to either set of Q_0, Q_1, Q_2 and Q_3 or Q_1, Q_2, Q_3 and Q_4 the values of 2.44 or 1.44 for [NBO]/[Si] are derived respectively instead of the stoichiometric value (2.00). Since the glass samples were all optically clear and no evidence of crystallization was detected, this disagreement could not be attributed to heterogeneity of glass samples.

If we assume instead that two types of the Q_2 species are present in the potassium silicate glasses and the two peaks at -82 ppm and -76 ppm observed in this glass are both assigned to Q_2 species, the [NBO]/[Si] ratio satisfies the stoichiometric value. The peak intensities and chemical shift values which are assigned as Q_2 species are shown in table 2 (Q_2 and Q_2'). While a direct evidence for the presence of two types of Q_2 species has not been presented exclusively in potassium silicate glass or crystals, the chemical shift difference between the Q_2 species in the chain and ring configuration were known in potassium silicate aqueous solutions almost in the same region with this experiment[31]. In the $CaO-SiO_2$ system, α-form (^{29}Si chemical shift is -83.5 ppm) and β-form (-89.0 ppm) are known to consist of ring and chain configuration, respectively.

2-4. Discussion

2-4-1 Linewidth

As noticed earlier, the silicon chemical shift is sensitive to the variations in bond length and angles as well as the second and third neighbor environments around the silicon atom. So the wider variety of the atomic arrangements around silicon atom will result in broader linewidth(half width at half maximum : hwhm) in its ^{29}Si MAS-NMR spectrum. The linewidths of Q_n's(table 1, table 2) suggests that the distributions of bridging angle, bond length or third neighbor environments of a Q_n site become wider with (1)larger n value in Q_n's, (2)the greater cationic potential of alkali metal ions and thus (3)the wider Q_n distribution.

2-4-2 Reliability of the NMR peak area analysis

Figure 5 shows the numbers of non-bridging oxygen atoms per Si atom, ([NBO]/[Si]), calculated from Q_n distribution for each alkali silicate

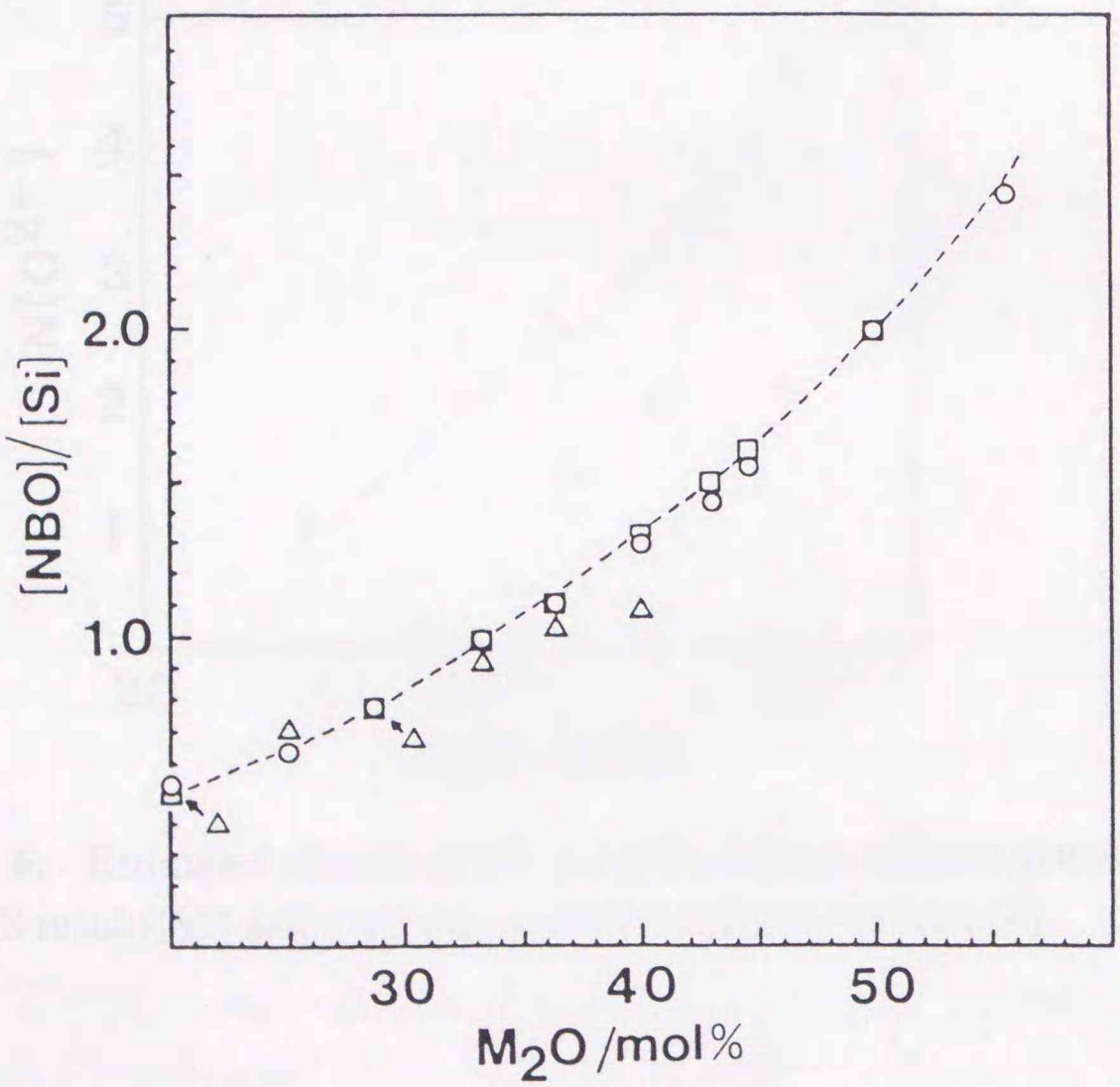

Figure 5. Numbers of non-bridging oxygen per Si tetrahedron as a function of composition. Symbols denote NMR results of lithium(Δ), sodium(❑) and potassium(○) silicate glasses, respectively. (- - - -) expectative value(see text).

glass. In potassium and sodium silicate glass, the ([NBO]/[Si]) values were in good agreement with those calculated from glass composition if no free alkali oxide ions (M_2O) were assumed to remain in the glasses. It had been shown that the free Na_2O ions do not exist in the sodium silicate glasses of the composition range studied in this work from the thermodynamic measurement on the melts[32,33,34] as well as XPS measurement on the glasses[16].

However, in Li_2O-SiO_2 glasses,experimental [NBO]/[Si] value became appreciably smaller than the calculated ones as Li_2O content increased as shown figure 6. If we assume the remaining part of oxygen atom to be extra Li_2O (O^{2-}), the amount of O^{2-} per numbers of the total oxygen atom, $N(O^{2-})$, can be obtained from equation;

$$N(O^{2-}) = \frac{[NBO]_{calc.} - [NBO]_{obs.}}{[NBO]_{calc.}}, \qquad (4)$$

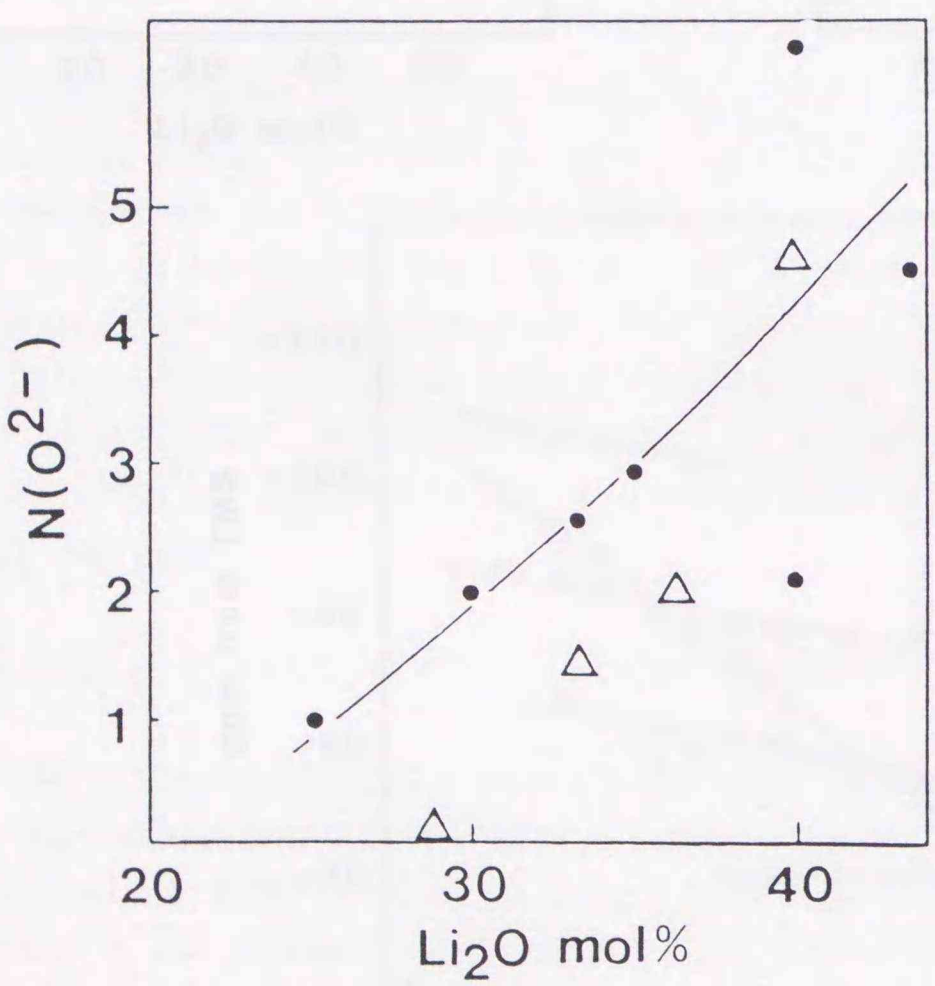

Figure 6. Estimated amount of O^{2-} ion in the lithium silicate glasses. (●), XPS results[35] and (Δ), this experiment from equation(4).

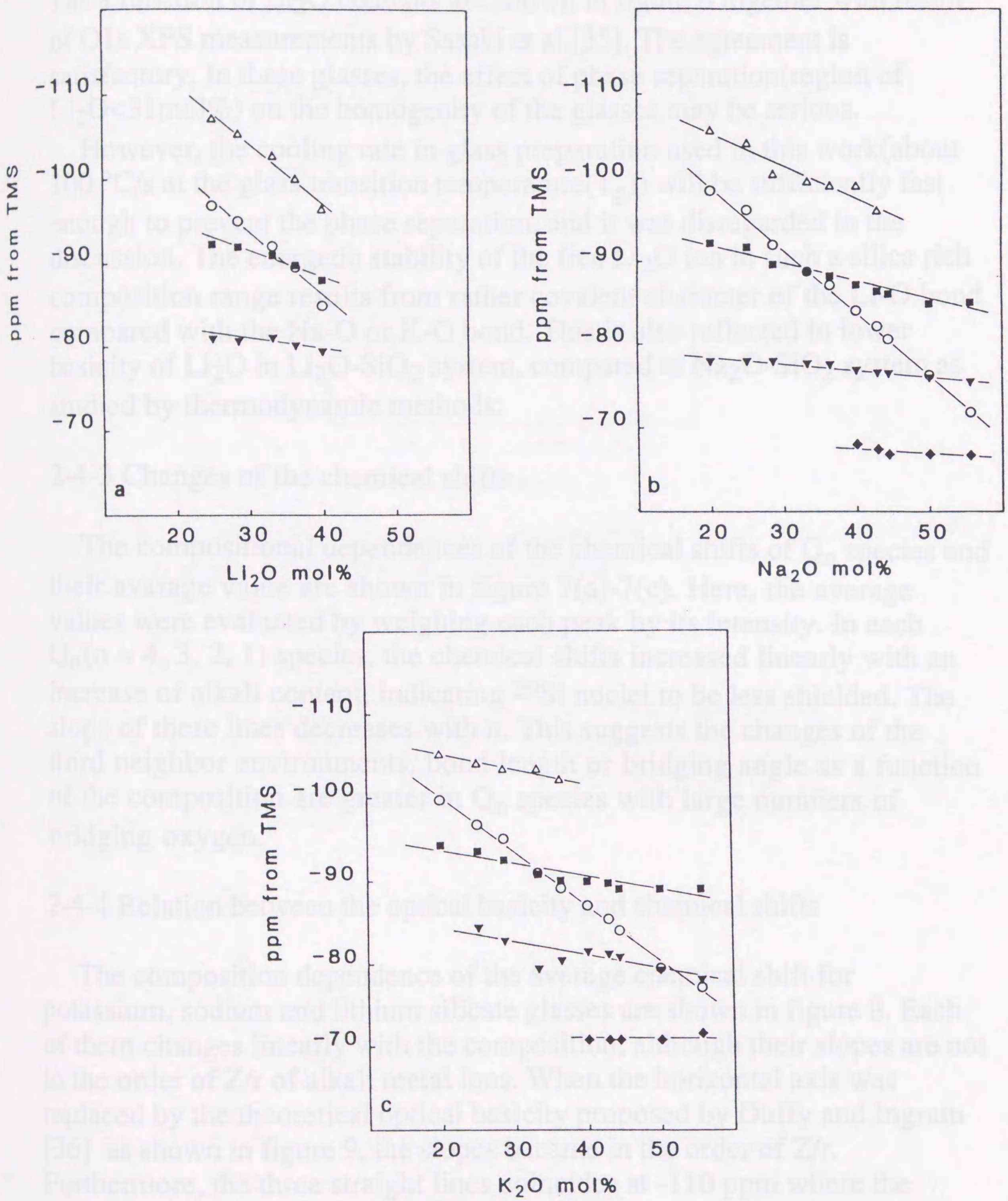

Figure 7. ^{29}Si chemical shifts for Q_n species as functions of alkaline oxide contents for (a) lithium, (b) sodium and (c) potassium silicate glasses. Δ, Q_4; ■, Q_3; ▼, Q_2; ◆, Q_1; and ○ averaged.

where $([NBO]/[Si])_{calc}$ and $([NBO]/[Si])_{obs}$ denote [NBO]/[Si] value derived from composition and Q_n distribution, respectively. The amounts of $N(O^{2-})$ as a function of Li_2O contents are shown in figure 6 together with result of O1s XPS measurements by Sasaki et al.[35]. The agreement is satisfactory. In these glasses, the effect of phase separation(region of Li_2O<31mol%) on the homogenity of the glasses may be serious.

However, the cooling rate in glass preparation used in this work(about 100 °C/s at the glass transition temperature(T_g)) will be sufficiently fast enough to prevent the phase separation, and it was disregarded in the discussion. The energetic stability of the free Li_2O ion in such a silica rich composition range results from rather covalent character of the Li-O bond compared with the Na-O or K-O bond. This is also reflected in lower basicity of Li_2O in Li_2O-SiO_2 system, compared to Na_2O-SiO_2 system as studied by thermodynamic methods.

2-4-3 Changes of the chemical shifts

The compositional dependences of the chemical shifts of Q_n species and their avarage value are shown in figure 7(a)-7(c). Here, the average values were evaluated by weighing each peak by its intensity. In each Q_n(n = 4, 3, 2, 1) species, the chemical shifts increased linearly with an increase of alkali content, indicating ^{29}Si nuclei to be less shielded. The slope of these lines decreases with n. This suggests the changes of the third neighbor environments, bond length or bridging angle as a function of the composition are greater in Q_n species with large numbers of bridging oxygen.

2-4-4 Relation between the optical basicity and chemical shifts

The composition dependence of the average chemical shift for potassium, sodium and lithium silicate glasses are shown in figure 8. Each of them changes linearly with the composition, although their slopes are not in the order of Z/r of alkali metal ions. When the horizontal axis was replaced by the theoretical optical basicity proposed by Duffy and Ingram [36] as shown in figure 9, the slopes became in the order of Z/r. Forthermore, the three straight lines coincides at -110 ppm where the optical basicity of Λ=0.49(corresponding to the pure SiO_2 glass).

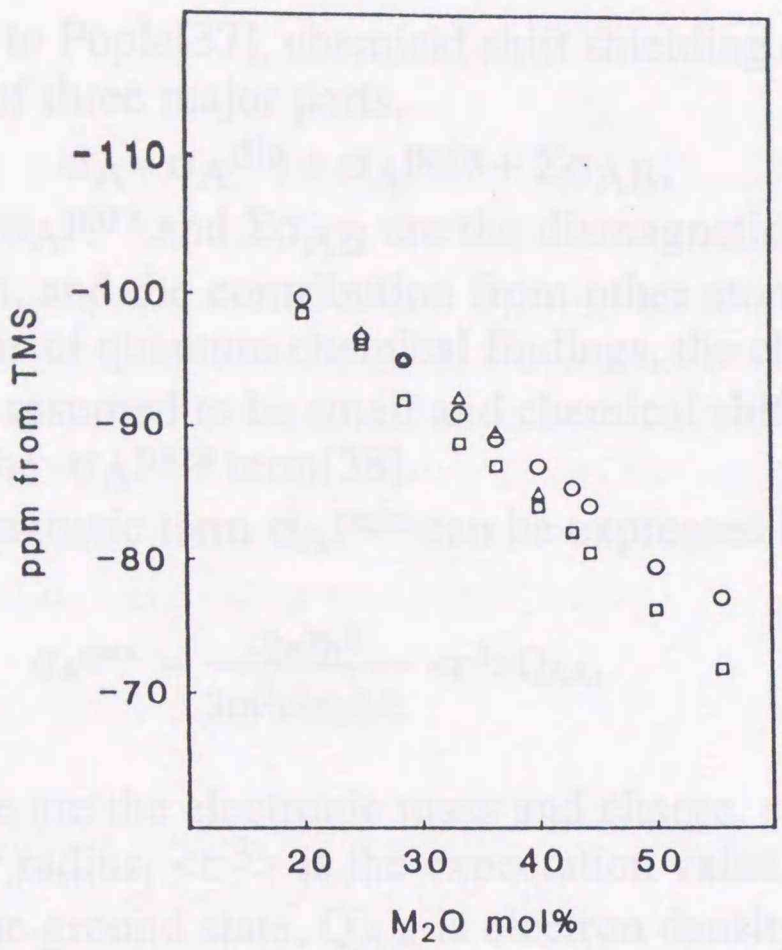

Figure 8. Averaged ^{29}Si chemical shifts as functions of alkaline oxide contents for (Δ) lithium, (❑) sodium and (○) potassium silicate glasses.

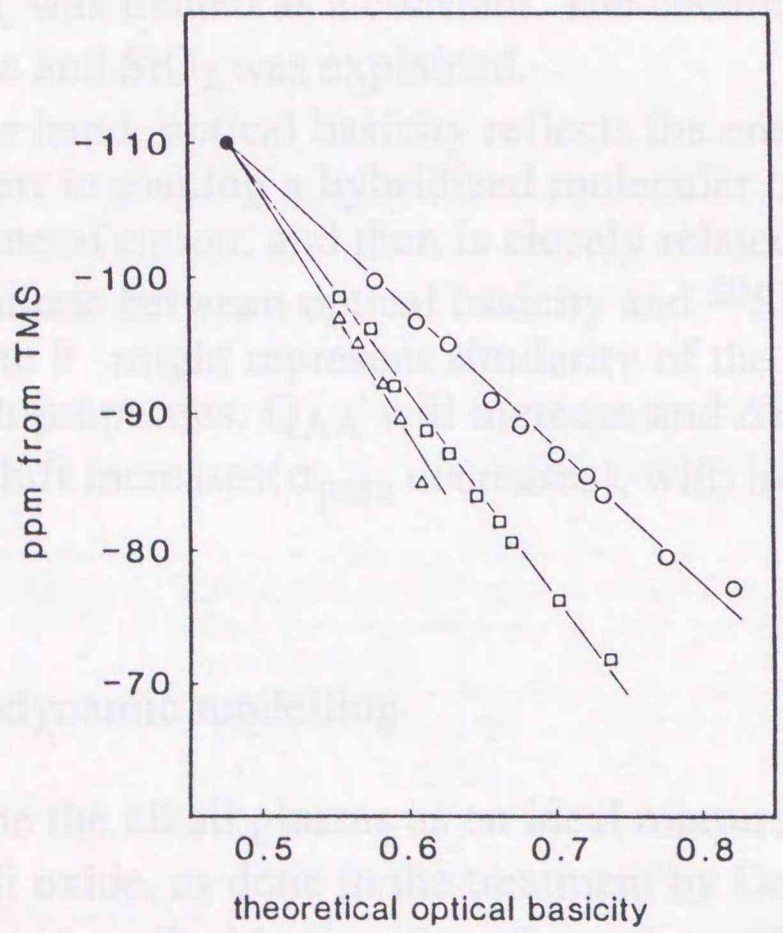

Figure 9. Averaged ^{29}Si chemical shifts as functions of theoretical optical basicity[36] for (Δ) lithium, (❑) sodium and (○) potassium silicate glasses.

According to Pople[37], chemical shift shielding constant of atom A, σ_A, consists of three major parts,

$$\sigma_A = \sigma_A^{dia} + \sigma_A^{para} + \Sigma\sigma_{AB}, \qquad (5)$$

where σ_A^{dia}, σ_A^{para} and $\Sigma\sigma_{AB}$ are the diamagnetic term, local paramagnetic term, and the contribution from other atoms B, respectively.

On the basis of quantum chemical findings, the changes in σ_A^{dia} for silicates were assumed to be small and chemical shift difference were attributed to the σ_A^{para} term[38].

The paramagnetic term σ_A^{para} can be expressed by,

$$\sigma_A^{para} = \frac{-2e^2h^2}{3m^2c^2a_0\Delta E} \langle r^{-3}\rangle Q_{AA}, \qquad (6)$$

where m and e are the electronic mass and charge, c is the speed of light, a_0 is the Bohr radius, $\langle r^{-3}\rangle$ is the expectation value of r^{-3} for valence p electrons in the ground state, Q_{AA} is electron density, and ΔE is an assumed average excitation energy. Among them, the dominant terms will be ΔE and Q_{AA}. Tossel[38] found a good relation between the ^{29}Si chemical shift and the ΔE value derived from X-ray emission spectra, where the Q_{AA} was treated as a constant. The chemical shift difference between olivine and SiO_2 was explained.

On the other hand, optical basicity reflects the energy level of oxygen which takes part in making a hybridized molecular orbital with silicon and the other metal cation, and then is closely related to the ΔE and Q_{AA}. The linear relations between optical basicity and ^{29}Si chemical shift shown in figure 9 might represent similarity of the mechanism which determine both properties. Q_{AA} will increase and ΔE will decrease, thus the chemical shift increases(σ_{para} decreases), with increasing alkali oxide content.

2-4-5 Thermodynamic modelling

If we assume the alkali glasses as an ideal mixtures of Q_n's (n = 0-4), SiO_2 and alkali oxide, as done in the treatment by Dorfeld [39], the glass structure can be described by a series of reactions (7),

$$SiO_2 + (2\text{-}n/2)\ M_2O \overset{K_n}{\leftrightarrow} Q_n \quad (7),$$

where M_2O represents an alkali oxide(M=Li,Na,K) which remains unreacted. Once four equilibrium constants for reaction (7) (K_3~K_0) are determined, the distributions of the Q_n species and the free alkali oxide concentration could be calculated as a function of the composition. However, the equilibrium constants determined from the present experiments were not K_n but the constants for equation (1) (k_3, k_2, k_1). The absolute value of K_n can be determined by the free energy for mixing $\Delta G_n{}^0$ referred to pure silica and alkali oxide,

$$\Delta G_n{}^0 = -RT\ln(K_n). \quad (8)$$

These equilibrium constants, K_n's, must be related to the other set of constants, k_n's, by the following relation,

$$k_n = \frac{K_{n-1} \times K_{n+1}}{K_n^2}. \quad (9)$$

Table 4. Standard free energies of formation for sodium silicate compounds of Q_n stoichiometry relative to SiO_2 and Na_2O determined by Dorfeld.[39]

Temperature (K)	Standard free energies (kJ/mol)			
	Q_3	Q_2	Q_1	Q_0
373	−124.5	−241.0	−332.6	−415.1
773	−125.6	−236.1	−327.6	−402.2
1073	−125.5	−232.0	−322.3	−390.4
1473	−125.7	−226.6	−315.1	−374.6

We now get the suitable set of K_n values so that the $\Delta G_n{}^0$ for Q_n species of equation (8) may coincide with the experimental standard free energies for equations (7). The latter have been estimated by Dorfeld[39] from JANAF tables[40] using the standard free energy of formation of silicate crystals which consist exclusively of particular Q_n(table4). The glass can be assumed to keep the thermodynamic state of the liquid at its glass transition temperature.

In sodium silicate glasses, T_g decreases linearly with Na_2O contents for the composition range of 10-45 Na_2O mol%[41]. The temperature variation of $\Delta G_n{}^0$ (exp.) is shown in table4. The K_n's were obtained assuming $\Delta G_n{}^0$ of equation (8) at each T_g to coincide with $\Delta G_n{}^0$ (exp.) at 773K. The results are summarized in table5.

If we define the thermodynamic activity of Na_2O to be equal to the concentration of Na_2O in equation(7) as,

$$a(Na_2O) = \frac{[Na_2O]}{\sum^{n} [Q_n] + [Na_2O]}, \qquad (10)$$

the present data can give $a(Na_2O)$ as functions of composition and temperature. The results are in semiquantitative accordance with the thermodynamic activity of sodium oxide[32,33,34] as shown in figure 10.

Table 5. Equilibrium constants(K_n) for equation(7) and standard chemical potentials for Q_n species($\mu_i{}^o$) in sodium silicates which gave the best fits for standard free energies(table4 at 773K) at each T_g's.

	Q_3	Q_2	Q_1	Q_0
μ_i^0 (kJ/mol)	−130	−235	−321	−395
K_n for eq. (7)	6.0×10^{8}	7.2×10^{15}	5.2×10^{21}	5.2×10^{26}

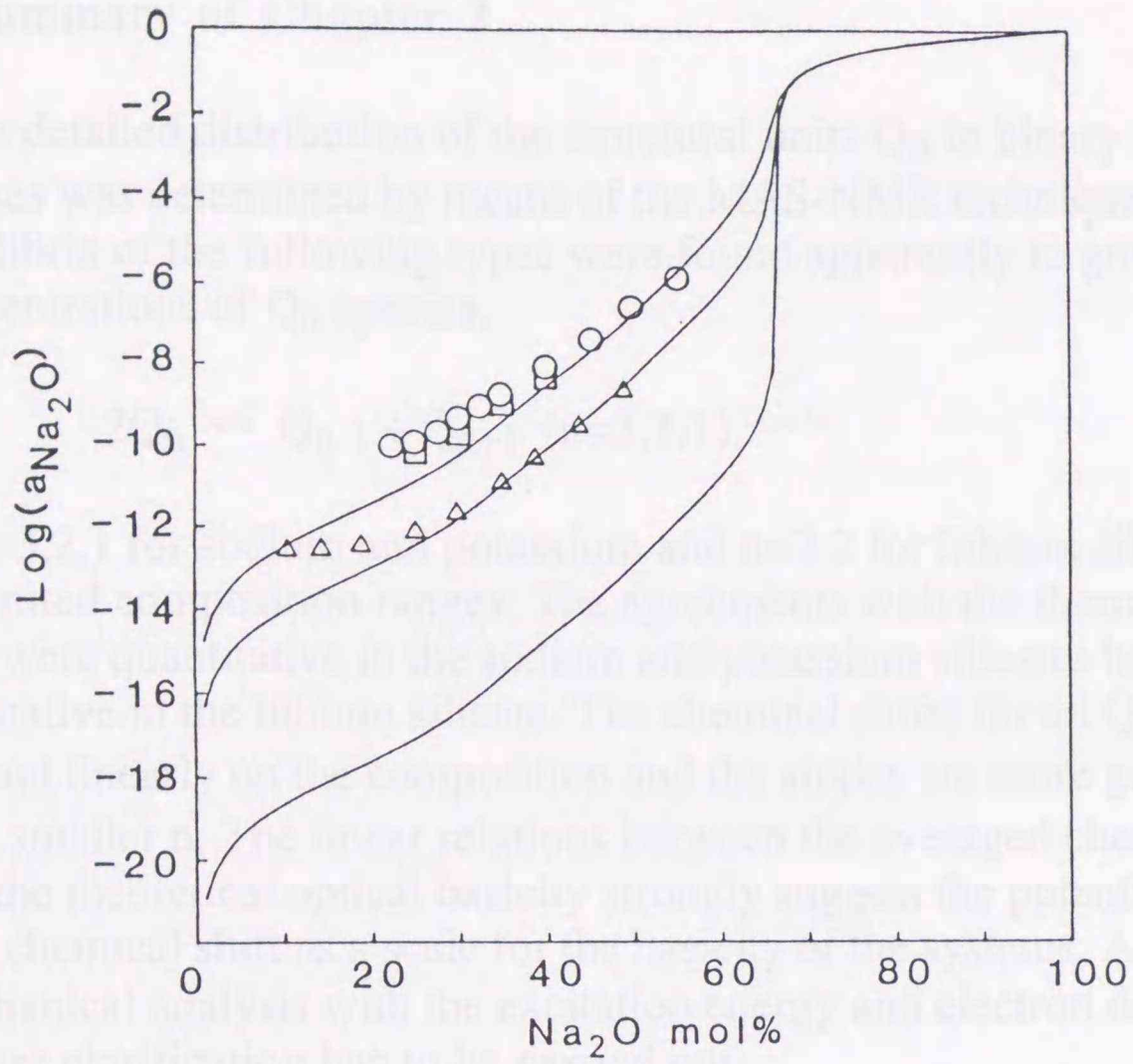

Figure 10. Comparison between the compositional dependence of sodium oxide activities. Solid lines calculated from equation(7) at 773, 1073 and 1273K. Symbols represent thermodynamic sodium oxide activities from E.M.F. measurements[36-38], at (Δ)1073K, (❑)1273K and (○)1300K, respectively.

A similar treatment was extended to the lithium silicate to reproduce the Li_2O contents determined from the present investigation as shown in fig.7. However, it leads to ΔG_n^0 values of a few ten kJ/mol too small compared with the free energy of formation of the crystalline silicates[40]. This discrepancy suggests that the Q_n treatment might not be suitable, especially in the less basic alkali system (i.e, Li_2O-SiO_2 system). One must also take into consideration the non-ideal interaction among Q_n species, as the activity of charged ions cannot be approximated by their concentration in the absence of any supporting electrolytes of constant ionic strength. One must also ask whether Q_n species can be treated as real chemical entities or not.

5. Summary of Chapter 2

The detailed distribution of the structural units Q_n in binary silicate glasses was determined by means of the MAS-NMR technique. The equilibria of the following types were found apparently to govern the concentrations of Q_n species,

$$2Q_n \leftrightarrow Q_{n-1} + Q_{n+1} \quad (n=3,2,1),$$

of n=3,2,1 for sodium and potassium and n=3,2 for lithium silicate glasses in limited composition ranges. The agreements with the thermodynamic data were quantitative in the sodium and potassium silicates but only qualitative in the lithium silicate. The chemical shifts for all Q_n species depend linearly on the composition and the slopes are more gentle for Q_n with smaller n. The linear relations between the averaged chemical shift and the theoretical optical basicity strongly suggest the potential use of the ^{29}Si chemical shift as a scale for the basicity of the systems. A quantum mechanical analysis with the excitation energy and electron density for further clarification has to be carried out.

references

(1)) R.L.Mozzi and B.E.Warren, J.Appl.Cryst., **2**, 164(1969).

(2) Y.Waseda and J.M.Toguri, Metal.Trans., **9B**, 595(1978).

(3) M.Imaoka, H.Hasegawa, and I.Yasui, Phys.Chem.Glasses, **24**, 72(1983).

(4) C.D.Yin, M.Okuno, H.Morikawa, and F.Marumo, J.Non-cryst.Solids, **55**, 131(1983).

(5) J.R.Sweet and W.B.White, Phys.Chem.Glasses **10**, 246(1969).

(6) N.Kikuchi, T.Maekawa, and T.Yokokawa, Bull.Chem.Soc.Japan, **52**, 1260(1979).

(7) B.H.W.S.deJong, K.D.Keefer, G.E.Brown Jr, and C.M.Taylor, Geochim.Cosmochim.Acta, **45**, 1291(1981).

(8) S.A.Brawer and W.B.White, J.Chem.Phys., **63**, 2421(1975).

(9) D.Virgo, B.O.Mysen, and I.Kushiro, Science, **208**, 1371(1980).

(10) B.Piriou and P.McMillan, Am.Mineral., **68**, 426(1983).

(11) P.McMillan, Am.Mineral., **69**, 622(1984).

(12) B.O.Mysen, D.Virgo, and C.M.Scarfe, Am.Mineral., **65**, 690(1980).

(13) S.K.Sharma, J.F.Mammone, and M.F.Nicol, Nature, **292**, 140(1981).

(14) G.N.Greaves, A.Fontaine, P.Lagarde, D.Raoux, and S.J.Gurman, Nature, **293**, 611(1981).

(15) M.C.Eckersley and P.H.Gaskell, J.Non-cryst.Solids, **106**, 132(1988).

(16) R.Bruckner, H.-U.Chun, H.Goretzki, and M.Sammet, J.Non-cryst.Solids, **42**, 49(1980).

(17) E.Lippmaa, M.Magi, A.Samoson, G.Engelhardt, and A.-R.Grimmer, J.Am.Chem.Soc., **102**, 4889(1980).

(18) A.-R.Grimmer, M.Magi, M.Hahnert, H.Stade, A.Samoson, W.Wieker, and E.Lippmaa, Phys.Chem.Glasses, **25**, 105(1984).

(19) R.Dupree, D.Holland, and D.S.Williams, J.Physiq., **C8**, 119(1985).

(20) J.F.Stebbins, Nature, 330 (1987)465., J.Non-cryst.Solids, **106**, 359(1988).

(21) J.F.Emerson, P.E.Stallworth, and P.J.Bray, J.Non-cryst.Solids, **113**, 253(1989).

(22) J.B.Murdoch, J.F.Stebbins, and I.S.E.Carmichael, Am.Mineral., **70**, 332(1985).

(23) E.Schneider, J.F.Stebbins, and A.Pines, J.Non-cryst.Solids, **89**, 371(1987).

(24) C.M.Schramm, B.H.W.S.de Jong, and V.Parziale, J.Am.Chem.Soc., **106**, 4396(1984).

(25) N.Janes and E.Oldfield, J.Am.Chem.Soc., **107**, 6769(1984).

(26) S.Ramdas and J.Klinowski, Nature, **308**, 521(1984).

(27) M.Magi, E.Lippmaa, A.Samoson, G.Engelhardt, and A.-R.Grimmer, J.Phys.Chem., **88**, 1518(1984).

(28) B.L.Sherriff and J.S.Hartman, Can.Mineral., **23**, 205(1985).
(29) T.Watanabe, H.Shimizu, A.Masuda, and H.Saito, Chem.Lett.,1293(**1983**).
(30) B.O.Mysen, D.Virgo, and F.A.Seifert, Am.Mineral., **69**, 834(1984).
(31) R.K.Harris, and C.T.G.Knight, J.Chem.Soc., Faraday Trans., 393(**1980**).
(32) D.A.Neudorf and J.F.Elliott, Metal. Trans., **11B**, 607(1980).
(33) B.A.Shakhmatkin and M.M.Shul'tz, Fizika Khim.Stekla, **6**, 129(1980).
(34) H.Itoh and T.Yokokawa, Trans.Japan Inst. Metals, **25**, 879(1984).
(35) T.Sasaki, M.Kawaguchi, M.Yamane, and Y.Suginohara, J.Japan Inst.Metals, **45**, 790(1981).
(36) J.A.Duffy and M.D.Ingram, J.Non-cryst.Solids, **21**, 373(1973).
(37) J.A.Pople, Discuss Faraday Soc. **34**, 7(1962).
(38) J.A.Tossell, Phys.Chem.Minerals, **10**, 137(1984).
(39) W.G.Dorfeld, Phys.Chem.Glasses, **29**, 179(1988).
(40) M.W.Chase Jr., C.A.Davies, J.R.Downey Jr., D.J.Frurip, R.A.McDonald, and A.N.Syverud, *JANAF Thermochemical Tables* Third Edition., American Institute of Physics, Inc.(1985)
(41) B.C.Schmid, A.N.Finn, and J.C.Young, J.Res.Natl.Bur.Std.,12,421(1934).

CHAPTER 3

STRUCTURAL STUDIES OF TERNARY SILICATE GLASS SYSTEM Na_2O-Al_2O_3-SiO_2 BY MEANS OF ^{29}Si NMR

Abstract of Chapter 3

Sodium aluminosilicate glasses with composition range of [Na]/[Al] ≥ 1 were investigated by means of ^{29}Si MAS-NMR. Line shape and chemical shift analysis suggested that numbers of non-bridging oxygen atoms(N_{nbo}) increase linearly with the ratio defined by {[Na]-[Al]}/[Si], which is in agreement with the classical structural model. An addition of alumina into sodium silicate glasses caused an increase of the chemical shift and the line width of Q_n peak having the largest n value among several Q_n peaks, where Q_n represents the SiO_4 tetrahedron with n bridging oxygen atoms connected to adjacent Si atom. This fact suggested that an aluminum atom tends to connect with most polymerized SiO_4 tetrahedra among all structural units constructing the glass network. The results could be interpreted in terms of thermodynamic acid and base concepts. Thus Al_2O_3 is a stronger acid than SiO_2 and tends to be associated with Na_2O to form $NaAlO_2$, while $NaAlO_2$ is no more acidic than SiO_2 and additional Na_2O modifies not $NaAlO_2$ but SiO_2.

The reaction between Q_n structure units,

$$2Q_n \leftrightarrow Q_{n-1} + Q_{n+1},$$

seemed to proceed to the left direction with increasing contents of $NaAlO_2$ into the sodium silicate glasses reflecting the basic character of $NaAlO_2$.

3-1. Introduction

Characterization of the structure and an understanding of the relationships between the structure and properties of aluminosilicate melts

and glasses are necessary in order to describe rock-forming igneous processes. As their melts are model compounds for acidic magmas, numerous models of structure and properties of natural magmatic liquids have, therefore, been based on simple aluminosilicate melts. In the view of glass industries, characterization of the structure is important because an introduction of aluminum oxide into silicate glasses proceeds their glass forming tendency.

The effect of composition on the properties of aluminosilicate melts and glasses have been extensively studied and interpreted in terms of simple structural models.[1-6] Densities, viscosities, refractive indices and thermal expansivities show drastic changes near the composition of atom ratio [Na]/[Al] = 1[1-5] and are thought to be accompanied by the change of coordination numbers of aluminum from 4 to 6 oxygen atoms. Thus, Galant[1] measured refractive indices of sodium aluminosilicate glasses and proposed a structural model that, in the composition range of [Na]/[Al]>1, all Al^{3+} form AlO_4 tetrahedra accompanied by Na^+ ion as the charge compensator and the excess sodium ions modify the silicate network which create non-bridging oxygen atoms (NBO's) bonded only to one silicon atom. While the observed physical properties suggest the validity of this structural model, spectroscopic observations have not always supported it. Bruckner et al.[7] and Smets and Lommen[8] concluded from O1s XPS spectra that number of NBO(N_{nbo}) goes zero even at the composition [Na]/[Al] > 0.7 and some AlO_6^{3-} might exist at the region of [Na]/[Al] = 1. On the other hand, Tasker et al.[9] showed that N_{nbo} linearly changes with {[Na] - [Al]}/[Si], and goes zero at [Na]/[Al] = 1, thus supporting the model. Other methods such as XRD[10], EXAFS[11], Raman spectroscopy[12] and MAS-NMR[13-17] were also employed to show wide varieties of the structural information. Among them, ^{29}Si, ^{27}Al, ^{23}Na MAS-NMR with compositions at around [M]/[Al] =1 (M = Li, Na, K, 0.5Ca) revealed the coordination number of aluminum to be four.[13-17] Furthermore, the validity of the Lowenstein's rule[18] and the variation of T-O-T(T=Si,Al) bond angles were also discussed in terms of the compositional dependence of ^{29}Si chemical shifts.[16]

On the other hand, the connectivity of the network-forming tetrahedra,

SiO_4 and AlO_4, were still unknown which would have significant influence on the physical properties of this system.

In the present work, we observed the compositional dependence of the ^{29}Si MAS-NMR spectra of sodium aluminosilicate glasses in wide composition range. The role of aluminum in the silicate network structure in relation with the connectivity of SiO_4 and AlO_4 will be discussed based on the ^{29}Si NMR chemical shift analysis and peak separation.

3-2. Experimental Section

All samples were prepared from reagent grade Na_2CO_3, Al_2O_3 and SiO_2. Mixed starting materials were carefully melted in Pt-crucible at 1250 -1400°C for 3 hours. Then, quenched into water or liquid nitrogen to get optically clear glasses. The nominal compositions of the glasses are cited in Table1-2(a-e) and figure1. They are composed of five series in addition to the binary sodium silicates.[19] Series 1(a-d) are the glasses with composition of constant [Na]/[Si] ratios, while in series 4 is kept $N_{nbo}+N_{Al}=1.5$ with the following definition of N_{nbo},

Table 1. ^{29}Si chemical shift for glasses of series 1(see text).

syst	composition	chem. shift
Na_2O–SiO_2	$1Na_2O$–$3SiO_2$	−94.8
	$1Na_2O$–$2SiO_2$	−87.7
	$2Na_2O$–$3SiO_2$	−83.5
	$1Na_2O$–$1SiO_2$	−75.1
1a, Na_2O:SiO_2 = 1:3	$3Na_2O$–$1Al_2O_3$–$9SiO_2$	−92.0
1b, Na_2O:SiO_2 = 1:2	$20Na_2O$–$1Al_2O_3$–$40SiO_2$	−87.4
	$9Na_2O$–$2Al_2O_3$–$18SiO_2$	−85.8
	$4Na_2O$–$1Al_2O_3$–$8SiO_2$	−87.0
	$3Na_2O$–$1Al_2O_3$–$6SiO_2$	−87.8
	$2Na_2O$–$1Al_2O_3$–$4SiO_2$	−85.0
	$3Na_2O$–$2Al_2O_3$–$6SiO_2$	−84.7
	$11Na_2O$–$9Al_2O_3$–$22SiO_2$	−85.3
1c, Na_2O:SiO_2 = 2:3	$6Na_2O$–$1Al_2O_3$–$9SiO_2$	−81.2
	$4Na_2O$–$1Al_2O_3$–$6SiO_2$	−81.5
	$2Na_2O$–$1Al_2O_3$–$3SiO_2$	−80.9
1d, Na_2O:SiO_2 = 1:1	$9Na_2O$–$1Al_2O_3$–$9SiO_2$	−74.6
	$3Na_2O$–$1Al_2O_3$–$3SiO_2$	−75.0
5, Na_2O:Al_2O_3 = 1:1	SiO_2	−110.9
	$1Na_2O$–$1Al_2O_3$–$6SiO_2$	−97.9
	$1Na_2O$–$1Al_2O_3$–$4SiO_2$	−92.8
	$1Na_2O$–$1Al_2O_3$–$2SiO_2$	−86.0

Table 2. ^{29}Si chemical shift, peak intensity, and half width of each Q_n species. Numbers of non-bridging oxygen calculated from peak intensity are also shown on the right side.

N_{Al}		chem shift, ppm	intensity	half-width, ppm	NBO calc	N_{Al}		chem shift, ppm	intensity	half-width, ppm	NBO calc
				(a) Series 2a							
0.0	Q_2	−77.0	3	4.0	0.49	0.4	Q_3	−90.7	52	5.7	0.52
	Q_3	−92.2	47	5.6			Q_4	−101.0	48	7.2	
	Q_4	−105.6	50	6.5		0.5	Q_3	−89.9	52	6.0	0.52
0.1	Q_3	−92.2	50	5.5	0.50		Q_4	−99.3	48	7.4	
	Q_4	−105.0	50	6.5		1.0	Q_3	−86.8	55	6.4	0.55
0.2	Q_3	−92.2	52	5.5	0.52		Q_4	−94.0	45	7.4	
	Q_4	−104.1	48	6.5		1.5	Q_3	−83.5	65	6.1	0.66
0.3	Q_3	−91.0	53	5.7	0.53		Q_4	−90.1	35	7.0	
	Q_4	−102.4	47	7.2							
				(b) Series 2b							
0.0	Q_1	−67.2	3	3.0	1.47		Q_3	−84.9	58	5.7	
	Q_2	−76.6	42	3.4		0.4	Q_1	−67.0	3	3.6	1.44
	Q_3	−86.4	55	5.1			Q_2	−76.0	38	3.6	
0.1	Q_1	−67.0	4	3.6	1.47		Q_3	−83.9	59	5.9	
	Q_2	−76.5	41	3.5		0.5	Q_1	−67.0	3	3.6	1.42
	Q_3	−86.0	55	5.2			Q_2	−75.8	36	3.8	
0.2	Q_1	−67.0	2	3.6	1.48		Q_3	−83.0	61	6.2	
	Q_2	−76.5	43	3.6		1.0	Q_2	−75.6	60	5.2	1.60
	Q_3	−85.5	55	5.4			Q_3	−82.6	40	6.0	
0.3	Q_1	−67.0	2	3.0	1.43	1.5	Q_2	−73.5	55	4.8	1.55
	Q_2	−76.3	40	3.6			Q_3	−80.1	45	5.2	
				(c) Series 2c							
0.0	Q_0	−59.5	3	3.0	2.48	0.3	Q_0	−59.5	4	3.0	2.46
	Q_1	−66.7	39	2.4			Q_1	−66.5	36	2.4	
	Q_2	−75.6	54	3.8			Q_2	−74.6	56	4.5	
	(Q_3)	−85.0	4	5.0			(Q_3)	−84.5	4	5.0	
0.1	Q_0	−59.5	3	3.0	2.48	0.4	Q_0	−59.5	5	3.0	2.47
	Q_1	−66.7	39	2.4			Q_1	−66.3	36	2.5	
	Q_2	−75.3	53	4.0			Q_2	−74.0	56	4.6	
	(Q_3)	−85.0	5	5.0			(Q_3)	−84.5	3	5.0	
0.2	Q_0	−59.5	3	3.0	2.49	0.5	Q_0	−59.4	5	3.0	2.43
	Q_1	−66.6	38	2.4			Q_1	−66.1	34	2.5	
	Q_2	−74.9	55	4.2			Q_2	−73.5	59	4.8	
	(Q_3)	−84.5	4	5.0			(Q_3)	−84.5	2	5.0	
				(d) Series 3							
0.0	(Q_2)	−77.0	3	4.0	0.53		Q_4	−104.0	69	7.5	
	Q_3	−92.2	47	5.6		0.3	Q_3	−91.8	20	5.7	0.20
	Q_4	−105.6	50	6.5			Q_4	−103.0	80	7.8	
0.1	(Q_2)	−78.0	1	4.0	0.41	0.4	Q_3	−91.2	10	5.7	0.10
	Q_3	−92.5	39	5.4			Q_4	−103.0	90	8.3	
	Q_4	−105.0	60	7.0		0.5	Q_3	−90.0	3	5.7	0.03
0.2	(Q_2)	−78.0	1	4.0	0.32		Q_4	−101.5	97	9.0	
	Q_3	−92.3	30	5.7							
				(e) Series 4							
N_{Al} = 0.0	Q_1	−67.2	3	3.0	1.48	N_{Al} = 0.3	Q_1	−68.0	1	3.0	1.19
N_{nbo} = 1.5	Q_2	−76.6	42	3.4		N_{nbo} = 1.2	Q_2	−76.9	20	3.4	
	Q_3	−86.4	55	5.1			Q_3	−86.3	76	5.4	
N_{Al} = 0.1	Q_1	−67.8	1	3.0	1.33		Q_4	−97.6	3	5.5	
N_{nbo} = 1.4	Q_2	−76.8	33	3.4		N_{Al} = 0.4	Q_2	−78.2	15	3.4	1.10
	Q_3	−86.5	64	5.2		N_{nbo} = 1.1	Q_3	−87.5	80	5.4	
	Q_4	−97.2	2	5.5			Q_4	−98.6	5	5.5	
N_{Al} = 0.2	Q_1	−67.8	1	3.0	1.25	N_{Al} = 0.5	Q_2	−77.8	10	3.5	1.03
N_{nbo} = 1.3	Q_2	−76.8	26	3.4		N_{nbo} = 1.0	Q_3	−87.2	83.	5.5	
	Q_3	−86.3	70	5.4			Q_4	−97.4	7	5.5	
	Q_4	−97.2	2	5.5							

[a] N_{Al} represents 4[Al]/([Al] + [Si]).

$$N_{nbo} = \frac{[Na] - [Al]}{[Si]}, \qquad (1)$$

and N_{Al},

$$N_{Al} = \frac{4[Al]}{[Al] + [Si]}. \qquad (2)$$

Thus, N_{nbo} represents the numbers of non-bridging oxygen atom per one silicon atom. N_{Al} is the numbers of bridging oxygen atom which is shared by both of SiO_4 and AlO_4 tetrahedra. Each notation have their own meanings when the structural model mentioned above is assumed.When the Lowenstein's rule is obeyed, the $N_{Al'}$ will be more significant instead of N_{Al}.

$$N_{Al'} = \frac{4[Al]}{[Si]}. \qquad (3)$$

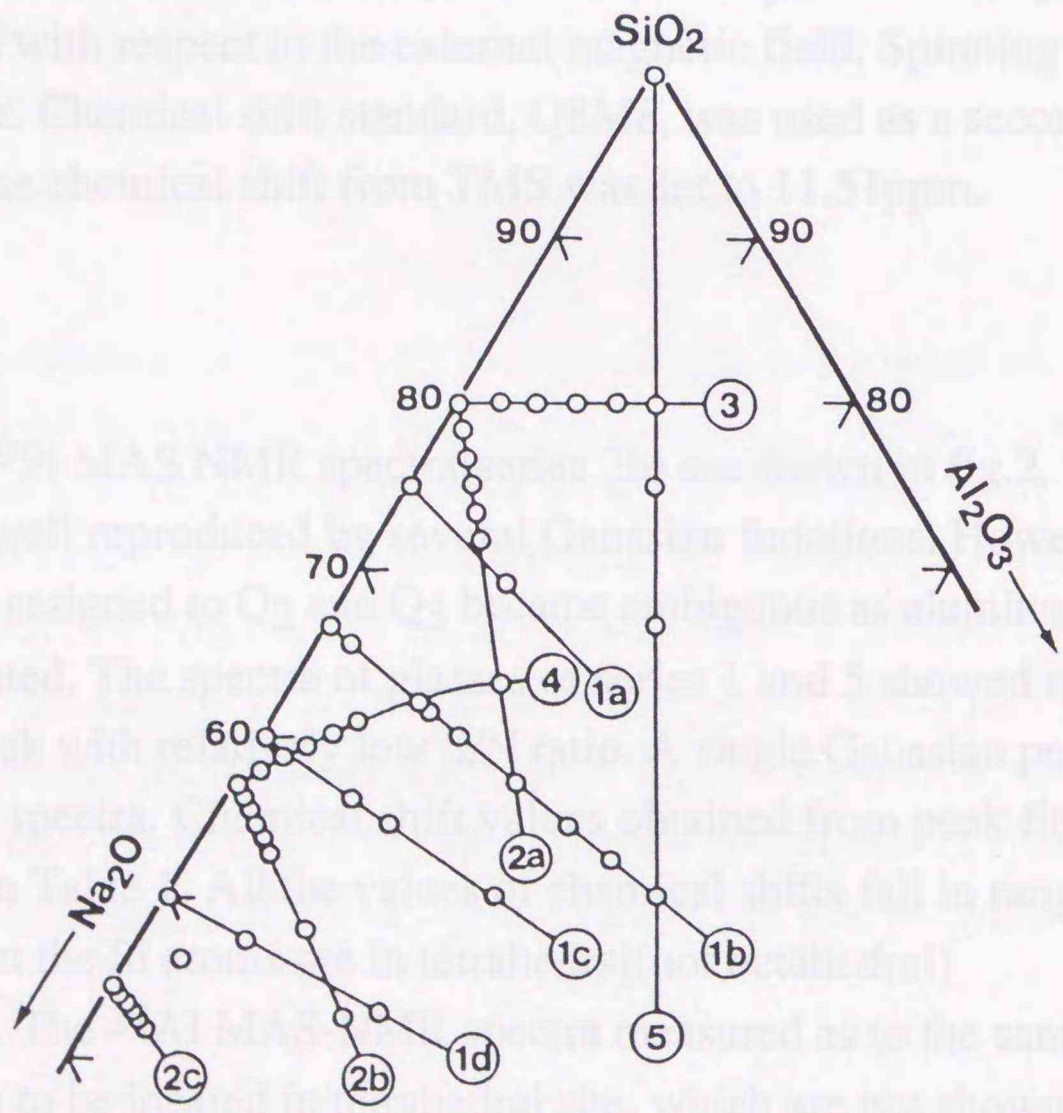

Figure 1. Five series of the glasses, investigated in the present study, shown in the somposition diagram for Na_2O-Al_2O_3-SiO_2 system.

Notations 2a, 2b and 2c represent systems having composition of $Na_2O \bullet 4SiO_2 + NaAlO_2$, $3Na_2O \bullet 4SiO_2 + NaAlO_2$ and $5Na_2O \bullet 4SiO_2 + NaAlO_2$, respectively, where N_{Al} ranged from 0 to 1.5 with constant N_{nbo} value, thus, the aluminum atom was introduced as $NaAlO_2$ into the binary sodium silicate glasses. Compositions of series 3 and 5 are $(1-x)Na_2O \bullet xAl_2O_3 \bullet 4SiO_2$ (x=0-0.5), and $xNaAlO_2 \bullet SiO_2$ (x=0-1.0), respectively. Each of the glass will be denoted such as 2a-1, 2a-2, 2a-3, ...etc.

0.05-0.1wt% Fe_2O_3 was added in some glasses(series 2,3,4) to reduce the relaxation time of ^{29}Si nuclei. No appreciable difference of the NMR spectra was found between glasses with and without Fe_2O_3. Measurements of ^{29}Si MAS-NMR was made with Bruker MSL-400(series 1 and 5 without addition of Fe_2O_3) and MSL-200 spectrometer(series 2,3,4) operated at 79.52 and 39.76 MHz for ^{29}Si, respectively. Typical accumulation time was 1 hour. Samples in an alumina sample holder were spun at the magic angle(54.74°) with respect to the external magnetic field. Spinning rate was 3500-4000 Hz. Chemical shift standard, Q8M8, was used as a secondary standard whose chemical shift from TMS was set to 11.51ppm.

3-3. **Results**

Typical ^{29}Si MAS NMR spectra(series 2b) are shown in fig.2. The spectra were well reproduced by several Gaussian functions. However, the distinct peaks assigned to Q_2 and Q_3 became ambiguous as aluminum ion was incorporated. The spectra of glasses of series 1 and 5 showed no more than single peak with relatively low S/N ratio. A single Gaussian peak was fitted in these spectra. Chemical shift values obtained from peak fitting are summarized in Table 1. All the values of chemical shifts fall in ranges expected when the Si atoms are in tetrahedral(not octahedral) environments. The ^{27}Al MAS-NMR spectra measured as to the same glasses show Al atom to be located in tetrahedral site, which are not shown here.

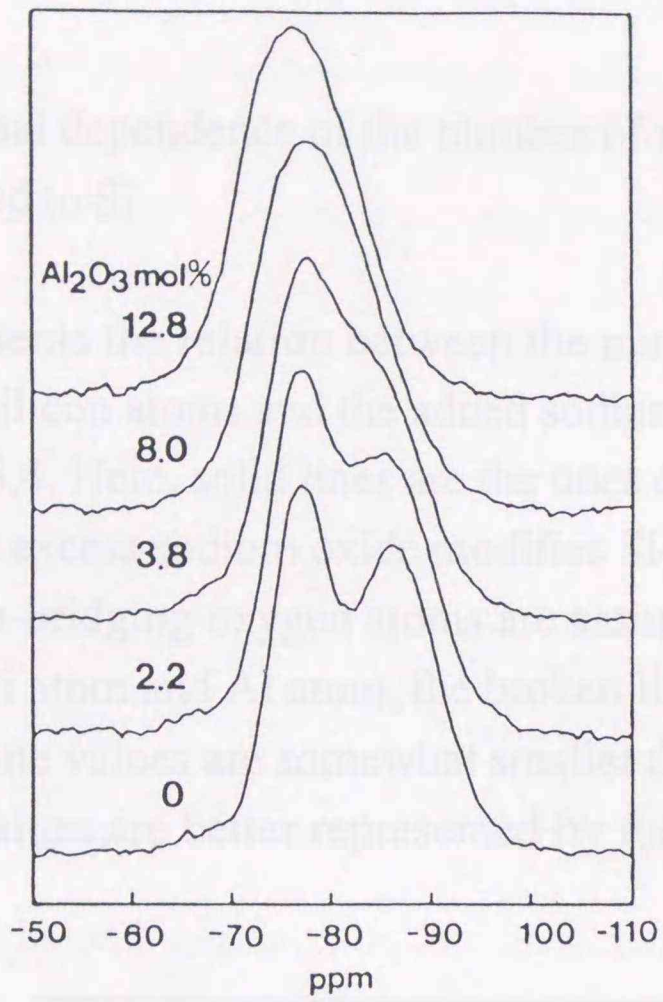

Figure 2. ^{29}Si MAS NMR spectra for series 2b glasses. Compositions are of the pseudo-binary $3Na_2O{\bullet}4SiO_2$-$NaAlO_2$.

While an addition of Al_2O_3 to sodium silicate glasses(series 1) caused mild change in ^{29}Si chemical shifts, the substitution of Si by NaAl(series 5) caused stronger shift to the positive direction.These trends are in agreement with the ^{29}Si NMR measurements for CaO-Al_2O_3-SiO_2 glass system.[17] Furthermore, as the results of the series 2 glasses(table 2(a-c)) clearly show, the effects of substitution of SiO_2 by $NaAlO_2$ upon the ^{29}Si chemical shifts are different for each Qn's. The peak position of the more polymerized site, for example Q_3 site in series 2b glasses, is strongly affected by the addition of $NaAlO_2$ than that of the less polymerized site.

3-4. Discussion

3-4-1. Compositional dependence of the number of non-bridging oxygen atoms connected to Si

Figure 3 represents the relation between the number of non-bridging oxygen atoms per silicon atoms and the added sodium aluminate in the glasses of series 2,3,4. Here, solid lines are the ones calculated with the assumption that the excess sodium oxide modifies Si-O-Si bond exclusively. Alternatively if non-bridging oxygen atoms are assumed to be associated equally with both Si atom and Al atom, the broken lines are obtained. Although the absolute values are somewhat smaller than the expected ones, the experimental values are better represented by the former postulate.

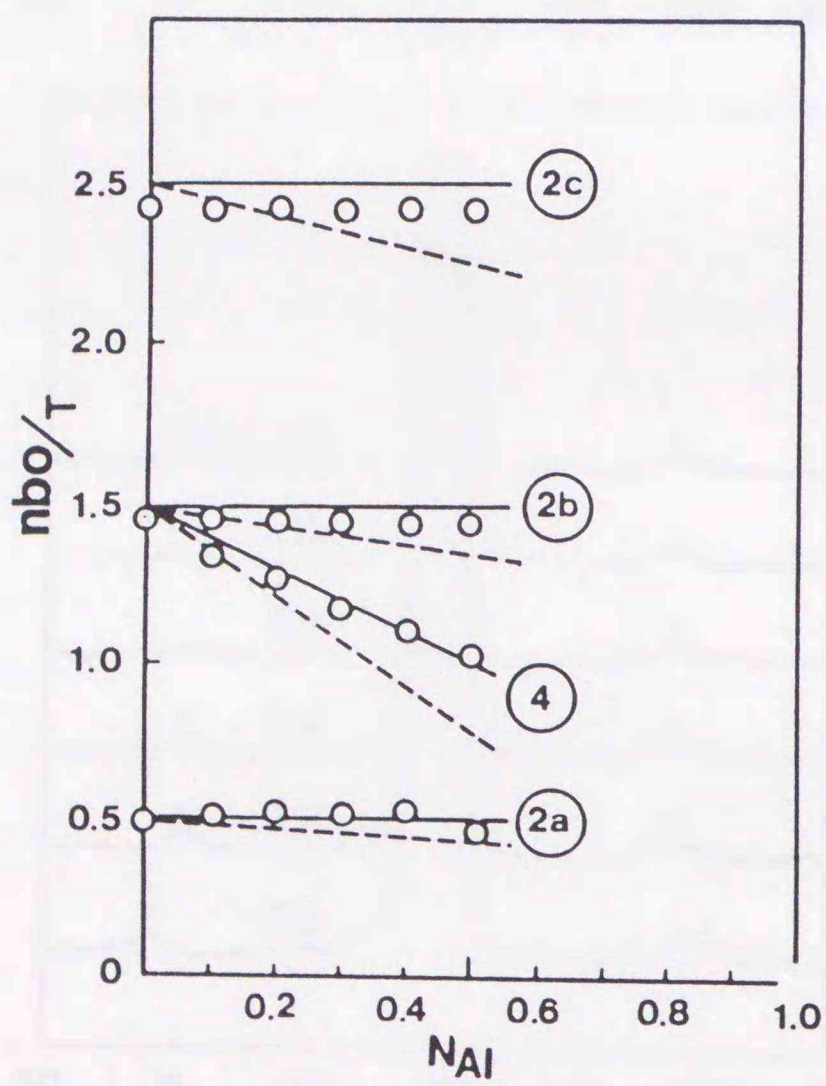

Figure 3. Numbers of non-bridging oxygen atoms per tetrahedral atom([Al]+[Si]). Open circles represent the results obtained from NMR peak area analysis. Lines represent values of {[Na]-[Al]}/[T] where [T] stands for [Si] which is shown by solid lines, and [Al]+[Si] by broken lines.

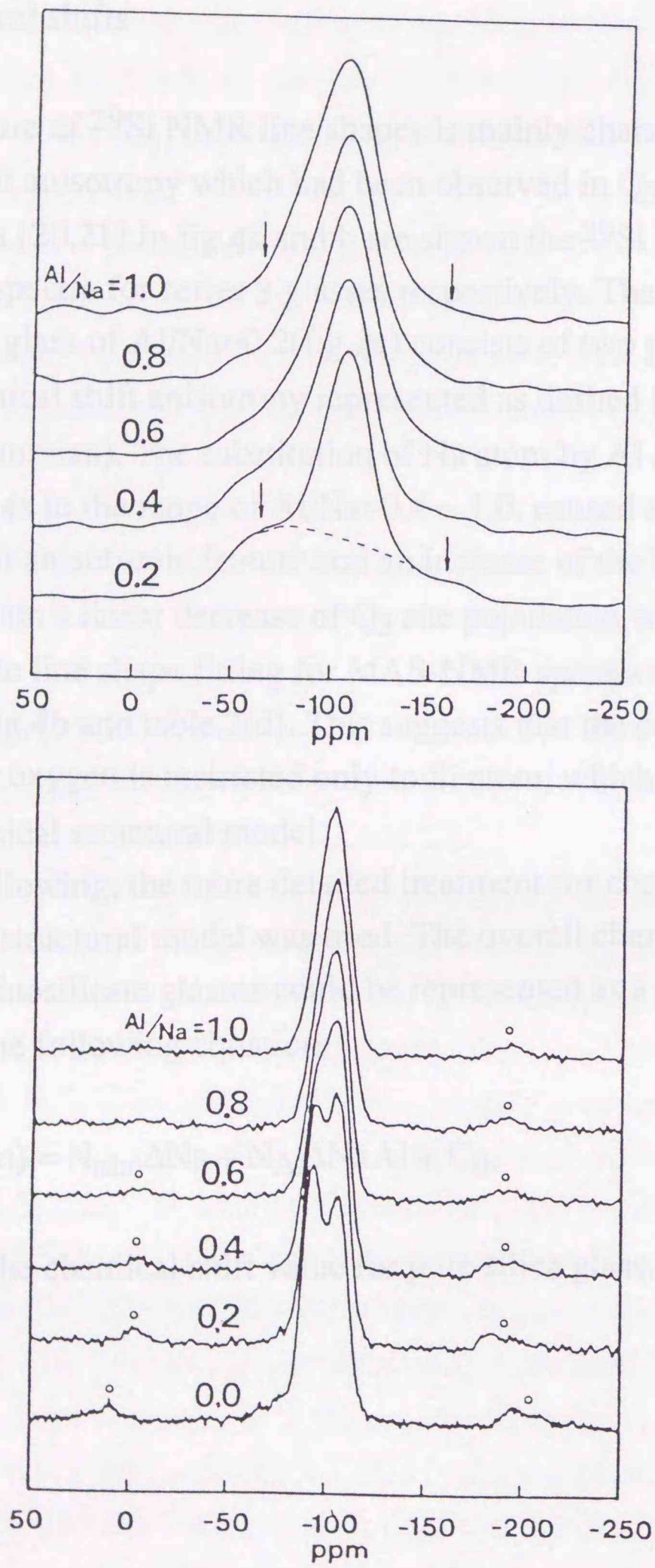

Figure 4. Broad line NMR(above) and MAS NMR(below) spectra for series 3 glasses. In the above, composition of the Al/Na=0.0 is missing. Open circles shown in the below represent spinning side bands.

3-4-2 Chemical shifts

The feature of ^{29}Si NMR line shapes is mainly characterized by the the chemical shift anisotropy which had been observed in Q_3 ,Q_2 and Q_1 environments.[20,21] In fig.4a and b are shown the ^{29}Si broad line and MAS-NMR spectra for series 3 glasses respectively. The broad line NMR spectrum for glass of Al/Na=0.2(fig.4a) consists of two peaks, Q_3 which showed chemical shift anisotropy represented as dashed line, and Q_4 site(single Gaussian). The substitution of Na atom by Al atom which is shown in fig.4a in the range of Al/Na=0.4 ~ 1.0, caused a decrease of chemical shift anisotropic feature and an increase of the broadening of Q_4 peak. We obtain a linear decrease of Q_3 site population with {[Na]-[Al]}/[Si] ratios from the line shape fitting for MAS-NMR spectra of this glass which is shown in fig.4b and table.2(d). This suggests that the connection of the non-bridging oxygen is restricted only to Si atom, which is in agreement with the classical structural model.

In the following, the more detailed treatment for chemical shift analysis based on the structural model was tried. The overall chemical shifts of sodium aluminosilicate glasses could be represented as a function of N_{nbo} and N_{Al} by the following equation.

$$\delta(\text{ppm}) = N_{nbo}\Delta Na + N_{Al}\Delta NaAl + C_0, \qquad (4)$$

where C_0 is the chemical shift value for pure silica glass. ΔNa and $\Delta NaAl$

represent the ^{29}Si chemical shift induced on a Si atom of interest. Each of them means the effect of substitution of the SiO_4 tetrahedra at the next nearest neighbor(NNN) from the silicon atom of interest by a Na, which cause a NBO formation, and a $NaAlO_4$, which cause a Si-O-Al bond formation, respectively.

As was seen in binary sodium silicate glasses, the chemical shifts do not depend linearly upon N_{nbo}.[19] The composition dependence of chemical shifts became gentle as alkali cation contents increased. Thus, the ΔNa and ΔNaAl will further depend on the bulk glass composition in the following way,

$$\Delta Na = C1 \bullet N_{nbo} + C2 \bullet N_{Al} + C3 \qquad (5)$$

$$\Delta NaAl = C2 \bullet N_{nbo} + C4 \bullet N_{Al} + C5, \qquad (6)$$

where ΔNa and ΔNaAl are assumed to depend linearly on the amount of Na and/or $NaAlO_4$ that already exist at the NNN of the Si atom in interest. They are represented by constants C1, C2 and C4.

The constants C0 to C5 were determined from the least square fit for 54 experimental values of weighted mean ^{29}Si chemical shifts in two cases. When the Lowenstein's rule was obeyed, in this case the N_{Al} can be expressed as 4[Al]/[Si], the constants were given as C0=-110.0, C1=-3.6, C2=-1.7, C3=24.2, C4=-0.8 and C5=9.7. When it was not obeyed, in this case the $N_{Al'}$ instead of N_{Al} is significant, the constants were given as C0= -111.0, C1=-3.5, C2=-2.8, C3=24.6, C4=-1.3 and C5=14.6. The standard deviation was 0.90 and 0.92, respectively. These results suggest the induced ^{29}Si chemical shift by one NNN substitution is almost twice as large for Na than $NaAlO_4$. The lines of iso-chemical shift calculated from the present experimental data with eqs.(4) to (6) are shown in fig.5a. Irrespective of the condition, whether the Lowenstein's rule is obeyed or not, both sets show reasonable fits. The iso-chemical shift lines change their slopes at the compositions near [Na]/[Al] = 1 and these changes are drastic in the SiO_2 poor region especially when the Lowenstein's rule was not taken into consideration. The chemical shift value for $CaAl_2SiO_6$ glass[16] was well

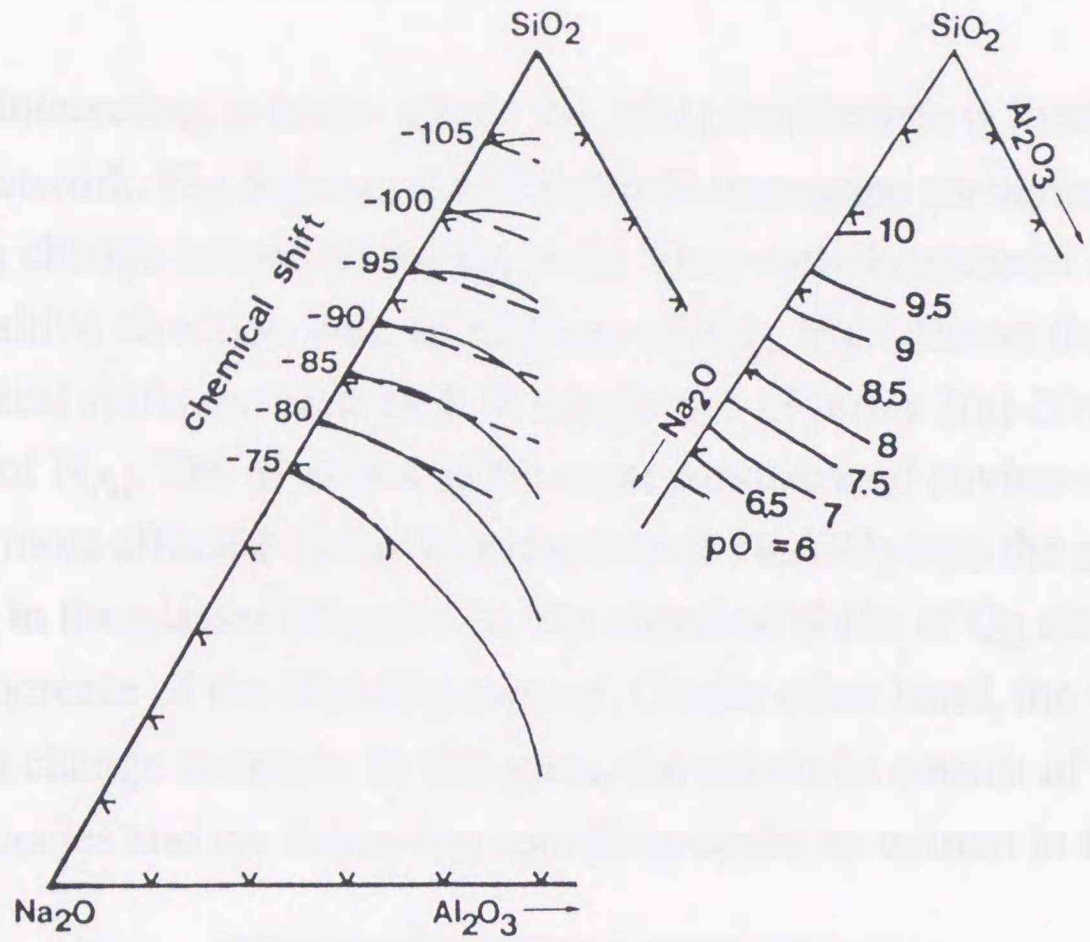

Figure 5. Left; ^{29}Si NMR iso-chemical shift lines as a function of the composition. Each line obtained from the best fit for experimental data by equation(2). Solid lines represent the results when the Lowenstein's rule is taken into consideration, whereas broken lines do not. Right; thermodynamic basicity derived from electro-motive force measurements.[22]

reproduced by the latter postulate.

It had been shown that the ^{29}Si NMR chemical shifts have a potential parameter for the scale for basicity.[19] The thermodynamic basicities for this system(fig.5b),[22] which was defined by $pO=-\log(a_{Na_2O})$ where a_{Na_2O} denotes the thermodynamic activity of Na_2O determined from E.M.F. measurements, show close similarity with ^{29}Si iso-chemical shift lines.

3-4-3 Location of AlO_4 tetrahedron

It is interesting to know where the AlO_4 tetrahedron is located in the silicate network. Fig.6 shows the ^{29}Si NMR line shape for series 2b glasses. The main change occurs on the Q_3 peak. They were broadened and shifted to the positive direction with an increase of N_{Al}. Fig.7 shows the changes of the chemical shifts for each peak in the glasses of series 2(a)-2(c) as a function of N_{Al}. The Si atoms in the most polymerized environment in the glass are most affected by the introduction of $NaAlO_2$ into the glass. For example, in the glasses of series 2c, the chemical shifts of Q_2 site increase with an increase of the $NaAlO_2$ content. On the other hand, the values for Q_1 do not change so much. In this glass, the networks consist of mainly Q_2 and Q_1 species and the following equilibria could be written in the

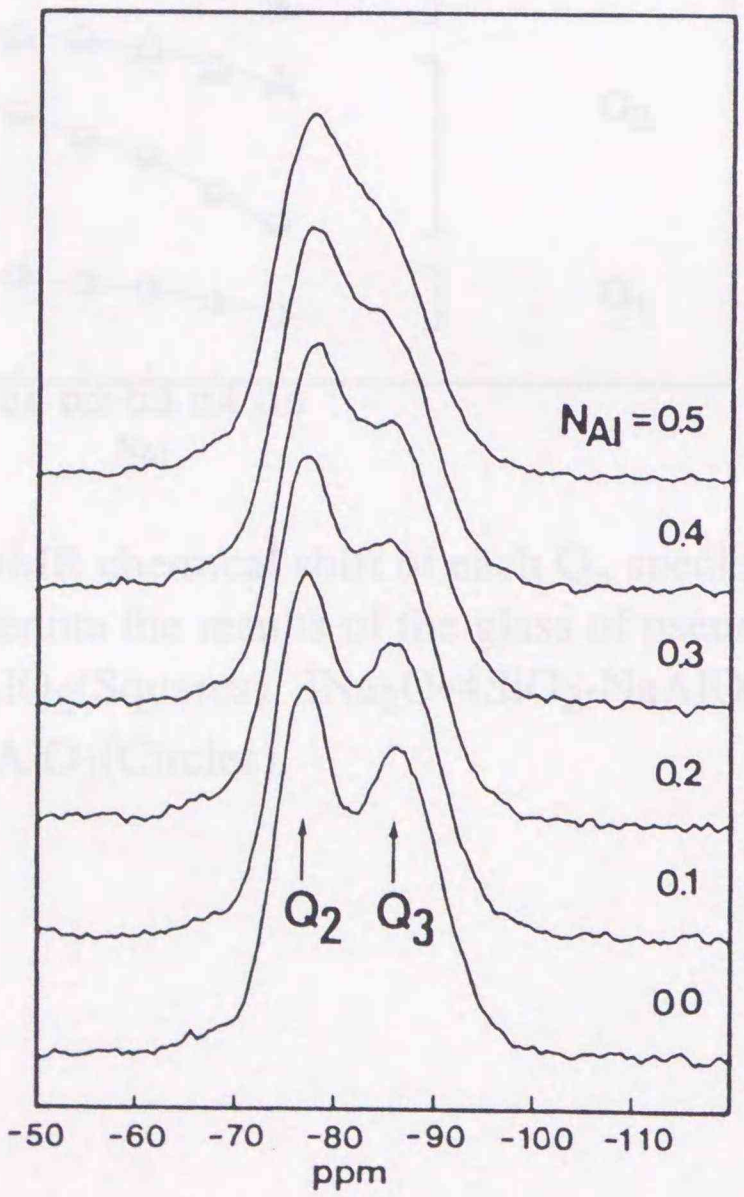

Figure 6. ^{29}Si MAS NMR spectra for series 2b glasses. Compositions are of the pseudo-binary $3Na_2O \bullet 4SiO_2$-$NaAlO_2$. An expansion plot of figure 2.

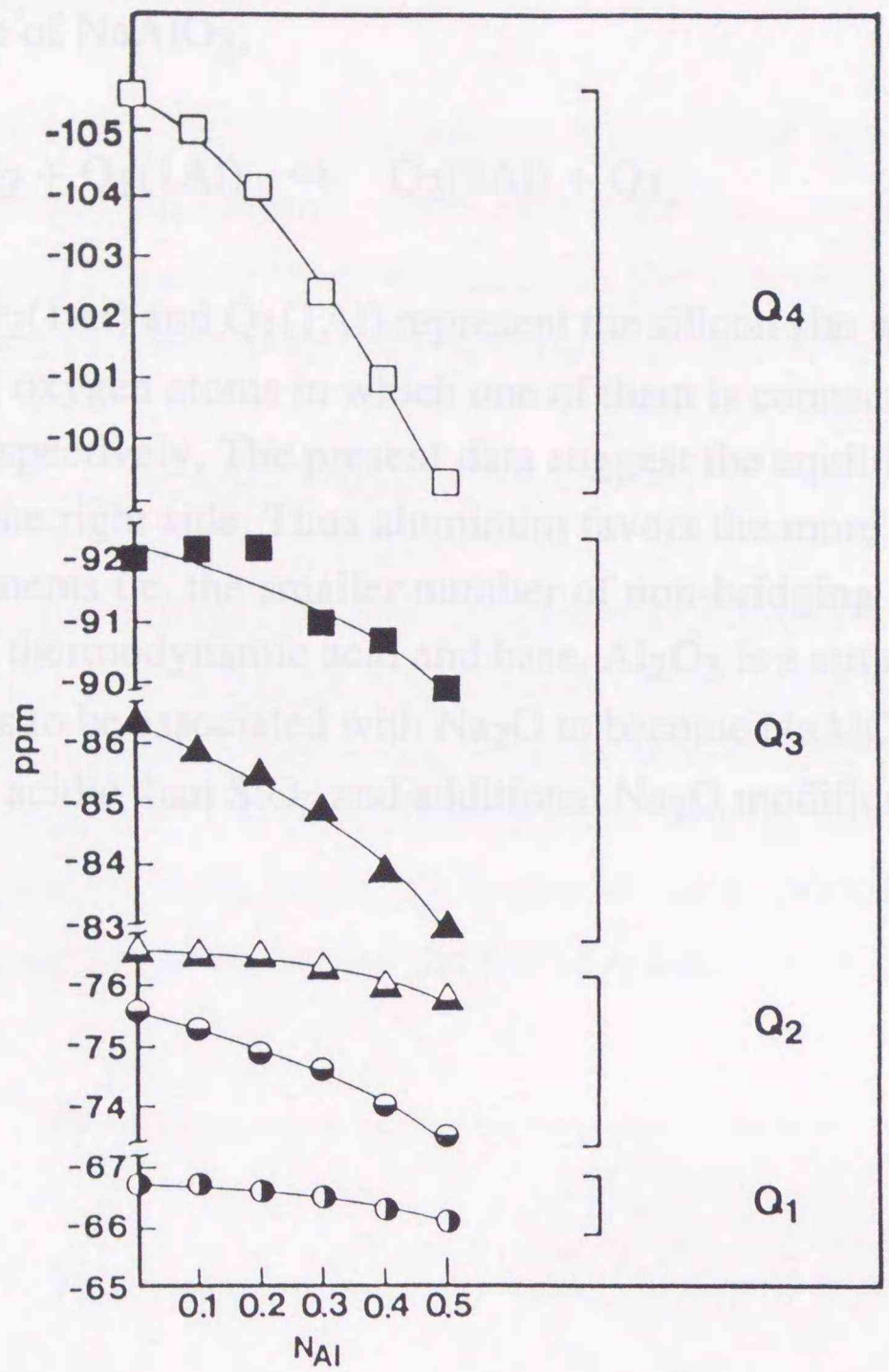

Figure 7. ^{29}Si NMR chemical shift of each Q_n species as a function of N_{Al} values. Symbols denote the results of the glass of pseudo-binary systems of $Na_2O{\bullet}4SiO_2$-$NaAlO_2$(Squares), $3Na_2O{\bullet}4SiO_2$-$NaAlO_2$(Triangless), and $5Na_2O{\bullet}4SiO_2$-$NaAlO_2$(Circles).

presence of $NaAlO_2$,

$$Q_2 + Q_1(1Al) \leftrightarrow Q_2(1Al) + Q_1, \qquad (7)$$

where $Q_2(1Al)$ and $Q_1(1Al)$ represent the silicon site with two and one bridging oxygen atoms in which one of them is connected to aluminum atom, respectively. The present data suggest the equilibria of reaction (7) shift to the right side. Thus aluminum favors the more polymerized environments i.e. the smaller number of non-bridging oxygen atoms. In terms of thermodynamic acid and base, Al_2O_3 is a stronger acid than SiO_2 and tends to be associated with Na_2O to become $NaAlO_2$, while $NaAlO_2$ is no more acidic than SiO_2 and additional Na_2O modifies not $NaAlO_2$ but SiO_2.

3-4-4 Q_n distribution

Basic oxides modify SiO_2 network depending upon their basicity or inversely upon the cationic power of the alkali cation which is defined by the charge(Z) divided by ionic radius(r). In addition to this, the resultant Q_n species are further affected by basicity in their distribution,

$$2Q_n \leftrightarrow Q_{n-1} + Q_{n+1}. \qquad (8)$$

Thus, the stronger the cationic power of the alkali cation the more the reaction (8) go to the right direction.[19] The Q_n distribution for N_{Al}=0.5 glasses derived from the present work is shown in fig.8 together with the previous results of sodium silicate glasses. The Q_n distribution suggests that the equation (8) shifts to the left with addition of $NaAlO_2$. This supports the opinion mentioned above that the $NaAlO_2$ acts as a base in sodium silicate glasses.

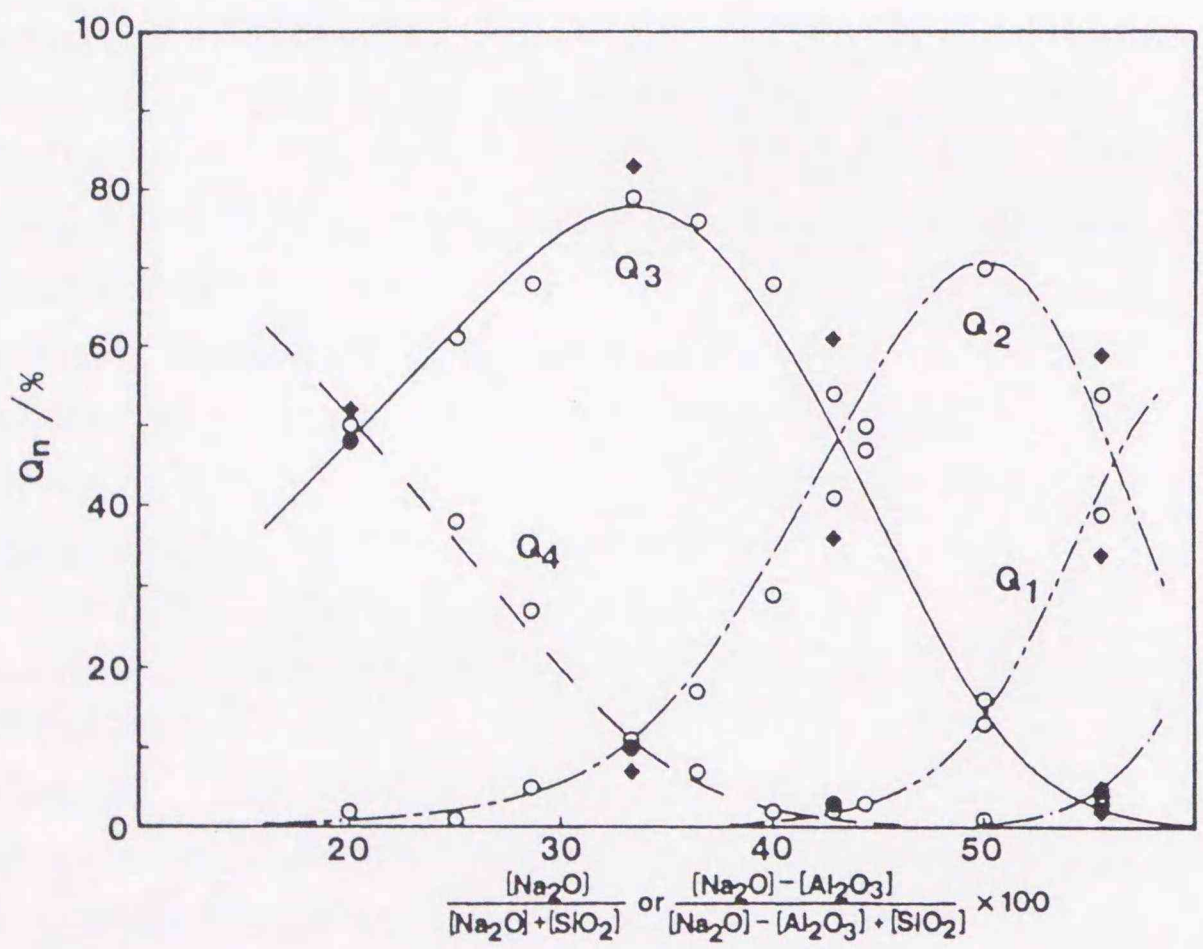

Figure 8. Q_n distributions as a function of contents of Na_2O.(○) binary sodium silicate glasses;[20], (◆) present work at N_{Al}=0.5.

3-5. Summary of Chapter 3

^{29}Si MAS NMR were investigated on sodium aluminosilicate glasses. The results indicate (1) that the number of non bridging oxygen atoms could be determined by excess amount of sodium ions over aluminum ions and in terms of thermodynamic acid-base, $NaAlO_2$ is no more acidic than SiO_2 and additional Na_2O modifies not $NaAlO_2$ but SiO_2, although Al_2O_3 is more acidic than SiO_2 and is preferentially attacked by Na_2O to become $NaAlO_2$, (2) that the aluminum ion favors the site in the rather polymerized part of silicate network, and (3) that introduction of Al_2O_3 induces the positive shift of ^{29}Si NMR peak in addition to the chemical rearrangement reactions.

references

1) Galant,E.I. The Structure of Glass(Translated from Russian) Consultants Bureau: New York, 1960, **Vol.2**, 451, Proceedings of the Third All-Union Conference on the Glassy State, Leningrad, 1959.
2) Day,D.E.; Rindone,G.E. J.Am.Ceram.Soc., **45**, 489(1962).
3) Lacy,E.D. Phys.Chem.Glasses, **4**, 234(1963).
4) Shelby,J.E. J.Appl.Phys., **49**, 5885(1979).
5) Riebling,E.F. J.Chem.Phys., **44**, 2857(1966).
6) Klonkowski,A. Phys.Chem.Glasses, **24**, 166(1983).
7) Bruckner,R.; Chun,H.-U.; Goretzki,H.; Sammet,M. J.Non-Cryst. Solids, **42**, 49(1980).
8) Smets,B.M.J.; Lommen,T.P.A. Phys.Chem.Glass., **22**, 158(1981).
9) Taskere,G.W.; Uhlmann,D.R.; Onorato,P.I.K.; Alexander,M.N.; Struck,C.W. J.Physiq, **C8**-273(1985).
10) Taylor,M.; Brown Jr,G.E., Geochim.Cosmochim.Acta, **43**, 1467(1979).
11) McKeown,D.A.; Waychunas,G.A.; Brown Jr,G.E., J.Non-cryst.Solids, **74**, 349(1985).
12) Domine,F.; Piriou,B. Am.Mineral., **71**, 38(1986).
13) Murdoch,J.B.; Stebbins,J.F.; Carmichael,I.S.E. Am.Mineral., **70**,332(1985).
14) Kirkpatrick,R.J.; Oestrike,R.; Weiss Jr,C.A.; Smith,K.A.;Oldfield,E. Am.Mineral., **71**, 705(1986).
15) DeJong,B.H.W.S.; Schramm,C.M.; Parziale,V.E. Geochim.Cosmochim.Acta, **47**, 1223(1983).
16) Oestrike,R.; Yang,W.-H.; Kirkpatrick,J.; Hervig,R.L.; Navrotsky,A.; Montez,B Geochim.Cosmochim.Acta, **51**, 2199(1987).
17) Engelhardt,G.; Nofz,M.; Wihsmann,F.G.; Magi,M.; Samoson,A.; Lippmaa,E. Phys.Chem.Glass., **26**, 157(1985).
18) Lowenstein,W. Am.Mineral., **39**, 92(1954).
19) Maekawa,H.; Maekawa,T.; Kawamura,K.; Yokokawa,T. J.Non-cryst.Solids, **127**, 53(1991)
20) Stebbins,J.F. Nature, **330**, 465(1987).
21) Wilson,M.A. NMR techniques and applications in geochemistry and soil chemistry, Pergamon press: Oxford, 1987, Chapter5.
22) Itoh,H.; Yokokawa,T., Trans.J.I.M., **25**, 879(1984).

CHAPTER 4

A HIGH TEMPERATURE ^{29}Si NMR STUDY OF SODIUM SILICATE MELT

Abstract of Chapter 4

A high temperature NMR probe which is suitable for the study of NMR chemical shifts and line shapes up to 1200°C was developed. This made possible in-situ high temperature measurements on sodium silicate melts for the nucleus of ^{29}Si in the temperature range of room temperature to 1200°C. Some experimental uncertainties, which came from the contamination of B_2O_3 from the sample container into sample having a basic composition(Na_2O>40%), were left unsolved. However, the composition variation of the temperature effects on silicate melts structure were investigated by means of chemical shift analysis. The peak position, referred to that of the glass sample having same composition, linearly shifted towards positive direction as increasing temperature in the composition of $Na_2O \bullet 3SiO_2$. However, as the Na_2O contents of the sample increased, the temperature effects gradually changed so that the ^{29}Si peak shifted to the negative direction as increasing temperature. Thus, the temperature effects on silicate melt structure seem to depend on the composition. The origin which causes ^{29}Si chemical shift seems complex, however, variation of Si-O-Si bond angles and the equilibrium among Q_n species seeming dominant.

On the other hand, ^{29}Si NMR spectra show narrowing just above the glass transition temperature, due to the exchange reaction among various structural species constructing the melt network. The line shapes were analysed by means of a multi-site exchange model, and averaged exchange rates(τ_{ex}), which contain both of the rearrangement, and the chemical exchange reaction were estimated. A rough relation between τ_{ex} and viscosities were observed.

4-1 Introduction

It is well known that the NMR spectroscopy provides useful information on structures and dynamics of liquids and solids. However, ordinary NMR apparatus is applicable only for measurements up to 500 °C. In the present paper, we describe a new probe suitable for NMR spectrometer with ppm resolution over 1200 °C. The purpose of this work is to solve some technical problems associated with high temperature experiments for NMR in order to observe the temperature variation of ^{29}Si NMR spectra for silicates in the glassy and molten states in which the structure and dynamic properties have not been well understood[1].

Recently, Stebbins et al. developed a high temperature and ppm resolution NMR apparatus and applied it to silicate melts[2]. In their apparatus, samples were rapidly shuttled between a furnace and a radio frequency(rf) coil which was kept cool by a rapid flow of air in order to avoid thermal and electric disturbances from the furnace. More recently, they used a new probe for relaxation measurement which was furnished with a heater at the center of the magnet, although the detail has not been described[3]. Coutures et al. reported a laser heated high temperature probe operated over 2000 °C, and applied it to the study of molten salts[4]. Because of the heating method, attainment of the thermodynamic equilibrium might be difficult. In the present work, we set two heating units on the upper and lower sides of the center of the magnet[5,6].

Silicates have three-dimensional network structure made from tetrahedron units whose corner oxygen atom is shared by another tetrahedron or modified by alkali oxide, as described in the preceding chapter. ^{29}Si NMR spectra of the silicate compounds give structural information about the coordination environment of the Si nucleus.

In the present investigation, high temperature ^{29}Si NMR measurements were made on sodium silicate melts up to 1200°C to study the temperature effect on the structure and dynamics of molten sodium silicates.

4-2 Description of the apparatus

Three types of high temperature probe have been developed. The first one is suitable for high resolution measurements up to 1200°C which we call HR-1. There are two other types HP-1 and HP-2 for high power measurements up to 1200°C(HP-1) and high power measurements up to 1800°C(HP-2), respectively. In this chapter, results obtained by HR-1 are presented. Details of HP-1 prove will be explained in chapter 7.

Figure 1(a) shows the details of the HR-1 prove[7]. Platinum wire (0.4 mmϕ) threaded through two-hole tube (3.0 mmϕ) of high purity alumina surrounds a core alumina tube (15 mmϕ) except for the zone of center of the rf coil made of 1.0 mmϕ platinum wire. The heater current flows through two platinum wires in the same alumina tube opposite in direction so as not to produce an additional magnetic field across the sample volume. Condensers of the tuning circuit were thermally insulated with a copper pipe cooled by water. The whole assembly of the high temperature probe loaded in a water jacket made of copper and brass was inserted in the superconducting magnet.

4-3 Experimental section

During experimental runs, the condition of the furnace was monitored by a mirror placed on the upper part of the magnet. The electrical power was supplied from a stabilized dc power unit. The heater current and the applied voltage was 20 A and 40 V, respectively at the maximum furnace temperature of 1450 °C. The maximum temperature was attained in two hours. The sample capsule made of boron nitride (Fig. 1 (b)) was placed in the center of the rf coil(non-spinning). In order to avoid the oxidation of the capsule, nitrogen gas atmosphere was maintained during experiments. However, the contamination of B_2O_3 from the sample container into sample having a basic composition(Na_2O>40%), was serious. To avoid this, measurement period must be minimized(less that a few seconds) for such samples. Sample temperature was measured by a Pt-Pt(Rh) thermocouple attached below the bottom of the capsule. The sample temperature was 1200 °C when the center of the furnace was 1450 °C. No drift of magnetic field was found during heating and cooling cycles. However, the quality factor of

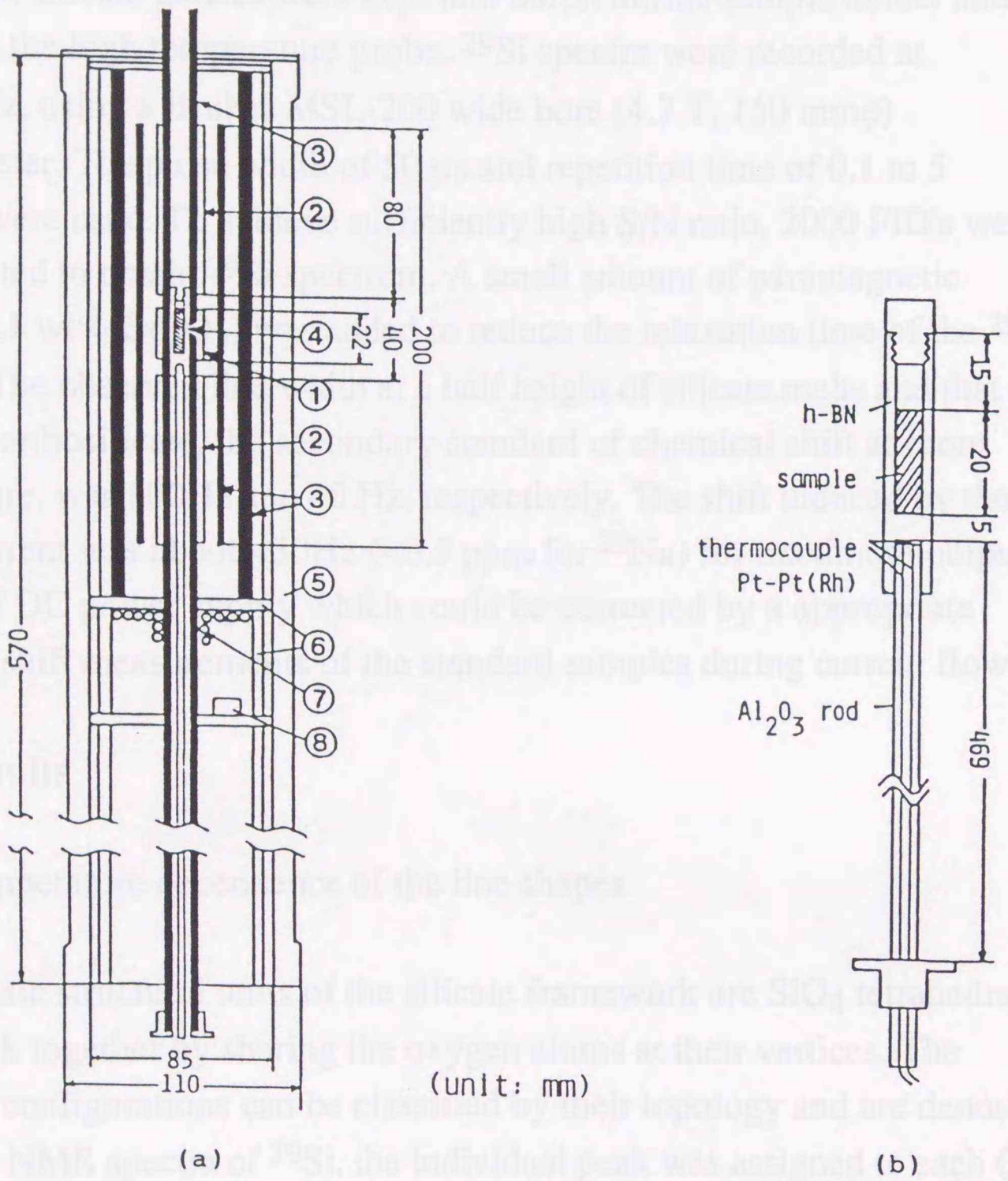

Figure 1. (a) Schematic representation of the high temperature NMR probe. 1:rf coil, 2:platinum heater (0.4 mmd), 3:Al_2O_3 tube, 4:h-BN sample holder, 5:Cu-brass water jacket, 6:Ti-Al alloy (KS-130AV) stand, 7:copper pipe water cooler, 8:tunning circuit. (b) Cross section of the sample holder.

the rf coil decreased considerably above 800 °C because of increase of its resistance.

Sodium silicate glasses were kept into boron nitride sample holder and melted in the high temperature probe. ^{29}Si spectra were recorded at 39.76MHz, using a Bruker MSL-200 wide bore (4.7 T, 150 mmϕ) spectrometer. The pulse width of 50 μs and repetition time of 0.1 to 5 seconds were used. To achieve sufficiently high S/N ratio, 2000 FID's were accumulated to obtain ^{29}Si spectrum. A small amount of paramagnetic reagent(0.1 wt% Gd_2O_3) was added to reduce the relaxation time of the ^{29}Si nucleus. The observed line width at a half height of silicate melts and that of tetraethylorthosilicate, the secondary standard of chemical shift at room temperature, was 100Hz and 40 Hz, respectively. The shift induced by the heater current was about <30Hz (<0.5 ppm for ^{23}Na) for maximum output current of DC power supply which could be corrected by a appropriate chemical shift measurements of the standard samples during current flow.

4-4 **Results**

4-4-1 Temperature dependence of the line shapes

The basic structural units of the silicate framework are SiO_4 tetrahedra which link together by sharing the oxygen atoms at their vertices. The resulting configurations can be classified by their topology and are denoted by Q_n. In NMR spectra of ^{29}Si, the individual peak was assigned to each Q_n species.(as shown in chapter2 and 3) For example, the broad line ^{29}Si NMR spectrum for $Na_2O{\bullet}3SiO_2$ glass (Figure 2(a)) consists of two components corresponding to Q_3 and Q_4 units shown by dashed and dotted lines, respectively. The Q_3 spectrum is asymmetric due to the chemical shift anisotropy.

As increasing temperature, a chemical exchange reaction between distinct chemical species is taking place. The resultant NMR spectrum will be modified, if the rate of the exchange reaction(r_{ex}) becomes comparable to the difference of the resonance frequency between distinct chemical

species($\Delta\nu_0$). r_{ex} is further related to the life time of the species(τ_{ex}) which will be given by the inverse of r_{ex}.

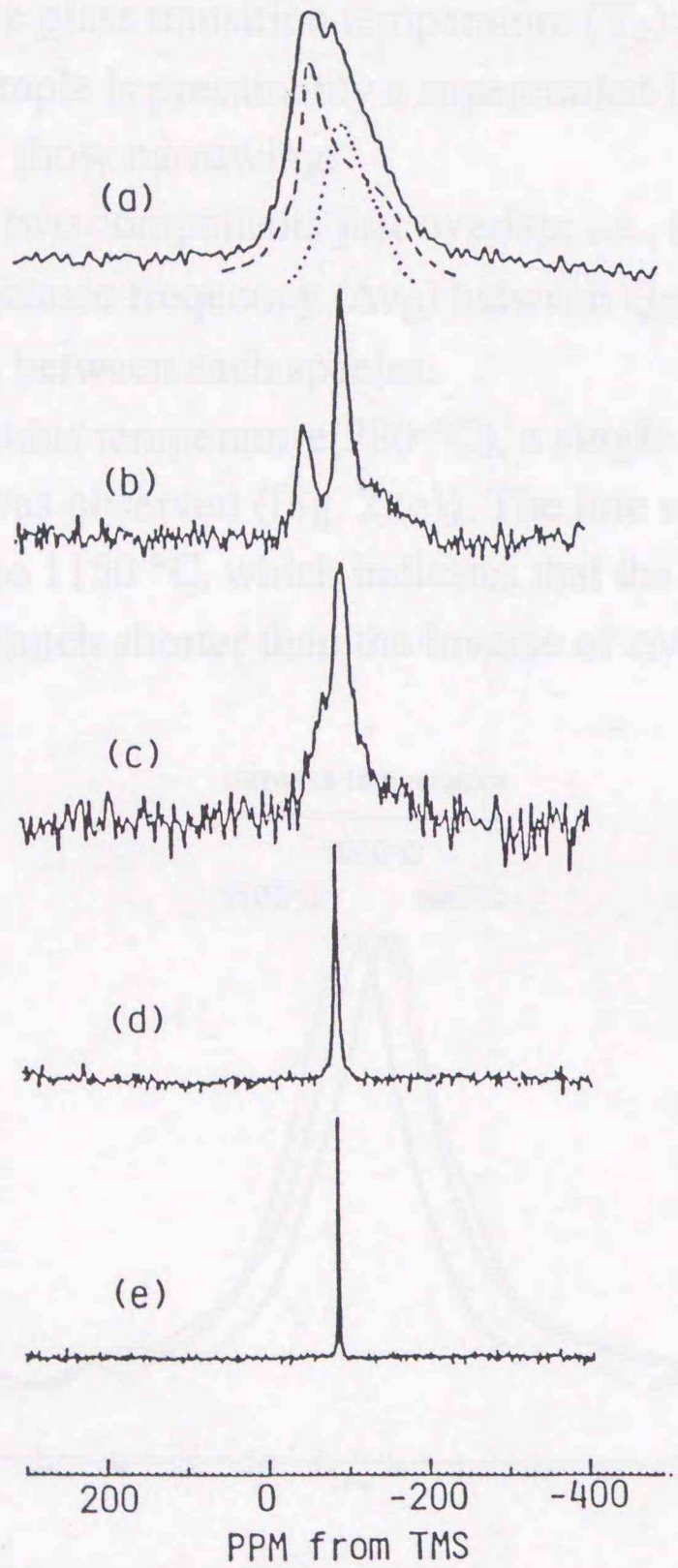

Figure 2. Temperature variation of ^{29}Si spectra for $Na_2O{\bullet}3SiO_2$ glass and liquid. (a) 20°C, (obtained by commercial broad line high power probe), (b) 550°C, (c) 670°C, (d) 770°C, and (e) 865°C.

In the glassy state, the rate of chemical exchange would be infinite. In the $Na_2O \bullet 3SiO_2$ glass, the difference of resonance frequency between Q_3 and Q_4 , ($\Delta\nu_0$) was derived to be 490 Hz from MAS-NMR of the same glass at room temperature.(Chapter 2) Shown in Fig.2(b)-(e) is the temperature dependence of ^{29}Si NMR spectra of $Na_2O \bullet 3SiO_2$ glass and melt. Around 550 °C (just above glass transition temperature (T_g) of this glass(T_g=505 °C), where the sample is presumably a supercooled liquid) the line width of both components show narrowing.

At 670 °C, the two components just overlap; i.e., the inverse of the difference of resonance frequency ($\Delta\nu_0$) between Q_3 and Q_4 sites becomes comparable to r_{ex} between each species.

Above the liquidus temperature(780 °C), a single and sharp profile of Lorentzian type was observed (Fig. 2 (e)). The line width does not change above 865 °C up to 1150 °C, which indicates that the lifetime of each species becomes much shorter than the inverse of $\Delta\nu_0$.

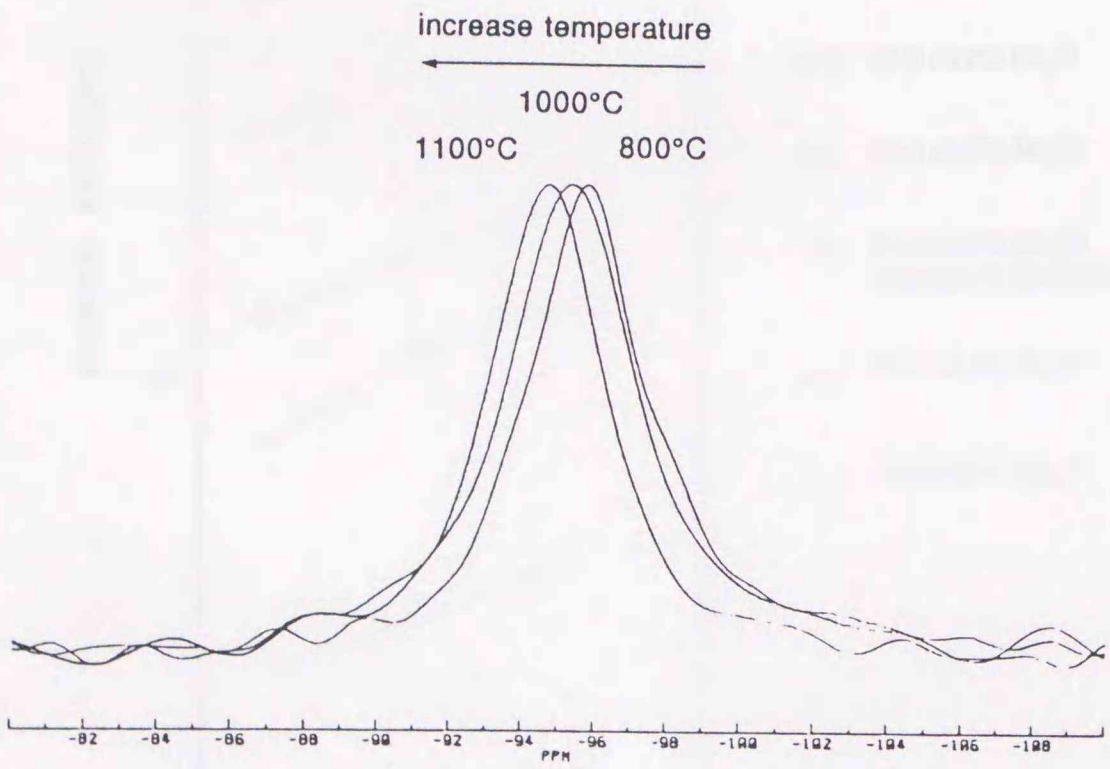

Figure 3. High temperature ^{29}Si NMR spectra for $Na_2O \bullet 3SiO_2$ melt.

4-4-2 Effect of temperature on ^{29}Si chemical shifts

As shown in figure 3, the peak position of ^{29}Si NMR spectrum for $Na_2O \bullet 3SiO_2$ melt shifted to positive direction (less shielded) as increasing temperature in agreement with the previous report which was made on sodium and lithium silicates by Stebbins and Farnan[8].

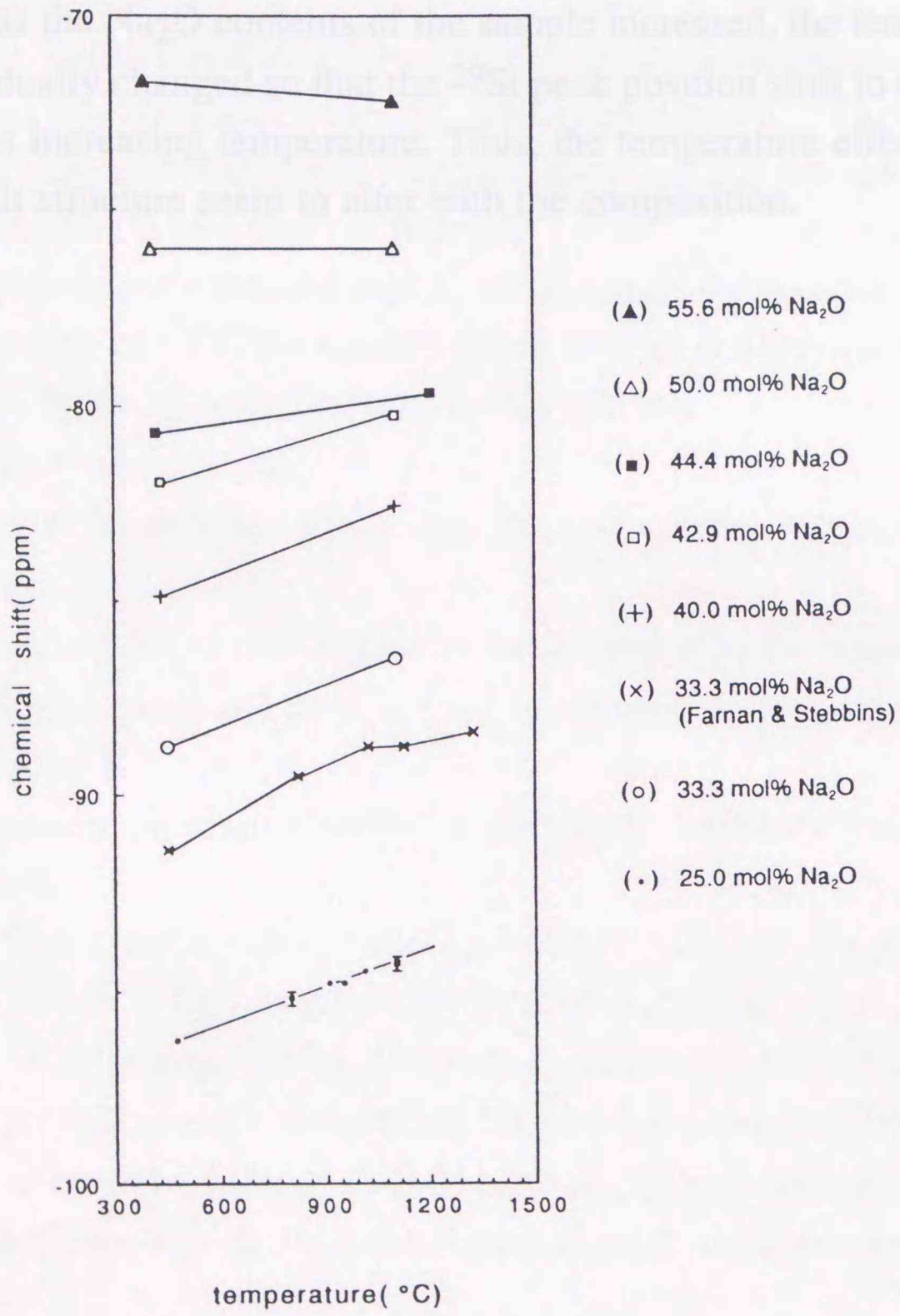

Figure 4. Temperature dependence of the ^{29}Si chemical shifts for Na_2O-SiO_2 system. Chemical shifts for glass samples(measured at room temperature) are plotted at T_g.

A series of measurements are made on sodium silicate melts of various sodium oxide contents. The results are summarized on figure 4. The center of gravity of MAS NMR spectra for glassy samples are plotted. A linear dependence upon temperature is observed when the value of glass is plotted at corresponding T_g's.

As shown in figure 4, the peak position, referred to that of the glass sample of the same composition, linearly shifted towards positive direction as increasing temperature in the $Na_2O \bullet 3SiO_2$ composition. However, as the Na_2O contents of the sample increased, the temperature effects gradually changed so that the ^{29}Si peak position shift to negative direction as increasing temperature. Thus, the temperature effect on silicate melt structure seem to alter with the composition.

4-5 Discussion

4-5-1 Relationships between chemical shift and melt structure

As shown above ^{29}Si NMR of the silicates, at the molten state, shows no more than a single peak because of the rapid exchange reactions between the structural units which may exist in the melts. The chemical shift value for the molten silicate, therefore, gives a structure averaged over the several structural units.

The ^{29}Si chemical shift is affected by the structural change associated with glass to liquid transition through supercooled liquid. The origin which causes ^{29}Si chemical shift seems complex. However, the possible structural changes would be summarized as follows.

1) An increase of Si-O-Si bond angles, which causes ^{29}Si positive shift[9] as demonstrated by MAS NMR measurements of various silicate crystals.

2) The equilibrium reaction between the Q_n species,

$$2Qn \leftrightarrow Q_{n-1} + Q_{n+1}, \qquad (1)$$

moves to the right direction with increasing temperature, which may cause negative shift.

3) An increase of Na_2O which remains unchanged after the reaction between alkaline oxide and silica at basic compositions. This effect causes ^{29}Si negative shift.

4) An increase of mean coordination number of Si, which causes ^{29}Si negative shift.

Among four reasons above, only one instance which causes positive shift is variation of the Si-O-Si bond angles. A relationship between Si-O-Si bond angles and ^{29}Si chemical shifts[9] in various silicate crystals are shown in figure5. The positive shift observed on $Na_2O \bullet 3SiO_2$ and $Na_2O \bullet 2SiO_2$ is likely caused by an increase of Si-O-Si bond angles with increase of temperature because of the well developed network structure expected on

the silica rich composition.

On the other hand, as the Na_2O content increased, the network structure becomes more modified and the units constructing the network structure become discrete each other. Thus the Si-O-Si angles might be less affected by the liquid formation. The negative shift of ^{29}Si peak position would be explained by the fact that the equilibrium reaction(1) moves to the right direction as increasing temperature, which would cause negative shift because the difference of chemical shift between Q_n species, $\delta(Q_{n-1}) - \delta(Q_n)$ getting smaller as decreasing n as shown in chapter 2.

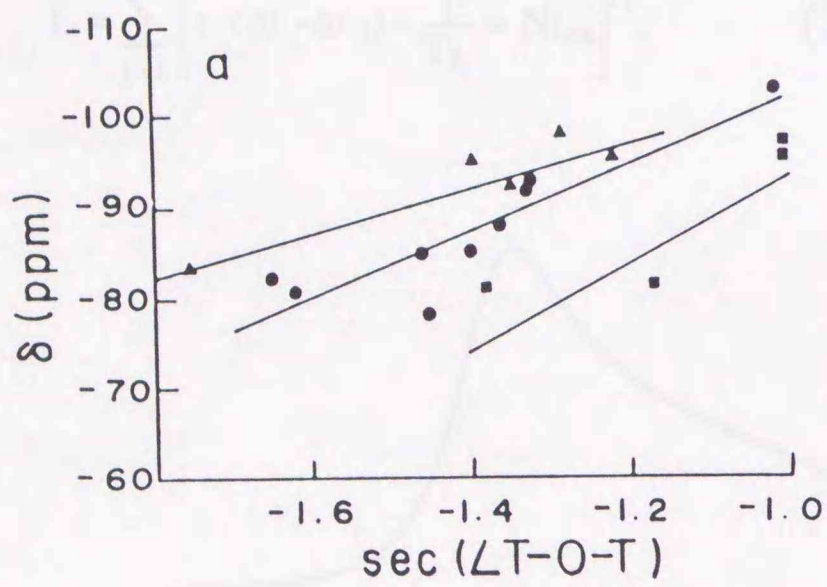

Figure 5. Relation between ^{29}Si chemical shift and mean secant Si-O-Si bond angle per tetrahedron. Symbols are in (a)Q_3(▲), Q_2(●), and Q_1(■).[9]

4-5-2 Estimation of the rates of exchange reaction between Q_n species

The temperature variation of ^{29}Si chemical shift has been successfully analysed in terms of multi-site exchange model[10], by Stebbins et al[11]. When the room temperature spectrum, having infinite life time of the species, is divided into N individual peaks with equilivalent intensities, thus the spectrum is assumed to be constructed from N numbers of micro-structural units, as shown in figure 6, then the line shape function($g(\omega)$) in the presence of the exchange reaction among N species with its rate of r_{ex} can be written as,

$$g(\omega) = \frac{1}{N} \frac{L}{1 - r_{ex} \cdot L}, \qquad (2)$$

where,

$$L = \sum_{j=1}^{N} \left[\imath\ (\omega - \omega_i) - \frac{1}{T_{2_j}} + N r_{ex} \right]^{-1}. \qquad (3)$$

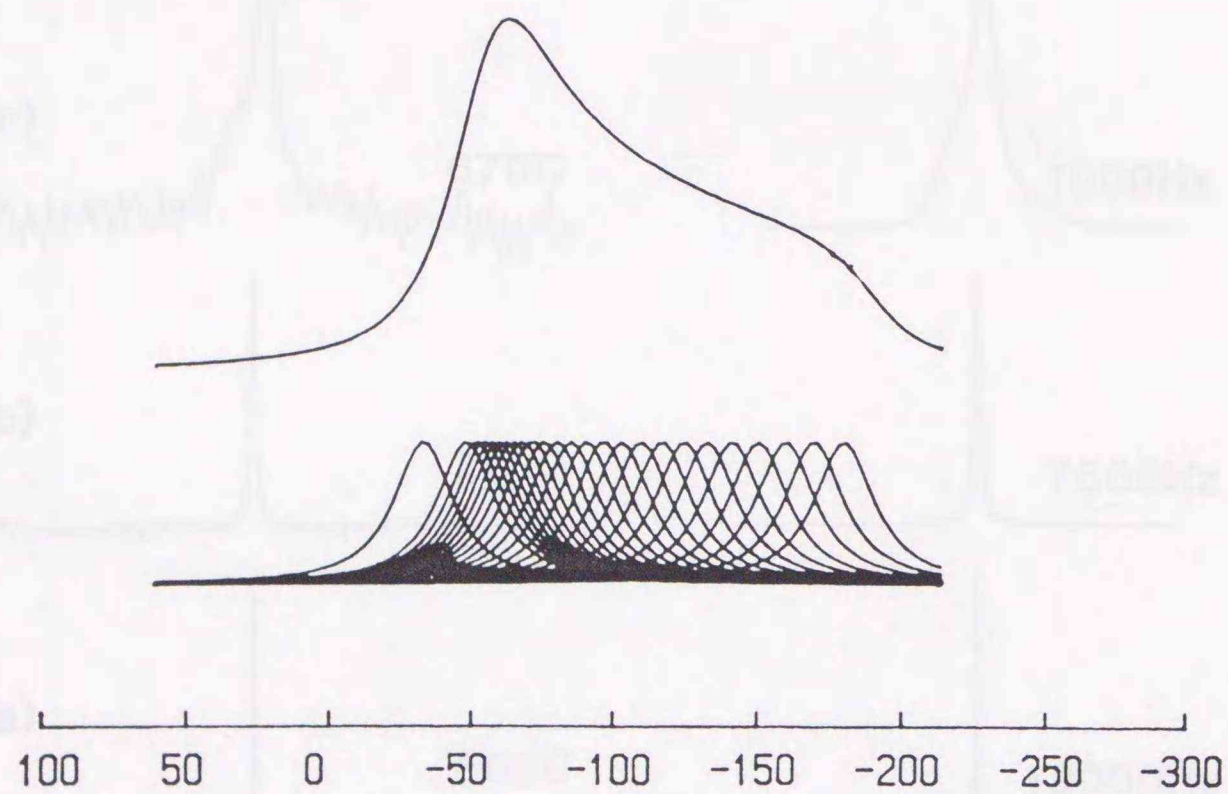

Figure 6. An example of peak separation of NMR spectrum into numbers of equal intensity peaks.

Here ω_j and $\frac{1}{T_{2_j}}$ is are the peak position and the line width of the j-th component, respectively.

The line shapes and their simulation by equation(2) and (3) applied to $Na_2O{\bullet}3SiO_2$ melts are shown in figure 7. The room temperature spectrum is split into 5000peaks with equal intensities concerning the dipolar-diploar broadening caused by the coupling between ^{29}Si and ^{23}Na nuclei. As temperature elevated up to 550°C, the dipolar broadening is no more taken into account due to the rapid motion of the sodium nucleus.

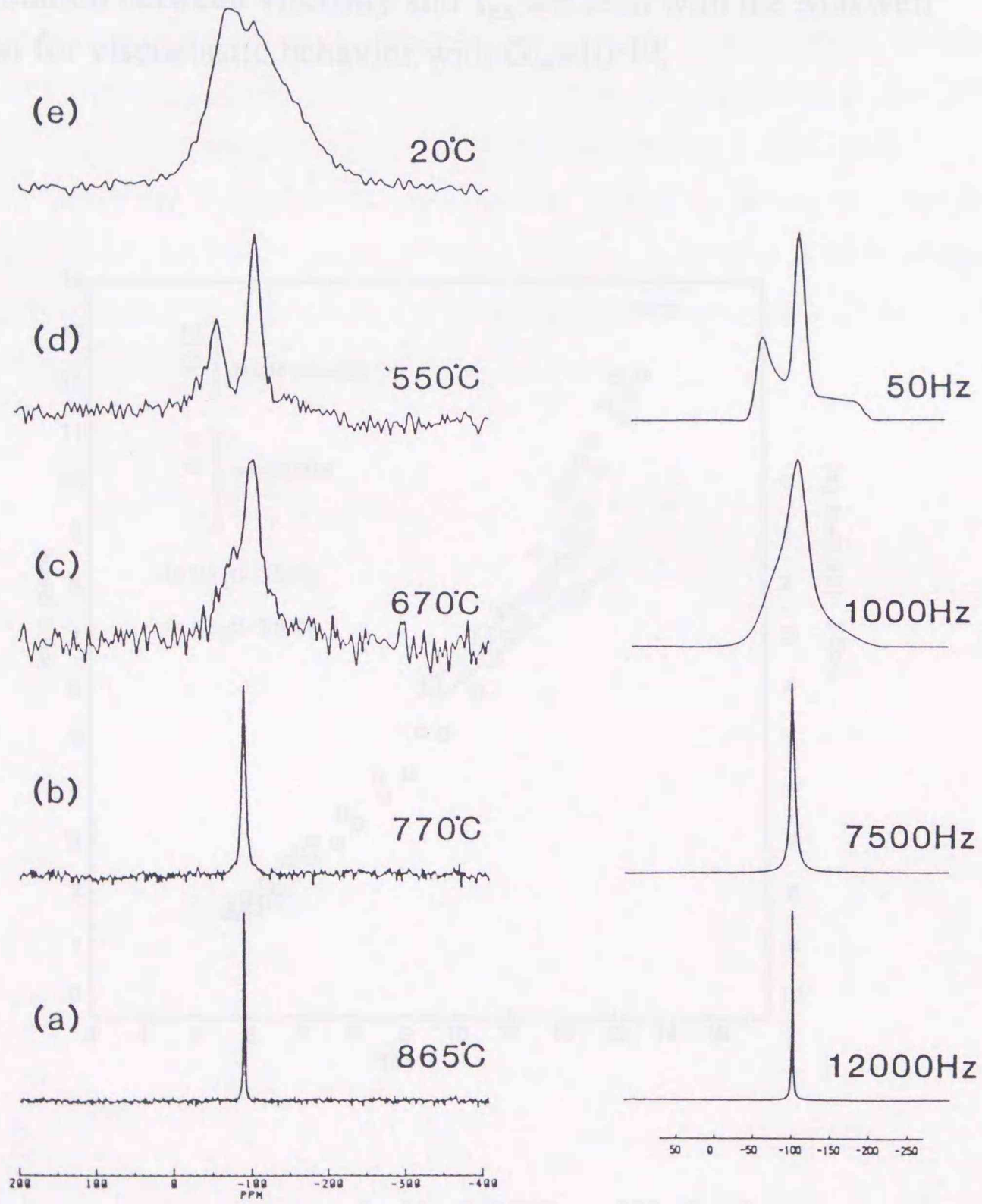

Figure 7. (Right) High temperature ^{29}Si NMR spectra for $Na_2O{\bullet}3SiO_2$ melt. (Left) Line shape simulation of multi-site exchange model with r_{ex} shown in the figure.(see text)

In the sense of equation (2) and (3), r_{ex} contains both of the rearrangement and the chemical exchange reaction. At the highest temperature, the exchange rates are underestimated due to the broadening of the line width caused by the limitation of the resolution of the apparatus. The exchange rates linearly increased as a function of the reciprocal absolute temperature with the activation energy of about 150kJ/mol, which is close to that derived from viscosities[12]. A comparison between viscosity and $\tau_{ex}(=1/r_{ex})$ are shown in figure 8. A rough relation between viscosity and τ_{ex} are seen with the Maxwell equation for viscoelastic behavior with $G_{\infty}=10^{-10}$.

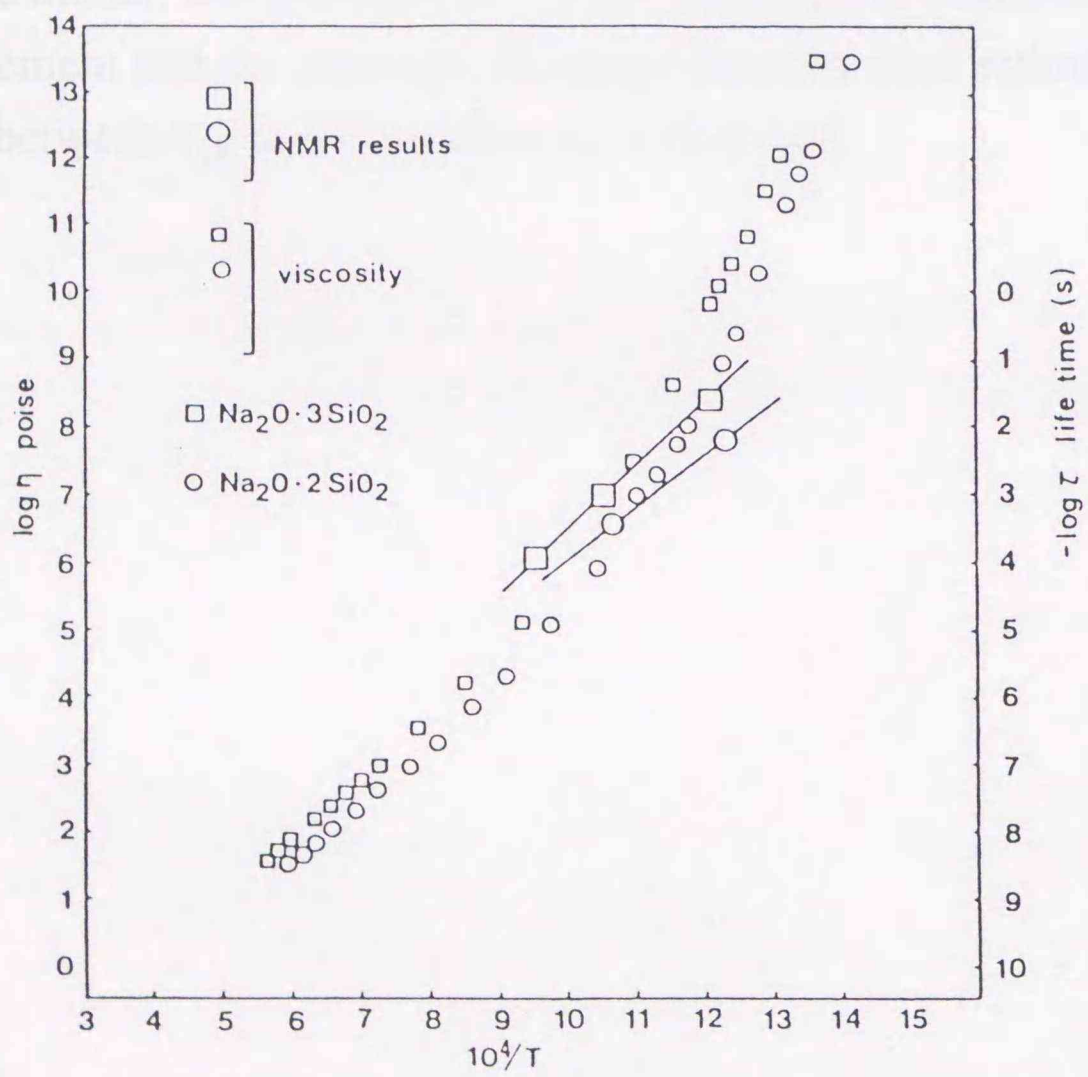

Figure 8. Relationships between τ_{ex} for $Na_2O{\bullet}2SiO_2$ and $Na_2O{\bullet}3SiO_2$ derived from line shape simulation and viscosities[12] plotted against inverse absolute temperature.

Summary of chapter 4

High temperature ^{29}Si NMR chemical shift and line shape measurements are made on sodium silicates up to 1200°C. The peak position, referred to that of the glass having the same composition, linearly shifted towards positive direction as increasing temperature in the composition of $Na_2O \bullet 3SiO_2$. However, as the Na_2O contents of the sample increased, the temperature effects gradually changed and the ^{29}Si shift moved to negative direction as increasing temperature. Thus, the temperature effects on silicate melt structure seem to alter with composition. The origin which causes ^{29}Si chemical shift seems complex. However, variation of Si-O-Si bond angles and the equilibrium among Q_n species seem dominant.

On the other hand, the line shapes were analysed by means of a multi-site exchange model, and averaged exchange rates(r_{ex}), in which both of the rearrangement and the chemical exchange reaction were estimated. A rough relation between τ_{ex} and viscosities were observed.

references

(1) B.O.Mysen, "*Structure and Properties of Silicate Melts*," in "Developments in Geochemistry, Vol. 4," Elsevier, Amsterdam(1988), p.27.

(2) J.F.Stebbins, E.Schneider, J.B.Murdoch, A.Pines, and I.S.E.Carmichael, Rev. Sci. Instrum., **57**, 39(1986).

(3) S.-B. Liu, A.Pines, M.Brandriss, and J.F.Stebbins, Phys.Chem.Minerals, **15**, 155(1987).

(4) J.P.Coutures, D.Massiot, J.C.Rifflet, and F.Taulelle, Bruker Report, **2**/1988, 9.

(5) T.H.DeFries and J.Jonas, J.Magn.Reson., **35**, 111(1979).

(6) S.Shimokawa and E.Yamada, J.Magn.Reson., **51**, 103(1983).

(7) S.Shimokawa, H.Maekawa, E.Yamada, T.Maekawa, Y.Nakamura, and T.Yokokawa, Chem.Lett., 617(1990/**4**)

(8) J.F.Stebbins and I.Farnan, Science, **255**, 586(1992)

(9) R.J.Kirkpatrick, K.A.Smith, S.Schramm, G.Turner, and W-H.Yang, Ann.Rev.Earth Planet.Sci., **13**, 29(1985)

(10) M.Mehring, in "*Principles of High Resolution NMR in Solids*", Springer-Verlag, New York(1983), pp 61

(11) I.Farnan and J.F.Stebbins, J.Am.Chem.Soc., **112**, 33(1990)

(12) J.O'M.Bockris, J.D.Mackenzie, and J.A.Kitchener, Trans.Faraday Soc., **51**, 1734(1955)

CHAPTER 5

A HIGH TEMPERATURE ^{23}Na NMR STUDY OF COORDINATION NUMBERS OF SODIUM ION IN SILICATE MELTS

Abstract of chapter 5

High temperature ^{23}Na NMR measurements were made on some sodium salts and silicates. The temperature dependence of the ^{23}Na NMR chemical shifts especially around their melting points have been observed for sodium salts. Simple ionic salts, such as NaCl, NaBr and $NaNO_3$, show positive shift of ^{23}Na NMR peak position on their solid-liquid transition which indicates the decrease of average coordination numbers around sodium ion on their molten states compared with corresponding crystalline state.

On the other hand, the ^{23}Na peak position of sodium silicate melts showed almost linear dependence on temperature. Comparison of the chemical shift of silicate melts with crystalline silicates suggested the coordination number of sodium ions in silicate melts to be 7 to 8 independent of the composition.

5-1. Introduction

Alkali cations are involved in most of multi-component silicate systems which compose geological and industrial materials. The alkali cations modify the silicate network to produce non-bridging oxygen. Little has been known about the coordination environment around alkali cations in the molten silicates compared with the network forming cations. The coordination environments of the alkali ion is often to be ill-defined, especially in the well developed network structure, e.g. framework aluminosilicates[1]. However, some structural studies concerning ^{23}Na NMR chemical shifts on alkali feldspars[2-4] demonstrated the ^{23}Na NMR is

a potential tool to study the structural information for both of crystalline and glassy samples.

On the other hand, in some high temperature ^{23}Na NMR study[5-7] ^{23}Na line shape has been discussed in terms of the dynamics. However, there has been paid relatively less attention to the structural sensitivity of the isotropic chemical shift for ^{23}Na.

In the present study, ^{23}Na NMR chemical shift measurements for sodium silicate and sodium aluminosilicates were made well above the melting points. The results are compared with the chemical shift of crystalline samples obtained from MAS NMR measurements. ^{23}Na chemical shifts of some inorganic salts below and above their melting points were also measured to compare with those of the results for silicates.

5-2.Experimental section

NMR measurements were carried out on Bruker MSL-200 spectrometer with wide bore(150mm) magnet operated at 52.938MHz for ^{23}Na nucleus. High temperature NMR line shapes and chemical shifts were observed with a home build high temperature NMR probe as described in chapter 4, HR-1, which was modified for this experiments. An rf coil was placed at the center of a single heater unit. A Helmholtz rf coil was made of platinum and wound 4 times and placed parallel to the applied magnetic field.

Temperature of the sample was measured by Pt-Pt(Rh) thermocouple placed 1mm below the bottom of the sample. Heater current was supplied by a stabilized DC power source controlled manually. Temperature drift was ±1°C during each experimental run. External chemical shift standard, 3M NaCl solution, was measured at the beginning and the end of the experiments with the current flow of the electric heater which influences on the position of the NMR peaks(heater current induces 0.5ppm shift at maximum output(800W)). The typical error for chemical shift was 1 ppm.

A series of MAS NMR measurements were made on crystals that contained sodium ions. The condition of MAS NMR was the same as that described in chapter 2. However, the excitation pulse width was kept at 0.6μs to avoid the nutation effects[8] which affect the line shapes and

relative intensities if NMR spectrum contains several peaks.

For high temperature NMR measurements, alumina sample container was used for sodium salts and boron nitride for silicates. NaCl, NaBr, Na_2CO_3 and $NaNO_3$ are purchased from commercial sources and used without further purification. Na_2SiO_3 and $Na_2Si_2O_5$ were crystallized from stoichiometric glasses. Other silicate and aluminosilicate samples were glassy.

To obtain the isotropic chemical shift from NMR peak position, the effect of dynamic frequency shift[9], which is caused by the second order nuclear quadrupolar interaction, have to be accounted. In the whole measurements of the present investigation, NMR spectrum has been measured at sufficiently high temperature, thus the motion of sodium ion is fast enough, for the dynamic shift to be neglected.

5-3.Results

5-3-1 ^{23}Na chemical shifts for silicate, borate and other inorganic crystals

Results of MAS NMR measurements are summarized in table 1. All samples have been identified to be single phase by powder X-ray diffraction. NMR spectrum for Jadeite($NaAlSi_2O_6$) has been measured by static condition, because the spinning rate of the MAS NMR probe was not sufficient to eliminate the spinning side bands. Except for Zeolite-A4, Sodalite and Tourmaline, all the spectra are well simulated by second order nuclear-quadrupolar MAS NMR line shape given as[10],

$$\Delta\nu_{\frac{1}{2}} = \left[\frac{\nu_Q^2}{6\nu_L}\right]\left[I\,(I+1) - \frac{3}{4}\right](A\cos^4\theta + B\cos^2\theta + C). \qquad (1)$$

Where,

$$A = \frac{21}{16} - \frac{7}{8}\eta \cos 2\phi + \frac{7}{48}\eta^2 \cos^2 2\phi ,$$

$$B = -\frac{9}{8} + \frac{\eta^2}{12} + \eta \cos 2\phi - \frac{7}{24}\eta^2 \cos^2 2\phi ,$$

$$C = \frac{5}{16} - \frac{\eta}{8} \cos 2\phi + \frac{7}{48}\eta^2 \cos^2 2\phi .$$

Here ν_L is the Lamor frequency. ν_Q is equal to $\frac{3e^2qQ}{2I(2I-1)h}$ where $\frac{e^2qQ}{h}$ is a quadrupole interaction parameter(in Hz) which is the multiple of the quadrupole moment of the nucleus(eQ) and the V_{ZZ} component of the EFG tensor(eq). η is an anisotropy of the EFG tensor($\frac{V_{yy} - V_{xx}}{V_{zz}}$). θ , ϕ is a Eular angles between the principle axis of the EFG tensor and the external magnetic field. For crystalline powder and glassy sample, θ and ϕ will be distributed spatially in the all directions. Thus the NMR line shapes will be given from the integration over $\cos\theta$ and ϕ for all possible directions. A line shape simulation was performed with appropriate sets of line shape functions with varying η value. As shown in table 1, isotropic chemical shifts, nuclear quadrupolar coupling constant and η have been obtained.

Table 1 ^{23}Na NMR parameters obtained from the present MAS NMR measurements.

compound	chemical shift (ppm)	Q.C.C. (MHz)	η
anhydrous silicates			
α-$Na_2Si_2O_5$	15±5	1.79	0.99
Na_2SiO_3	23	1.39	0.76
Jadeite($NaAlSi_2O_6$)	10±5	3.3±0.1	0.25
Zeolite-A4	10±5	<0.4	
Sodalite	6±2	<0.2	
Tourmaline	-15±2	<0.4	
hydrous silicates			
Natrolite	6±1	1.78	0.64
Analcime	14±1	2.3	0.02
borates			
Borax(1)	-0.9±0.2	0.85	0.13
Borax(2)	11.9±0.2	0.55	0.45
Ulexite	5.2±0.5	1.25	0.53
$NaBO_2$	1.5±1	1.18	0.0
Inorganic compounds			
Na_2SnO_3	49±1	2.05	0.0
Na_2ZrO_3	27±1	2.02	0.1
Na_2GeO_3	22.5±1	1.31	0.79
$NaPO_3$	2±1	1.56	0.58
$Na_2Ti_3O_9$	3±1	0.68	0.17
$NaNbO_3$	-5.0±0.5	1.0	0.87
Na_2WO_4	5±2	2.5	0.03
Na_2MoO_4	3±2	2.57	0.0
$Na_2WO_4(2H_2O)$	-1.2±1	0.87	0.39
$Na_2MoO_4(2H_2O)$	-2±1	0.89	0.1

5-3-2. ^{23}Na chemical shifts of simple ionic liquids

The temperature dependence of ^{23}Na NMR spectra for NaCl and NaBr around their melting points, 801°C and 747°C, respectively, are shown in figure 1. At the melting points, NMR spectra clearly split into two peaks corresponding to the liquid and solid states. The liquid states show more positive chemical shift values compared with that of crystalline states. These shifts can be interpreted by the decrease of the coordination number around sodium ion. The results are in accordance with X-ray and Neutron diffraction results.[11,12]

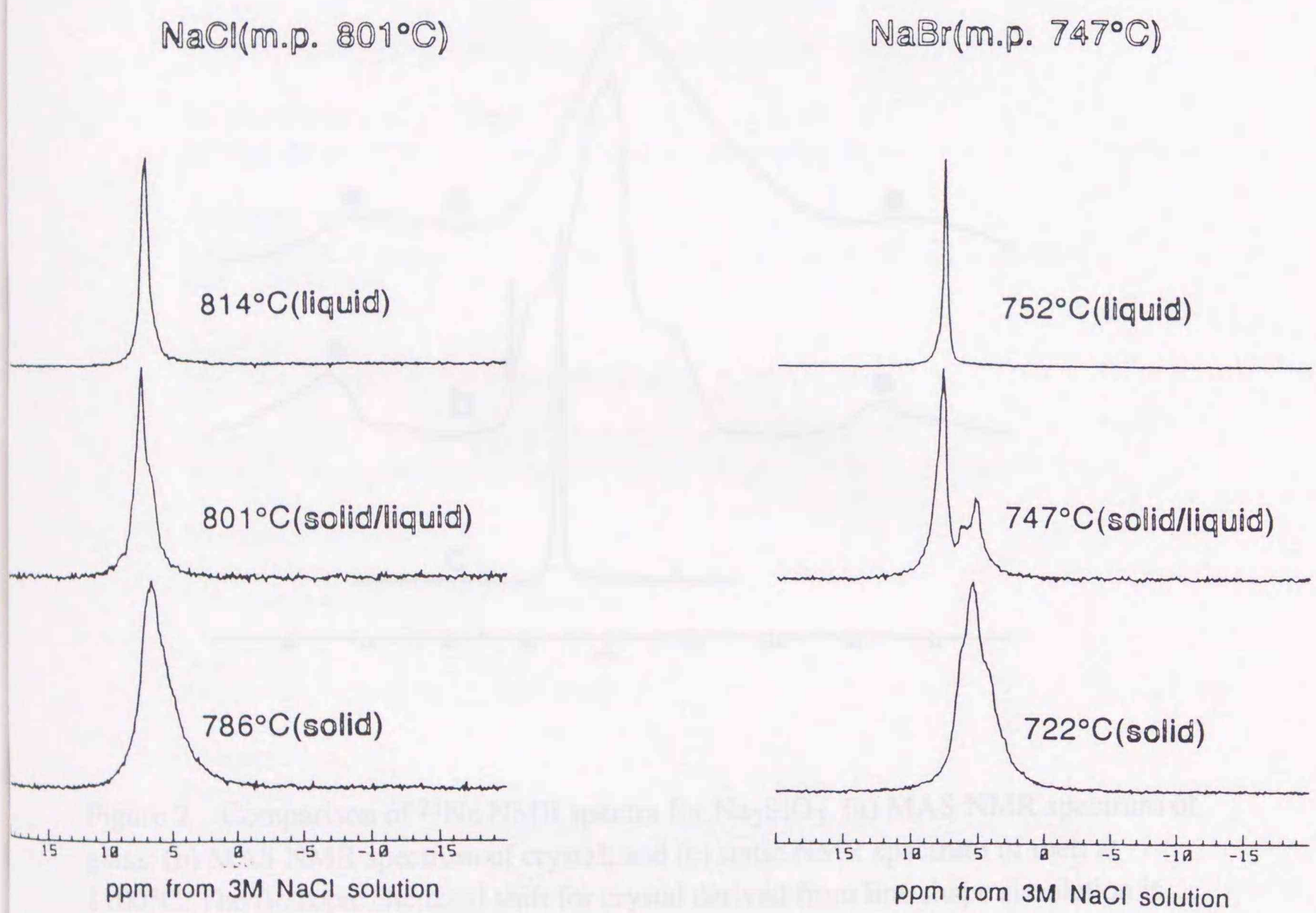

Figure 1 High temperature ^{23}Na spectra for NaCl(left) and NaBr(right) around the melting points.

5-3-3. ^{23}Na chemical shifts of silicate and aluminosilicate liquids

The ^{23}Na NMR spectra for sodium metasilicate(Na_2SiO_3) crystal, glass and melt(at 1100°C) are shown in figure2. The line shape of melt was observed as a single Gaussian peak. The dispersion v.s. absorption plot was circular, which indicates the effect of dynamic frequency shift is negligible, thus, the peak position can be directly related to the isotropic chemical shifts. The composition dependence of the isotropic chemical shift is shown in figure3(solid circle). As the number of non-bridging oxygen per tetrahedral cation(NBO/T) increases, thus the network is increasingly modified, ^{23}Na chemical shift increases linearly.

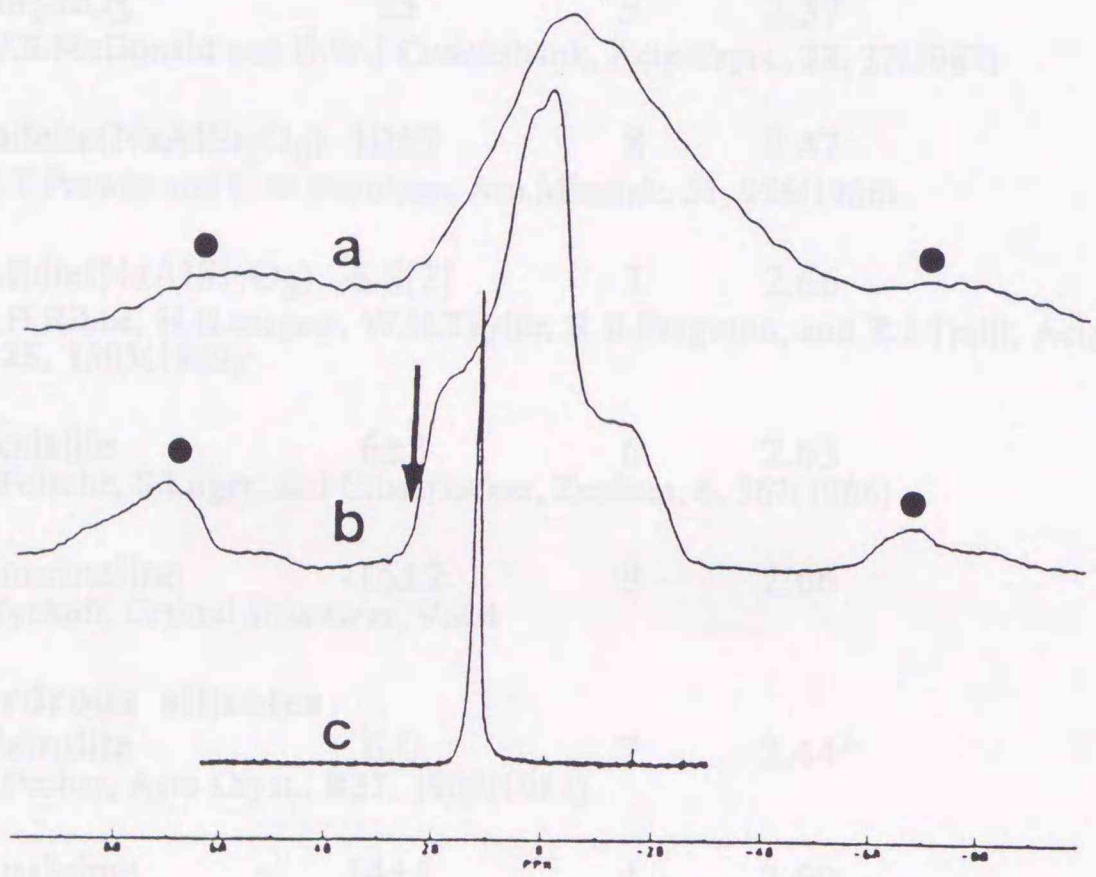

Figure 2 Comparison of ^{23}Na NMR spectra for Na_2SiO_3. (a) MAS NMR spectrum of glass; (b) MAS NMR spectrum of crystal; and (c) static NMR spectrum of melt at 1100°C. The isotropic chemical shift for crystal derived from line shape simulation is indicated by an arrow. Dots represent spinning side bands.

Table 2. ^{23}Na chemical shifts and structural parameters of silicates, germanete and borate.

compound	chemical shift (ppm)	coordination number and distance(Å)	
anhydrous silicates			
α-$Na_2Si_2O_5$	15±2	5	2.40
A.K.Pant and D.W.J.Cruickshank, Acta Cryst., **B24**, 13(1968)			
Na_2SiO_3	23	5	2.37
W.S.McDonald and D.W.J.Cruickshank, Acta Cryst., **22**, 37(1967)			
Jadeite($NaAlSi_2O_6$)	10±5	8	2.47
C.T.Prewitt and C.W.Burnham, Am.Mineral., 51, 956(1966)			
Albite($NaAlSi_3O_8$)	-6.8[2]	7	2.66
P.H.Ribbe, H.D.megaw, W.H.Taylor, R.B.Ferguson, and R.J.Traill, Acta Cryst., **B25**, 1503(1969)			
Sodalite	6±2	6	2.63
J.Felsche, S.Luger, and C.baerlocher, Zeolites, **6**, 367(1986)			
Tourmaline	-15±2	9	2.66
Wyckoff, *Crystal Structures*, Vol.4			
hydrous silicates			
Natrolite	6.0	7	2.44
F.Pechar, Acta Cryst., **B37**, 1909(1981)			
Analcime	14±1	4	2.60
I.R.Beattie, Acta Cryst., **7**, 357(1954)			
others			
Na_2GeO_3	22.5	5	2.40
D.W.J.Cruickshank, A.Kalman, and J.S.Stephens, Acta Cryst., **334**, 1333(1978)			
$NaBO_2$	1.5	7	2.53
Wyckoff, *Crystal Structures*, Vol.4			

5-4. Discussion

Some attempts were made to find a structural parameter to correlate the ^{23}Na chemical shifts obtained in the present investigation with coordination environments around sodium ions for the whole samples observed in the present work. There seems a rough relation between the coordination numbers and ^{23}Na chemical shifts. As the coordination number increased ^{23}Na chemical shift appears in the negative directions. A more quantitative analysis is now in progress.

On the other hand, the relation could simply be understood if only the

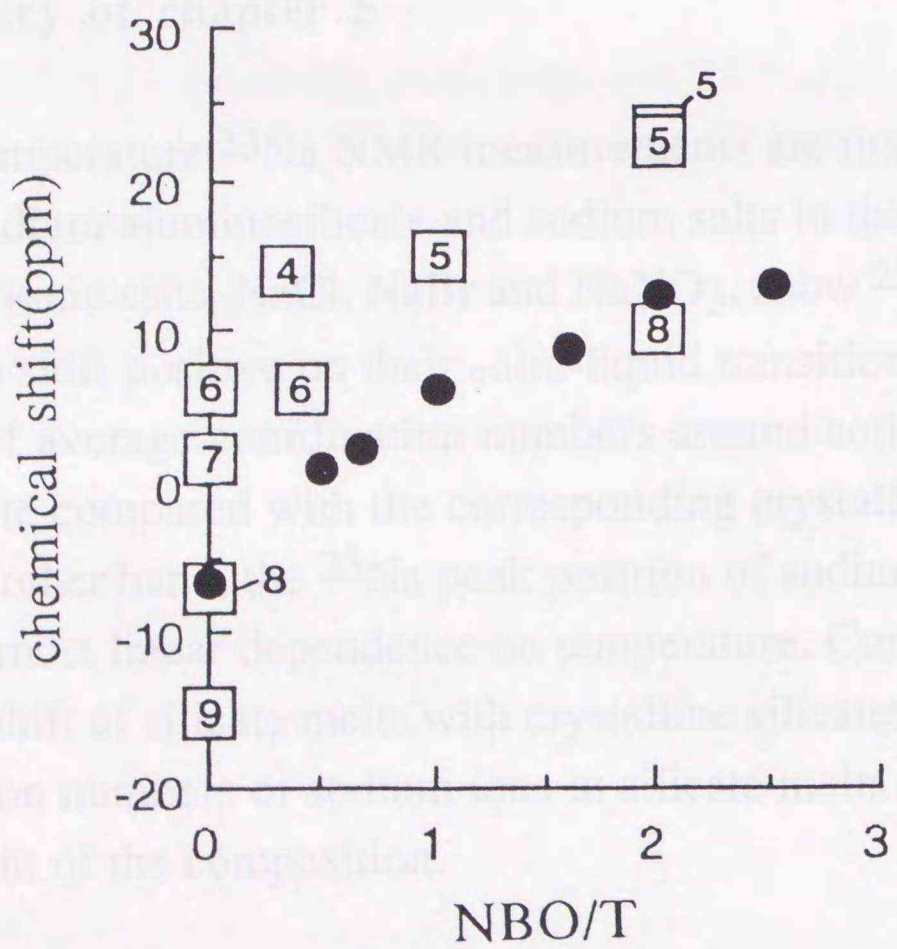

Figure 3 ^{23}Na chemical shift plotted against NBO/T for sodium silicate, aluminosilicate, germanate and borate crystals(❑) and melts(●). The data for the crystals are shown in table2. Data for melts are shown in figure3. The numbers indicated in the simbol represent the numbers of Na-O bonds within 3.2Å from Na atom.

network glass forming systems are taken into account. Table 2 summarizes the ^{23}Na chemical shift and coordination numbers around Na atom within the spheres of 3.2Å. The relationships are shown in figure3 as a function of NBO/T. The ^{23}Na chemical shift seem to depend not only on the coordination numbers but also for degree of polymerization. ^{23}Na chemical shifts for the materials having the same coordination number seems linearly depends on the NBO/T value. The isotropic chemical shift for silicate melts(solid circles in figure3) suggests the coordination number of sodium in silicate liquids to be 7 to 8, independent of compositional variation. This result is slightly different from that derived from X-ray diffraction measurements[13] which gave coordination numbers to be 4.1~6.1. The EXAFS study of sodium di-silicate glass[14] gave coordination numbers to be 5±0.5 while that of sodium aluminosilicate glasses[15] gave the coordination number of sodium in the whole composition range to be 5.1~7.6 in close to the present results.

Summary of chapter 5

High temperature ^{23}Na NMR measurements are made on sodium silicate, sodium aluminosilicate and sodium salts in their molten state.

Simple ionic salts, NaCl, NaBr and $NaNO_3$, show ^{23}Na NMR peak position to shift positive on their solid-liquid transition which indicates the decrease of average coordination numbers around sodium ion in their molten state compared with the corresponding crystalline state.

On the other hand, the ^{23}Na peak position of sodium silicate melts showed almost linear dependence on temperature. Comparison of the chemical shift of silicate melts with crystalline silicates suggested the coordination numbers of sodium ions in silicate melts to be 7 to 8 independent of the composition.

references

(1) P.H.Ribbe, H.D.Megaw, W.H.Taylor, R.B.Ferguson, and R.J.Traill, Acta Cryst., **B25**, 1503(1969)

(2) B.L.Phillips, R.J.Kirkpatrick, and G.L.Hovis, Phys.Chem.Minerals, **16**, 262(1988)

(3) G.L.Hovis, D.R.Spearing, J.F.Stebbins, J.Roux, and A.Clare, Am.Miner., **77**, 19(1992)

(4) G.Engelhardt and D.michel, "*High-Resolution Solid-State NMR of Silicates and Zeolites*", (John Wiley and Sons, Chichester, 1987)

(5) J.F.Stebbins, I.Farnan, E.H.Williams, and J.Roux, Phys.Chem.Minerals, **16**, 763(1989)

(6) J.F.Stebbins and I.Farnan, Science, **255**, 586(1992)

(7) J.F.Stebbins, J.B.Murdoch, E.Schneider, I.S.E.Carmichael, and A.Pines, Nature, **314**, 250(1985)

(8) A.Samoson and E.Lippmaa, Chem.Phys.Lett., **100**, 205(1983)

(9) L.Werbelow and G.Pouzard, J.Phys.Chem., **85**, 3887(1981).

(10) E.Kundla, A.Samoson, and E.lippmaa, Chem.Phys.Lett., **83**, 229(1981)

(11) G.Zarzycki, J. de Phys., **17**, 44(1956)

(12) F.G.Edwards, J.E.Enderby, R.A.Howe, and D.I.Page, J.Phys.C, **8**, 3483(1975)

(13) Y.Waseda, *The Structure of Non-crystalline Materials*, McGraw-Hill International Book Company

(14) G.N.Greaves, A.Fontaine, P.Lagarde, D.Raoux, and S.J.Gurman, Nature, **293**, 611(1981)

(15) D.A.McKeown, G.A.Waychunas, and G.E.Brown Jr., J.non-cryst.Solids, **74**, 325(1985)

CHAPTER 6
DYNAMICS OF INORGANIC NETWORK-GLASS-FORMING SYSTEM-
^{11}B NMR STUDIES OF B_2O_3 MELT AND GLASS

Abstract of chapter 6

High temperature ^{11}B NMR line shape and relaxation time measurements were made on B_2O_3 glass and melt in the region of room temperature to 1200°C. Peak positions and relaxation times were well interpreted in terms of double exponential relaxation and dynamic shift caused by the second order nuclear quadrupolar interaction. As the result, isotropic chemical shift(δ_{iso}) and reorientational correlation time(τ_c) were obtained. δ_{iso} for ^{11}B was in the range for BO_3 structural units and increased(less shielded) as increasing temperature, which is likely caused by the gradual change of the linkage of the BO_3 units, such as fragmentation of the ring structure into chains. Arrhenius plot of the correlation time showed two regions crossing each other around 750°C and each of them being responsible for two distinct reorientational processes. Below 750°C, a linear dependence of τ_c against the inverse of temperature with activation energy of 39kJ/mol was observed. This process persist below the glass transition temperature and was attributed to the restricted rotation of BO_3 triangle around its equilibrium position. Above 750°C, the τ_c was strongly temperature dependent and coincides with that of the ultrasonic longitudinal relaxation times.

6-1. Introduction

The structural changes associated with the glass formation in various systems are suggested to be closely related to their dynamics in the liquid region. The dynamical behavior above the glass transition temperature(T_g) has been described phenomenologically.[1,2] Structural

relaxation in glass forming systems is often characterized by two separate process; the α– and the β-processes.[3-11] The α process corresponds to those degrees of freedom which freeze out at T_g and is associated with the collective motion directly related to the liquid-glass transition. In the case of network forming glass with strong covalent bonds such as B_2O_3 and SiO_2 ,it has been proposed that the transformation to a liquid occurs through temperature-activated bond breaking, which may explain the nearly Arrhenius behavior of the viscosity and structural relaxation time in these systems.[12,13] The β process corresponds to those degrees of freedom which exist in both the liquid and glass and is associated with intra-molecular motion.

Studies concerning with the dynamical behavior of organic glass forming systems in these decades give the insights of the relationships between the structural relaxation and the dynamical behavior of molecular motion. In contrast, the dynamics of inorganic network glass forming systems such as silicates and borates has been poorly understood mainly due to experimental difficulties. Our previous ^{11}B NMR longitudinal-relaxation study[14] disclosed the temperature dependence of reorientational correlation time(τ_c) of binary Na_2O-B_2O_3 melts for the first time. A crossover was observed between two distinct orientational relaxation processes, which occurred well above the T_g. The non-Arrhenius character of τ_c of both processes had been discussed and analysed on the basis of strong-fragile classification of glasses.[15]

In the present study, we chose B_2O_3 which is one of the best studied examples of inorganic glass forming materials. The spin-lattice relaxation time and line shapes of ^{11}B in B_2O_3 glass and melt were measured with ppm resolution over a wide temperature range, from room temperature to 1200°C, in order to study the temperature effect on the structure and dynamics of the liquid state.

B_2O_3 is a typical network glass forming oxide with caloric Tg of 260°C and melting point of 577°C. The structure of B_2O_3 glass has been a much debated issue for many years.[16-23] It has been generally accepted that this glass is constructed from three dimensional random

network with structural unit of planer BO_3 triangle.[16-18] The manner in which the BO_3 triangles are connected has been much discussed.[16-23] Some experimental observations indicated boroxol ring(B_3O_6) to be the well defined molecular entities in the structure.[16-18] In contrast, some molecular-dynamics simulation studies[22,23] predicted structures that are absent of boroxol rings and still in good agreement with the structure factors determined from neutron and X-ray diffraction. The general view, however, seems to be that vitreous B_2O_3 consists of a large amount of boroxol rings. The glass forming of this material with ease seems to be correlated with this structural geometry while B_2O_3 crystal does not contain boroxol rings.[24] In the present study, special attention was paid to the the dynamic behavior of molten B_2O_3 in relation with the gradual decrease of the amount of boroxol rings as increasing temperature estimated from Raman vibrational spectroscopy.[19]

6-2. Experimental section

NMR measurements were carried out on a Bruker MSL-200 spectrometer with wide bore(150mm) magnet operated at 64.19MHz for ^{11}B. The high temperature NMR probe[25] specially reconstructed for this experiment was made of a platinum electric heater, wound non-magnetically, and an outer water jacket. The detachable detection coil was made of platinum wire turned solenoidally 6 times. Reagent grade anhydrous B_2O_3 was melted in a platinum crucible at 1200°C for 5 hours, quenched to glass, and put into alumina sample holder for high temperature NMR measurements.

In addition to FT-NMR spectra, spin-lattice relaxation time measurements were performed by inversion-recovery(180°-τ-90°) sequence. Saturation-recovery (90°-τ-90°) sequence was also employed to obtain some of the experimental points. However, both of them gave identical results. A 90° pulse width was kept at about 4μs from room temperature to 400°C. It gradually became longer as the temperature was raised up to 1200°C(12μs at 1000°C), because the quality factor of the detection coil got worse with temperature.

In the previous work by Rubinstein and Resing,[26] the ^{11}B relaxation

behavior of B_2O_3 melt had been analysed on the basis of Bloembergen, Purcell and Pound(BPP)[27] treatment. Thus, the decay of the magnetization had been assumed as single exponential, although the relaxation decay of nucleus with the spin numbers of I become the sum of $I+1/2$ exponential decays.[28] BPP treatment of relaxation data would have resulted in an extremely temperature dependent τ_c, in contrast with the present study as will be shown later. In the present investigation, the longitudinal relaxation and line shapes were analysed by means of the double exponential relaxation and the dynamic frequency shifts which successfully explained our previous longitudinal-relaxation data of Na_2O-B_2O_3.[14]

For the particular case of $I=3/2(^{11}B)$, the relaxation behavior of the longitudinal magnetization is given by the following expression,[28-32] if an isotropic motion of a single correlation time(τ_c), thus the Lorentian shape of the spectral density is assumed,

$$\langle S_z\rangle - \langle S_z\rangle^T = -2\langle S_z\rangle^T [(4/5)\exp(-a_1 t) + (1/5)\exp(-a_2 t)], \quad (1)$$

$$a_1 = 2C J_2,\ a_2 = 2C J_1, \quad (2)$$

$$J_n = t_c\ (1 + (n\,\omega\,\tau_c)^2)^{-1}, \quad (3)$$

$$C = (1/20)(e^2 q\, Q/h)^2, \quad (4)$$

where w is the Lamor frequency in radian and $e^2 q\, Q/h$ is a effective quadrupole-coupling constant. $\langle S_z\rangle$ and $\langle S_z\rangle^T$ represent the longitudinal magnetization and its equilibrium value, respectively.

The transverse relaxation following the $\pi/2$ pulse is given by,[31,32]

$$\langle S_x\rangle - i\,\langle S_y\rangle^T = \langle S_z\rangle^T\, i \exp[-i\,\omega\,(t-t_0)]\,[(3/5)\exp(-b_1 t) + (2/5)\exp(-b_2 t)] \quad (5)$$

where,

$$b_1 = C\ (J_0 + J_1 + i\,Q_1)$$
$$b_2 = C\ (J_1 + J_2 - i\,Q_1 + i\,Q_2) \quad (6)$$

The imaginary components of the spectral density,

$$Q_n = n\,\omega\,\tau_c^2\,(1 + (n\,\omega\,\tau_c)^2)^{-1}, \quad (7)$$

include hyperfine second-order dynamic quadrupolar shifts which cause a displacement of the satellite pairs and the central line relative to each other.

6-3. Results

Figure 1 shows the ^{11}B NMR spectra for B_2O_3 glass and melt. The spectra show little change until the Tg was reached. Above Tg, however, the line width decreased considerably until around 550°C. The full width at half maximum(fwhm) at 550°C was 480Hz(7.5ppm). Then, the fwhm increased again with increasing temperature. The spectra seem to be strongly influenced by the double exponential quadrupolar relaxation as described above.

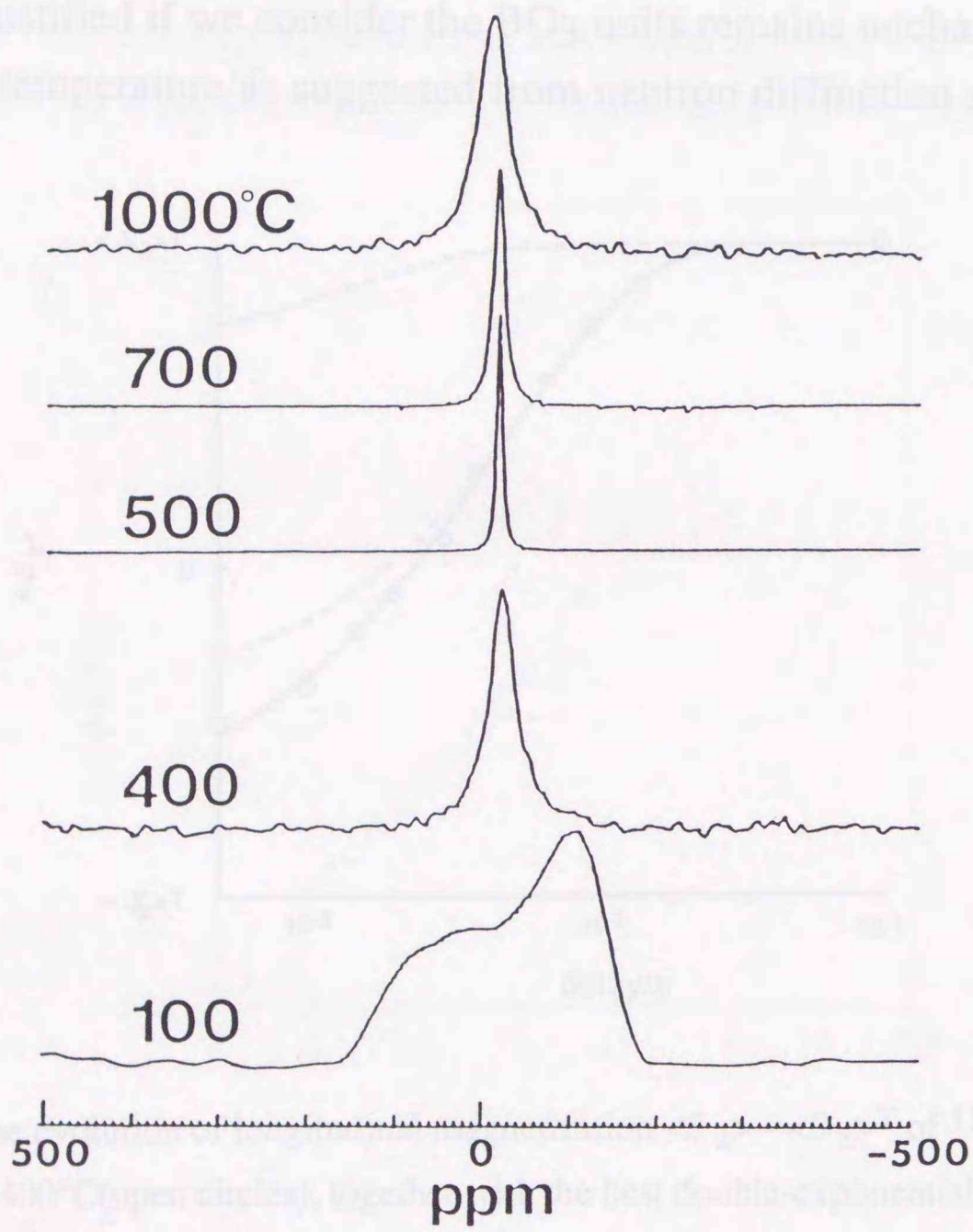

Figure 1. Temperature variations of the ^{11}B NMR spectra for B_2O_3.

Figure 2 shows time evolution of longitudinal magnetization, $\langle S_z \rangle - \langle S_z \rangle^T$, of ^{11}B in B_2O_3 melt at 400°C. The solid line in the figure is a theoretical function of equation(1) that gives the best fit to the experimental data. In the simulation, the dynamical quadrupolar coupling constant e^2qQ/h of 2.05MHz and $\tau_c=1.53\cdot10^{-7}$s were adopted. The quadrupolar coupling constant should be, in principle, determined at each temperature from the time evolution of $\langle S_z \rangle - \langle S_z \rangle^T$ together with τ_c. However, e^2qQ/h was assumed to be constant in the whole temperature range. Although the gradual change of the network structure as a function of temperature was observed from chemical shift analysis, the assumption would be justified if we consider the BO_3 units remains unchanged with increasing temperature as suggested from neutron diffraction study.[20]

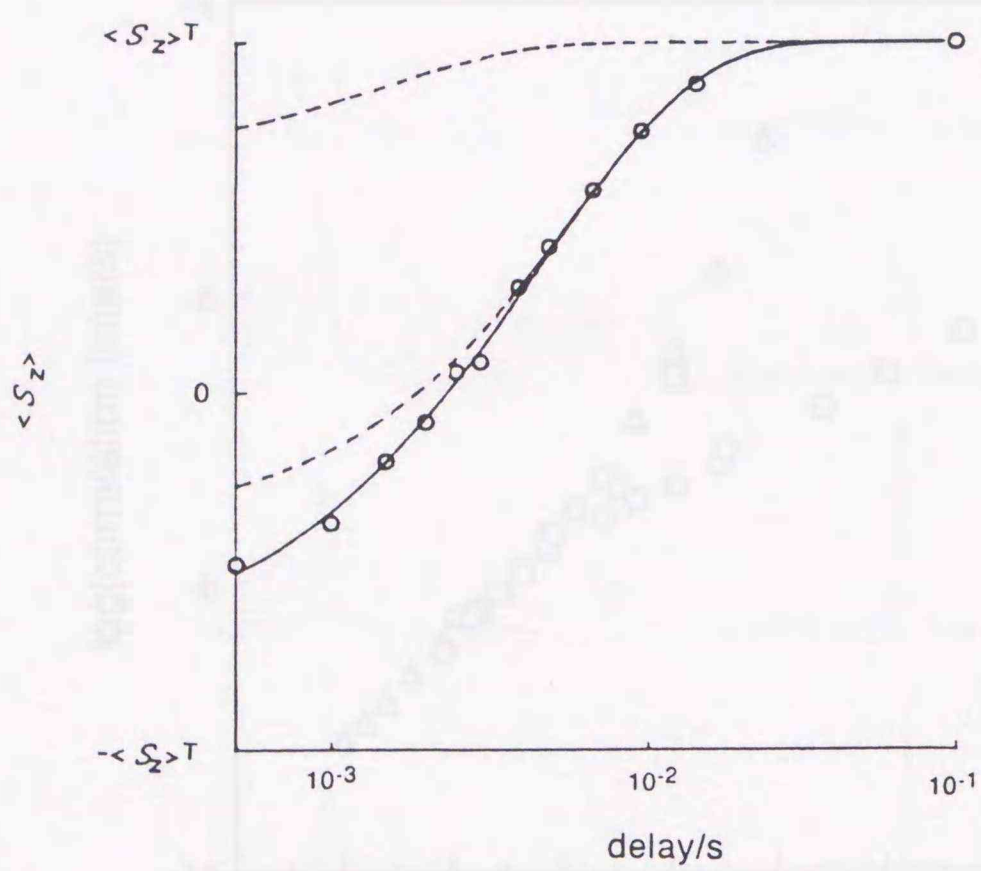

Figure 2. Time evolution of longitudinal magnetization $\langle S_z \rangle - \langle S_z \rangle^T$ of ^{11}B of B_2O_3 melt at 400°C(open circles), together with the best double-exponential fits of equation(1) with e^2qQ/h =2.05MHz and $\tau_c=1.53\cdot10^{-7}$s(solid line). Broken lines represent each exponents.

Furthermore, e^2qQ/h of BO_3 triangles obtained from line shape simulation on borate crystals and glasses[33] are almost constant over wide composition range and degree of polymerization. e^2qQ/h for pure B_2O_3 was determined from an extrapolation of the results of Na_2O-B_2O_3[14] to sodium free limit. Assuming e^2qQ/h to be 2.05MHz through the whole temperature range, τ_c have been determined as shown in figure3(open circles).

Using the results obtained from longitudinal relaxation, ^{11}B spectra have been calculated by Fourier transforming the transverse-relaxation function $\langle S_x \rangle + i \langle S_y \rangle$ of equation(5). In figure 4 is shown the comparison between experimental and calculated spectra. Calculated line shapes consist of a superposed two Lorenzians obtained by Fourier

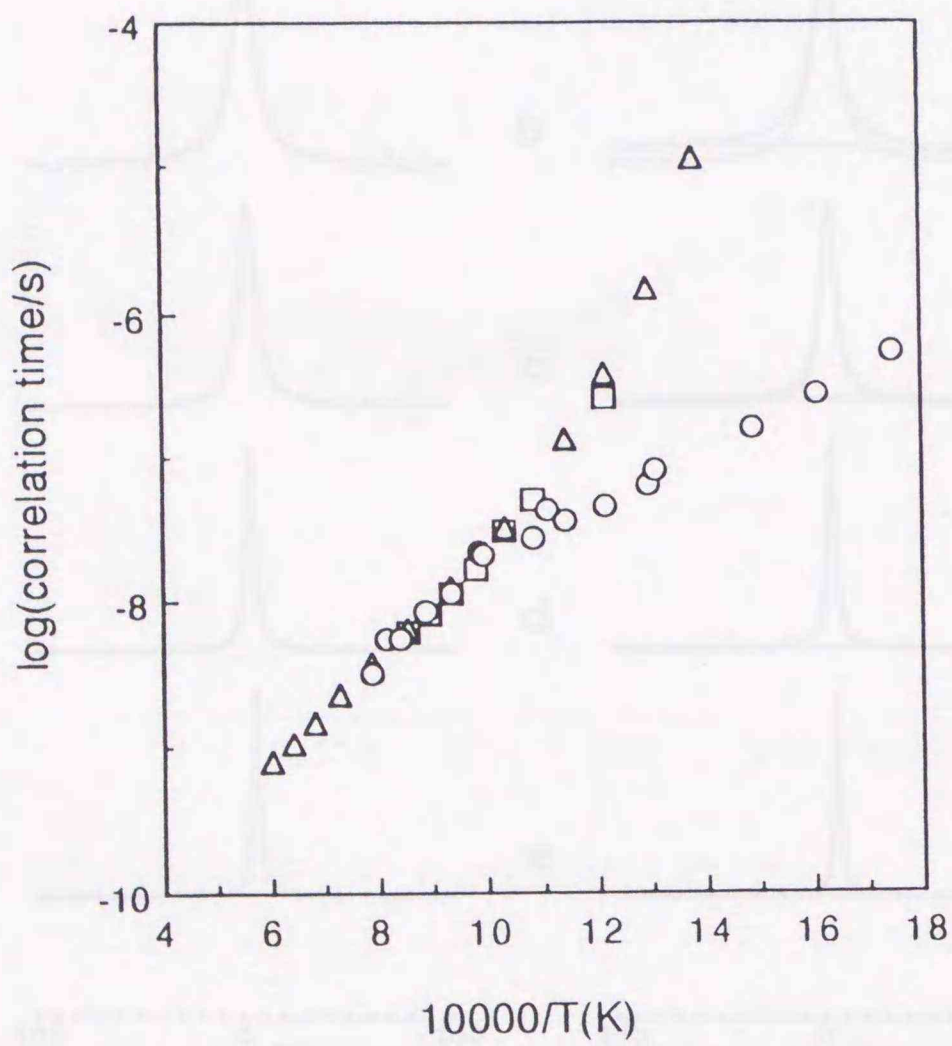

Figure 3. Temperature dependence of correlation times of B_2O_3 melt. (○) τ_c determined from ^{11}B longitudinal relaxation. (❑) averaged correlation times of the ultrasonic longitudinal relaxation.[36] (Δ) shear relaxation time of viscosity[13] estimated from Maxwell equations for viscoelastic behavior with $G_\infty = 10^{-10.4}$.

transforms of the function $<S_x> + i <S_y>$. At lower temperature, the second component becomes so broad as to be invisible. Reasonable fit suggests the Lorenzian shape of the spectral densities J_n in equation(3) seems to satisfactorily explain the experimental profiles. A non-Debye frequency behavior, which is frequently observed for organic glass forming systems,[5-7,9,11] has been analysed by the non-Lorenzian shape of J_n i.e., the distribution of τ_c. In contrast to these results, the deviation from Debye process seems to be considerably small in the present system. The same was true for Na_2O-B_2O_3 system.[14]

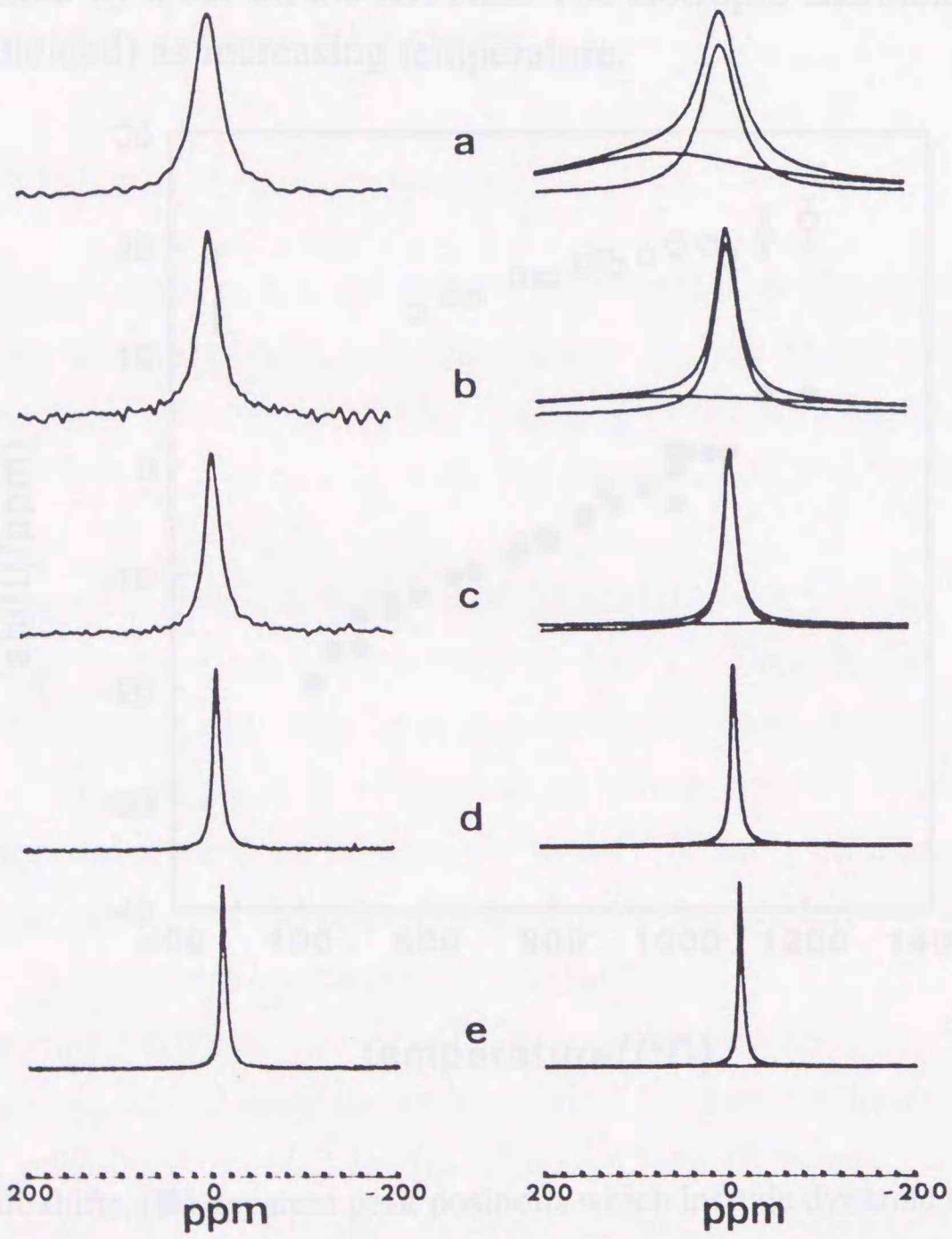

Figure 4. (Left)^{11}B NMR line shapes for B_2O_3 at a);950°C, b);860°C, c);790°C, d);650°C, and e);590°C. (Right)calculated line shapes obtained by the Fourier transforms of equation(5) using the parameters of the longitudinal relaxation. a); $\log(\tau_c)$=-8.25, b); $\log(\tau_c)$=-8.00, c); $\log(\tau_c)$=-7.75, d); $\log(\tau_c)$=-7.45, e); $\log(\tau_c)$=-7.25.

Because the peak positions of ^{11}B NMR spectra are also affected by the quadrupolar interaction, for which the term Q_n in equation(7) is responsible, the isotropic chemical shift values could not be obtained directly from the raw spectra. They can be estimated from the experimental spectra correcting the dynamic frequency shifts of equation(5) using parameters obtained from the line shape simulation. Both of the apparent chemical shift and the estimated isotropic chemical shift are shown in figure5. ^{11}B chemical shift range for BO_3 triangles is also shown figure5 by a bar on the left side. The isotropic chemical shifts increase(less shielded) as increasing temperature.

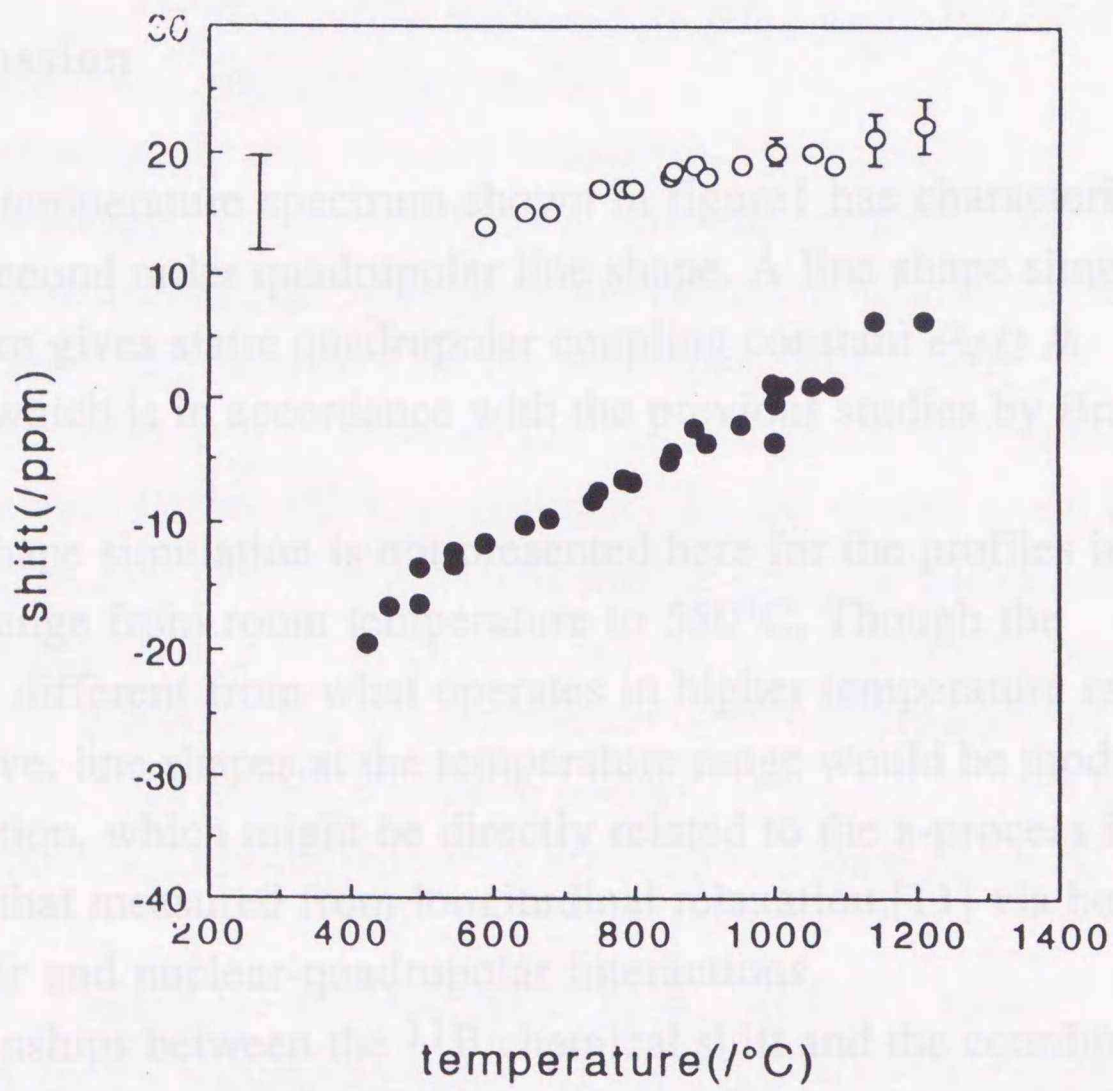

Figure 5. ^{11}B NMR shifts. (●) apparent peak positions which include dynamic shifts caused by Q_n of equation (7). (○) isotropic chemical shifts estimated from the line shape simulation.

The temperature dependence of τ_c plotted in figure3 shows a bend at a temperature at which the value of the correlation time is of the order of 10^{-8} s. This indicates the presence of two dynamical processes which are responsible for ^{11}B relaxation. Because the condition $\omega\tau_c>1$ is fulfilled in the whole temperature range of the present study, the longitudinal relaxation is governed by the motion of higher frequency within the Larmor precession frequency. Therefore the bend in figure3 corresponds to the crossover between the correlation times of two dynamical processes, each of which has higher frequency in the temperature range above and below the crossover temperature.

6-4. Discussion

The room temperature spectrum shown in figure1 has characteristic of rigid-lattice second order quadrupolar line shape. A line shape simulation of the spectrum gives static quadrupolar coupling constant e^2qQ/h of 2.6±0.1MHz which is in accordance with the previous studies by Bray et al..[18]

Any line shape simulation is not presented here for the profiles in the temperature range from room temperature to 550°C. Though the mechanism is different from what operates in higher temperature range discussed above, line shapes at the temperature range would be modulated by slower motion, which might be directly related to the a-process in contrast with that measured from longitudinal relaxation,[11] via both of dipolar-dipolar and nuclear-quadrupolar interactions.

The relationships between the ^{11}B chemical shift and the coordination environment around boron nucleus were studied for some minerals[33] Chemical shift of BO_3 is located in the range 12.7 to 19.0 ppm, while that of BO_4 in the range -3.3 to 2.0 ppm referred to that of $BF_3 \bullet Et_2O$. The chemical shift for B_2O_3 melt(figure5) estimated from the line shape simulation comes roughly in the range for BO_3 in the whole temperature range studied. The progressive shift with temperature towards positive direction is likely caused by the gradual change of the connectivity of the

BO_3 units. The progressive fragmentation of the boroxol ring into chains has been suggested from both of Raman[19] and neutron scattering studies.[20] The B-O-B bond angles in the boroxol ring was shown to be 120° while that at the oxygen of chain was approximately 130°.[16-18] The fragmentation of the boroxol rings into chains as increasing temperature would result in the chemical shift of ^{11}B of BO_3 group. The chemical shift of RBO_2(R=alkyl group) compound where the two oxygens incorporate B atom into five-member ring show 5~6 ppm positive shift resulting from the strain at B, compared with that in case of six-member ring.[34] The positive shift of ^{11}B in B_2O_3 melt might be caused by the deviation of the B-O-B and O-B-O bond angles from 120°, though the quantitative estimation needs further study.

The NMR quadrupole relaxation is proposed to proceed by the fluctuation of the electric field gradients around the nucleus under investigation. For the case of B_2O_3 melt, the rotational motion of the BO_3 triangle must play the major role on the relaxation. In figure3, temperature dependence of τ_c show almost linear dependence against the inverse temperature below 750°C in contrast with the results given by Rubinstein and Resing.[26] The low activation energy for this motion (39kJ/mol) suggests that it is not directly related to the diffusion process. The translational diffusion has to presume simultenious breaking of the strong B-O bonds with higher activation energy, as the B_2O_3 melt is constructed from the fully polymerized three dimensional network structure.

On the other hand, τ_c of this process at T_g was at 10^{-6} s which coincides with the corresponding value for $0.09Na_2O \bullet 0.91B_2O_3$ and $0.20Na_2O \bullet 0.80B_2O_3$ systems.[14] The Na_2O-B_2O_3 glass is suggested to have fully polymerized network structure within the composition range of Na_2O<30mol%. $0.33Na_2O \bullet 0.67B_2O_3$ glass has a certain amount of non-bridging oxygens which terminate the network, and τ_c was smaller by about one order of magnitude.[14,35] These facts suggest that the restricted rotation (rotational vibration) of the structural units around its

equilibrium positions in cooperation with the adjacent groups probably be responsible for this β-process.

On the other hand, above 750°C τ_c become strongly temperature dependent. In this region, an Arrhenius law also holds with the activation energy of 72kJ/mol. τ_c coincides with the averaged correlation time for ultrasonic longitudinal relaxation[36] and also coincides with the shear relaxation time of viscosity estimated from Maxwell equations for viscoelastic behavior,

$$\tau_c = \frac{G_\infty}{\eta} \qquad (8),$$

if $G_\infty = 10^{-10.4}$ is adopted as shown in the figure3. The Arrhenius behavior suggests the strong character of this compound in the framework of strong-fragile classification.[15]

6-5. Summary of chapter 6

High temperature NMR line shape and relaxation time measurements were made on ^{11}B in B_2O_3 melts. Longitudinal relaxation times and line shapes were well analysed by double exponential relaxation and dynamic frequency shifts caused by nuclear quadrupole interaction. The isotropic chemical shifts and reorientational correlation times of the BO_3 triangle were obtained. The shift gradually moved to positive direction with increasing temperature. Below 750°C, the temperature dependence of the reorientational correlation time shows characteristics for the β-relaxation process which is attributable to the restricted rotation of BO_3 triangles around its equilibrium position in cooperation with the adjacent groups.

On the other hand, above 750°C the correlation times show strong temperature dependence, characteristic to the so-called α-process.

References

(1) See, for example, *Proceedings of the International Discussion Meeting on Relaxations in Complex Systems* [J. Non-cryst.Solids, **131-133**,(1991)].

(2) C.A.Angell, Chem.Rev., **90**, 523(1990).

(3) G.P.Johari and M.Goldstein, J.Chem.Phys., **53**, 2372(1970).

(4) D.Kivelson, J.Phys.Chem., **95**, 709(1991).

(5) E.Rössler and H.Sillescu, Chem.Phys.Lett., **112**, 94(1984).

(6) Th.Dries, F.Fujara, M.Kiebel, E.Rössler, and H.Sillescu, J.Chem.Phys., **88**, 2139(1988).

(7) J.Colmenero, A.Alegría, J.M.Alberdi, and F.Alvarez, Phys.Rev.**B44**, 7321(1991).

(8) B.Bagchi, A.Chandra, and S.A.Rice, J.Chem.Phys., **93**, 8991(1990).

(9) E.Rössler, J.Chem.Phys., **92**, 3725(1990).

(10) D.Kivelson and S.A.Kivelson, J.Chem.Phys., **90**, 4464(1990).

(11) S.Kaufmann, S.Wefing, D.Schaefer, and H.W.Spiess, **93**, 197(1990).

(12) G.Urbain, Y.Bottinga, and P.Richet, Geochim.Cosmochim.Acta, **46**, 1061(1982).

(13) A.Napolitano, P.B.Macedo, and E.G.Hawkins, J.Am.Ceram.Soc., **48**, 613(1965).

(14) Y.Inagaki, H.Maekawa, T.Yokokawa, and S.Shimokawa, Phys.Rev., **B47**, 674(1993).

(15) C.A.Angell, J.Non-cryst.Solids, **102**, 205(1988).

(16) *Borate Glasses*, (Proc. Conf. on Boron in Glass and Glass Ceramics, Alfred, New York, June 5-8, 1977), eds. L.D.Pye, V.D.frechette, and N.J.Kreidl (Plenum, New York, 1978)

(17) R.L.Mozzi and B.E.Warren, J.Appl.Cryst., **3**, 251(1970).

(18) A.H.Silver and P.J.Bray, J.Phys.Chem., **29**, 984(1958).

(19) A.K.Hassan, L.M.Torell, L.Börjesson, and H.Doweida, Phys.Rev., **B45**, 12797(1992).

(20) M.Misawa, J.Non-cryst.Solids, **122**, 33(1990).

(21) P.L.Hanst, V.H.Early, and W.Klemperer, J.Chem.Phys., **42**, 1097(1965).

(22) T.F.Soules, J.Chem.Phys., **73**, 4032(1980).

(23) Q.Xu, K.Kawamura, and T.Yokokawa, Nippon Seramikkusu Kyokai gakujyutu Ronbunshi, **97**, 1416(1989).

(24) S.L.Strong and R.Kaplow, Acta.Cryst., **B24**, 1032(1968).

(25) S.Shimokawa, H.Maekawa, E.Yamada, T.Maekawa, Y.Nakamura, and T.Yokokawa, Chem.Lett., 617(**1990/4**).

(26) M.Rubinstein and H.A.Resing, Phys.Rev., **B13**, 959(1976).

(27) N.Bloembergen, E.M.Purcell, and R.V.Pound, Phys.Rev., **73**, 679(1948).

(28) P.S.Hubbard, J.Chem.Phys., **53**, 985(1970).

(29) A.G.Redfield, IBM J.Res.Dev., **1**, 19(1957).

(30) G.Jaccard, S.Wimperis, and G.Bodenhausen, J.Chem.Phys., **85**, 6282(1986).

(31) L.Werbelow and G.Pouzard, J.Phys.Chem., **85**, 3887(1981).

(32) L.G.Werbelow, J.Chem.Phys., **70**, 5381(1979).

(33) G.L.Turner, K.A.Smith, R.J.Kirkpatrick, and E.Oldfield, J.Magn.Reson., **67**, 544(1986).

(34) R.G.Kidd, in *NMR of Newly Accessible Nuclei*, Vol.2, ed. P.Lasszlo(Academic Press, New York,1983), p.56

(35) P.J.Bray and J.G.O'Keefe, Phys.Chem.Glasses, **4**, 37(1963).

(36) P.Macedo and T.A.Litovitz, Phys.Chem.Glasses, **6**, 69(1965).

ACKNOWLEDGEMENTS

The author wishes to express his sincere gratitude to Professor Toshio Yokokawa for his fruitful suggestion, lively discussion and continuous encouragement throughout this work. The author is also indebted to Professor Takashi Maekawa, Professor Katsuyuki Kawamura, Dr. Shigezou Shimokawa and Mr.Eiji Yamada for their informative advice and discussions. Hearty thanks are made to Professor Yoshio Nakamura, Professor Yoichi Sasaki, Professor Jonathan F. Stebbins and Dr. Dominique Massiot for their informative advice and discussions. Thanks are also due to Dr. Hidero Unuma, Mr. Yousuke Inagaki, Mr. Masato Nakamura, Mr. Satoshi Kato and Mr. Hajime Kiyono for their encouragement and collaboration.

Finally, it is also his pleasure to thank his wife, Mrs. Tamako Maekawa, his parents, Mrs. Nobuko Maekawa, Mr. Kinya Maekawa, Mrs. Masami Sato and Mr. Takefumi Sato, and his grandmother, Mrs. Hatsuko Munemasa, and his brother, Mr. Tomoki Maekawa, and his sister Ms. Yuko Sato for their continuous understanding and encouragement.

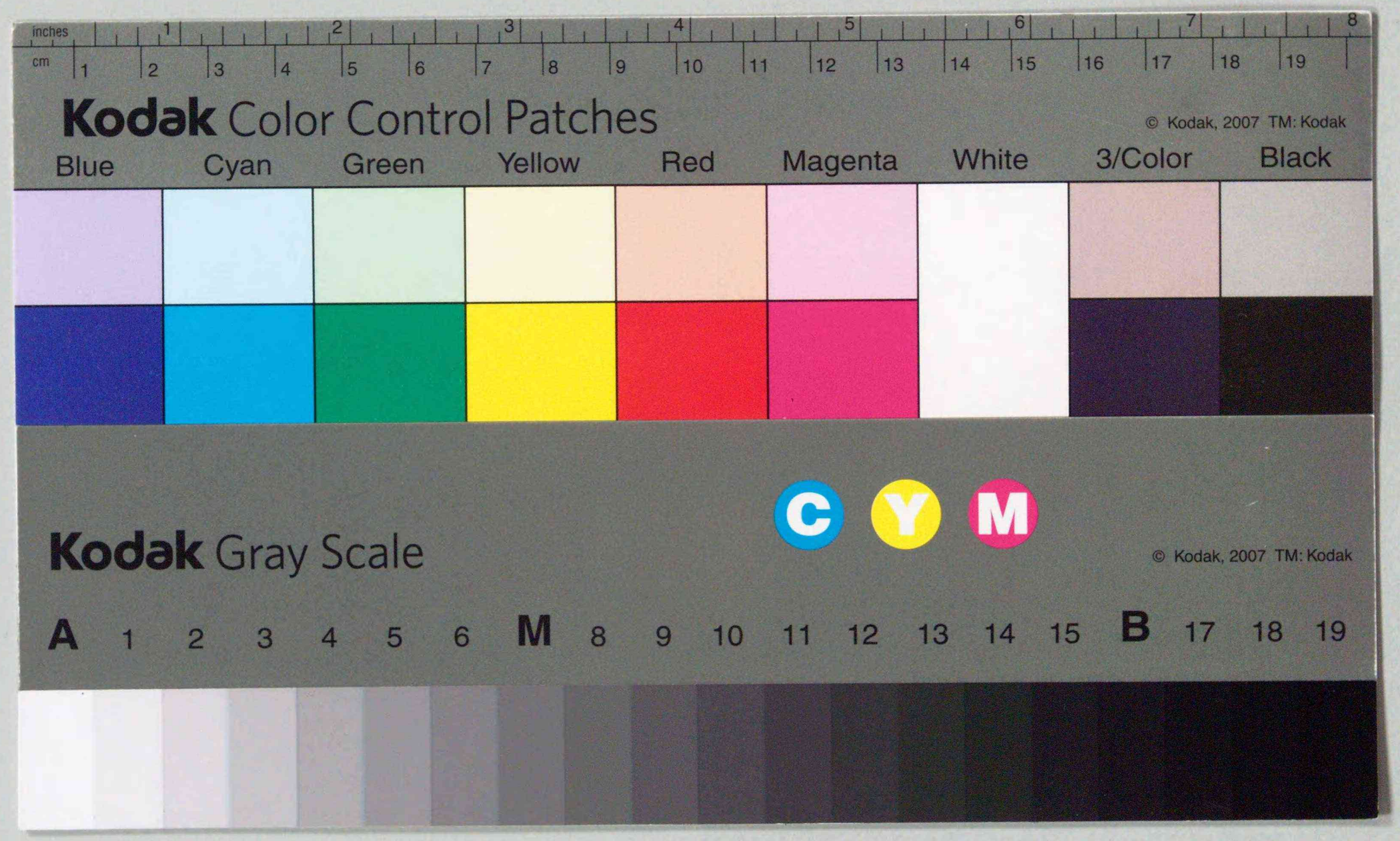
inches
1 2 3 4 5 6 7 8
cm
1 2 3 4 5 6 7 8 9 10 11 12 13 14 15 16 17 18 19
Kodak Color Control Patches
© Kodak, 2007 TM: Kodak
Blue Cyan Green Yellow Red Magenta White 3/Color Black
Kodak Gray Scale
C Y M
© Kodak, 2007 TM: Kodak
A 1 2 3 4 5 6 M 8 9 10 11 12 13 14 15 B 17 18 19